Measurement and Control of Dynamic Effects

Saturation, hysteresis, and eddy currents in iron-dominated magnets

Marco Buzio, Test & Measurement Section, Magnet, Superconductors and Cryostats Group

CAS course on “Normal- and Superconducting Magnets”, 19.11–02.12.2023 Pölten, Austria

Contents

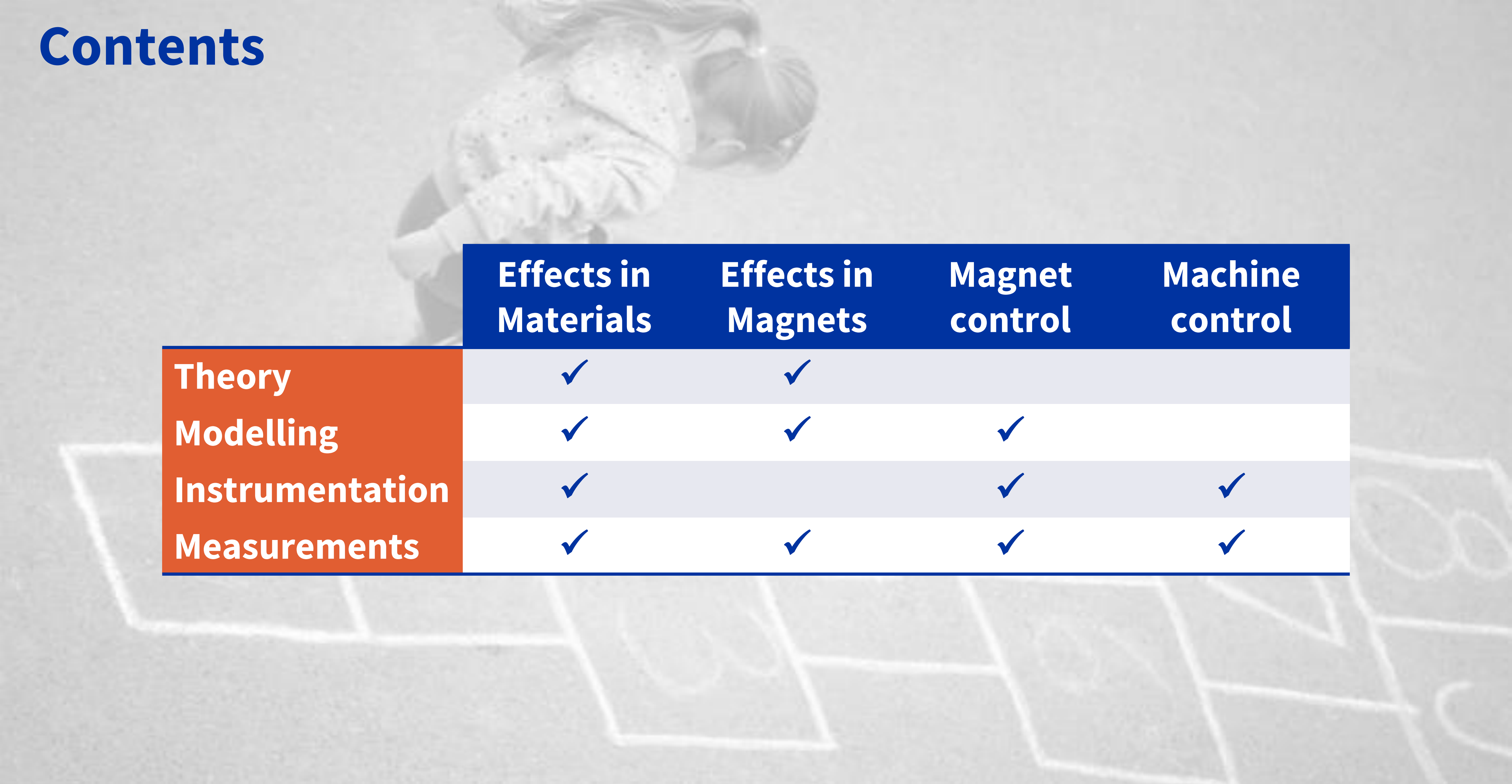

	Effects in Materials	Effects in Magnets	Magnet control	Machine control
Theory	✓	✓		
Modelling	✓	✓	✓	
Instrumentation	✓		✓	✓
Measurements	✓	✓	✓	✓

Acknowledgement

Thanks for scientific and technical support to present and past members of the TE-MSC-TM Section:

Luca Bottura, Didier Cornuet, Stephan Russenschuck, Louis Walckiers

Anthony Beaumont, Ricardo Beltron Mercadillo, Matthias Bonora, Regis Chritin, Guy Deferne, Lucio Fiscarelli, David Giloteaux, Giancarlo Golluccio, Christian Grech, Melvin Liebsch, Anton Lu, Unai Martinez, Vincenzo di Capua, Olaf Dunkel, Carlo Petrone

Special thanks for material properties instrumentation and measurements:

Mariano Pentella

Part I – Magnetic materials

Phenomenology and measurement of dynamic phenomena
hysteresis, saturation, eddy currents and more

Phenomenology

Eddy currents

- Time-varying *B* propagates through conducting bodies (length scale ℓ) with time constant $\boldsymbol{\tau_{\mathrm{E}}} \propto \ell^2 \frac{\mu}{\rho}$
- AC fields at frequency *f* penetrate a conductor with exponential decay with characteristic length δ (skin depth)
- Corollary: eddy currents problems are 1st order → exponential transients (no oscillations!)
- **High μ, low ρ** → long time constant, small skin depth → **increased shielding**

Magnetic field diffusion in a homogeneous, isotropic medium:

$$\begin{cases} \nabla \times \boldsymbol{E} = -\frac{\partial \boldsymbol{B}}{\partial t}, \nabla \times \boldsymbol{B} = \mu \boldsymbol{J}, \nabla \cdot \boldsymbol{B} = 0 \\ \text{Ohm's law:} \quad \boldsymbol{E} = \rho \boldsymbol{J} \end{cases} \Rightarrow$$

$$\nabla^2 \boldsymbol{B} = \frac{\mu}{\rho} \frac{\partial \boldsymbol{B}}{\partial t}$$

Non-linear medium → differential permeability

$$\nabla^2 H = \frac{1}{\rho} \frac{\partial}{\partial t} (\mu(H) H) = \frac{1}{\rho} \frac{\partial}{\partial t} B\big(H(t)\big) = \frac{1}{\rho} \frac{dB}{dH} \frac{\partial H}{\partial t}$$

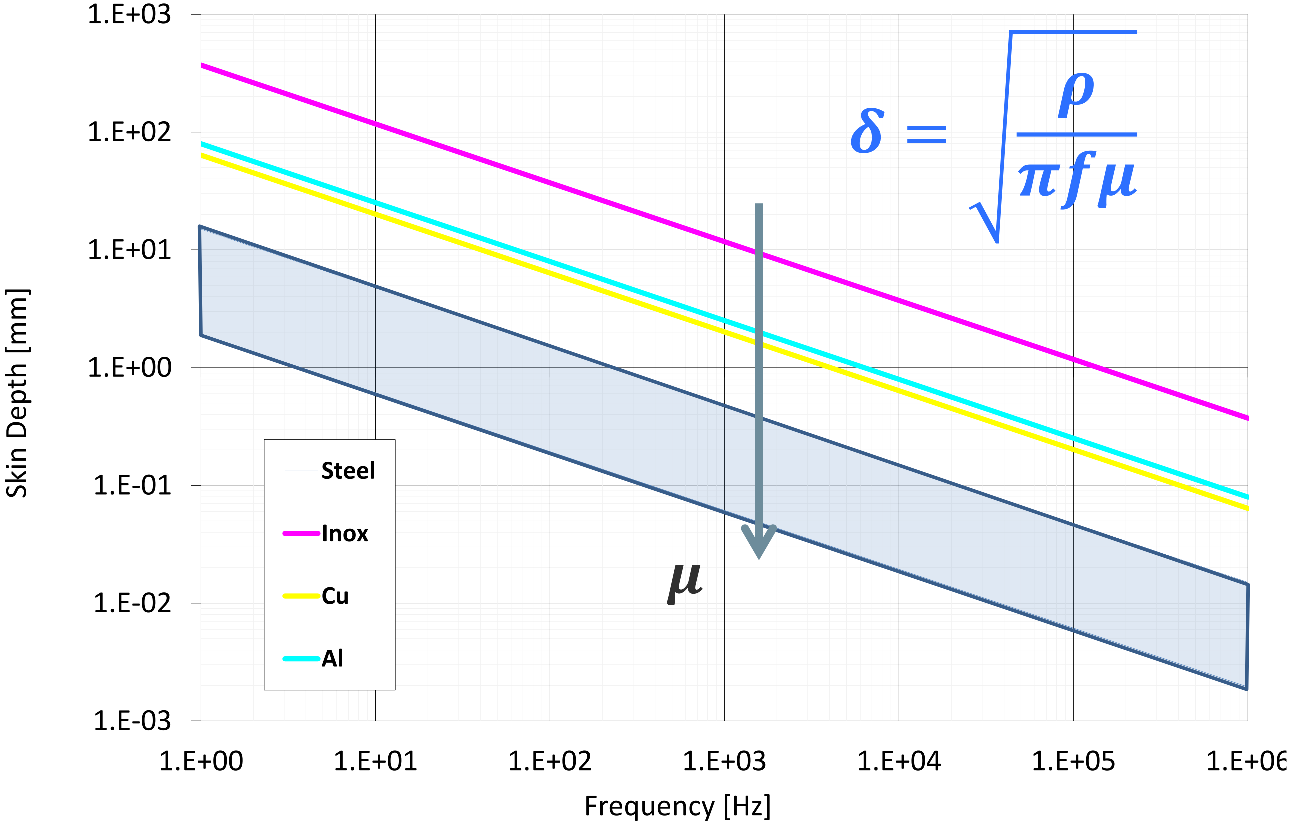

$$\boldsymbol{\delta} = \sqrt{\frac{\boldsymbol{\rho}}{\boldsymbol{\pi f \mu}}}$$

Eddy currents in a slab (out-of-plane *B*)

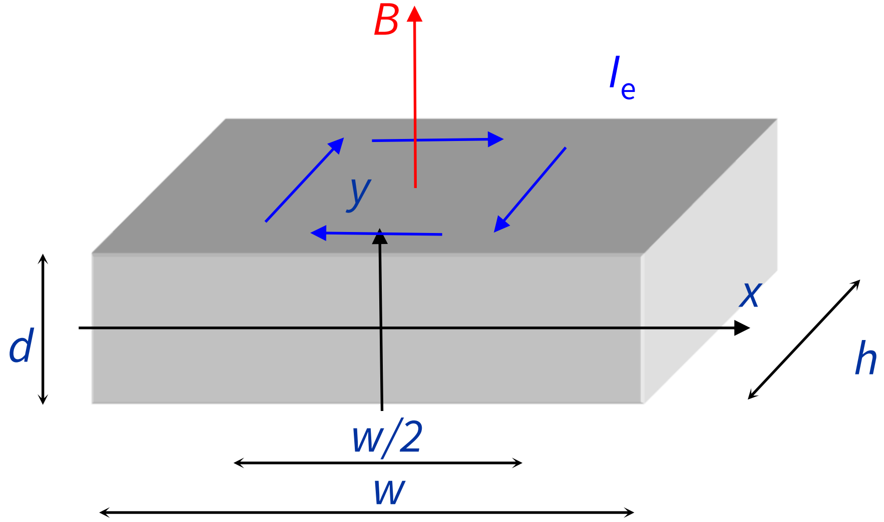

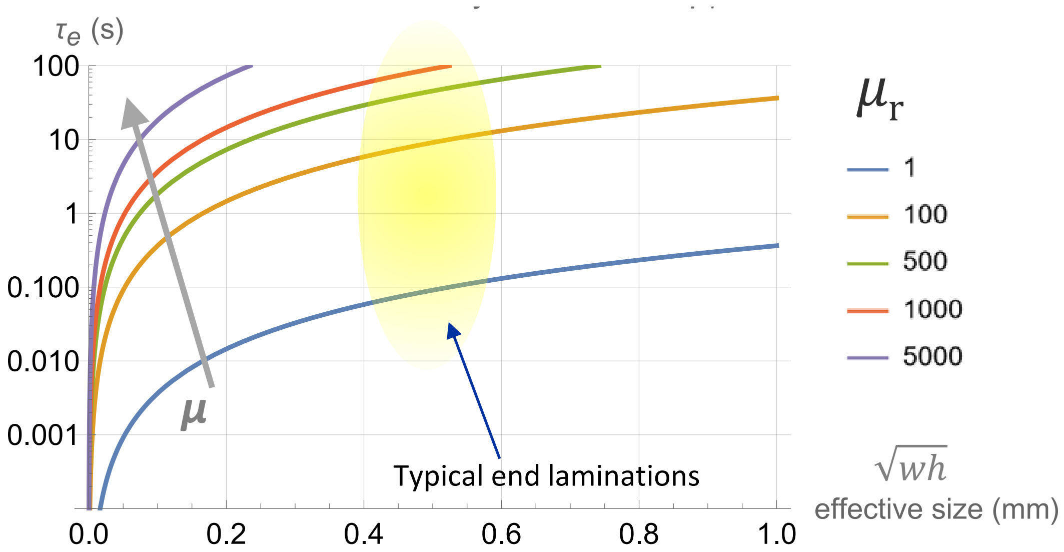

Typical end laminations

Assume:

- Negligible skin depth (=low frequency=full penetration)
- Lumped eddy currents
- Self magnetic field << external *B* (≠ self-consistent case)

- Flux linked area: $A_e = \frac{1}{2} wh$
- Eddy resistance: $R_e = 4\rho \frac{w+h}{wh}$
- Eddy current: $V_{loop} = \dot{B} A_e,\ \ I_e = \frac{V_{loop}}{R_e} = \frac{1}{16}\frac{w^2h^2}{w+h}\frac{\dot{B}}{\rho}$
- Self magnetic field: $B_e = \frac{4}{\pi}\frac{w+h}{wh}\mu I_e = \frac{1}{4\pi}\frac{\mu}{\rho} wh\dot{B}$
- Self magnetic flux: $\Phi_e = B_e A_e = \frac{2}{\pi}\mu(w+h) I_e$
- Self-inductance: $L_e = \frac{\Phi_e}{I_e} = \frac{2}{\pi}\mu(w+h)$
- Decay time: $\tau_e = \frac{L_e}{R_e} = \frac{1}{2\pi}\frac{\mu}{\rho} wh = \frac{B_e}{\dot{B}}$

Eddy currents in thin laminations (in-plane *B*)

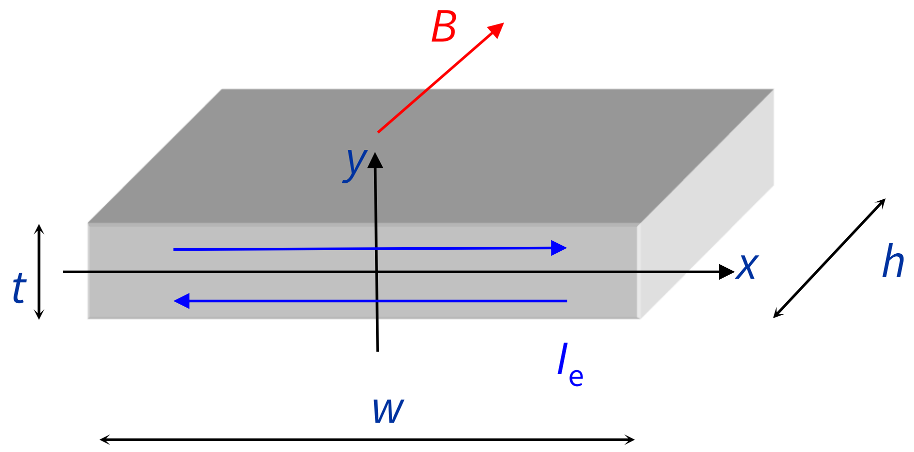

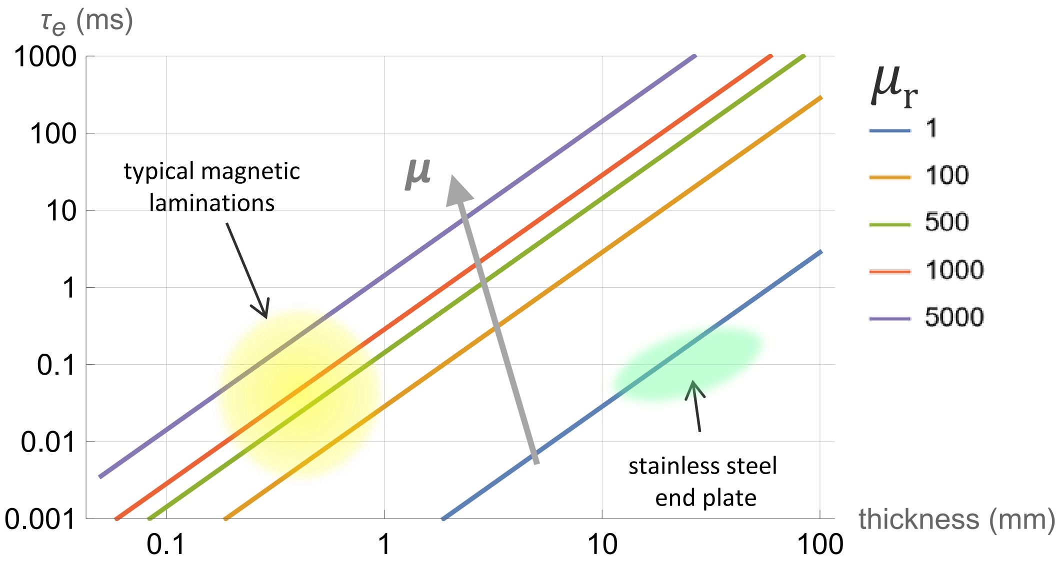

- Flux linked area: $A_e = \frac{t}{2} w$
- Eddy resistance: $R_e = \frac{2\rho}{t/2}\frac{w}{h}$
- Eddy current: $V_{loop} = \dot{B} A_e,\ I_e = \frac{V_{loop}}{R_e} = \frac{1}{8}\frac{t^2 h}{\rho}\dot{B}$
- Eddy magnetic field: $B_e = \frac{\mu I_e}{h} = \frac{1}{8}\frac{\mu}{\rho} t^2 \dot{B}$
- Eddy magnetic flux: $\Phi_e = B_e A_e = \frac{1}{2}\mu\frac{tw}{h} I_e$
- Self-inductance: $L_e = \frac{\Phi_e}{I_e} = \frac{1}{2}\mu\frac{tw}{h}$
- Decay time: $\tau_e = \frac{L_e}{R_e} = \frac{1}{8}\frac{\mu}{\rho}t^2 = \frac{B_e}{\dot{B}}$

Ferromagnetic metals

Stefano Sgobba
this CAS

- Magnetically soft metals: Fe, Ni, Co and vast majority of their alloys
  Main contribution: electron spin from incomplete inner (3d) shells (exception: austenitic stainless steels)
- Ferromagnetic domains ~10 µm, spontaneously magnetized up to saturation, randomly distributed in the virgin state → macroscopic (average) ***M***=0
- Shape, orientation and distribution of the domains seek to minimize energy ***M·H***
- Major magnetization processes:
  - Domain wall movement inside a grain: irreversible, due to wall pinning by inclusions/micro-stresses
    jerky movement → Barkhausen noise
  - Rotation of the magnetization: reversible, depends on alignment of ***H*** to crystallographic axes

Differential domain enlargement

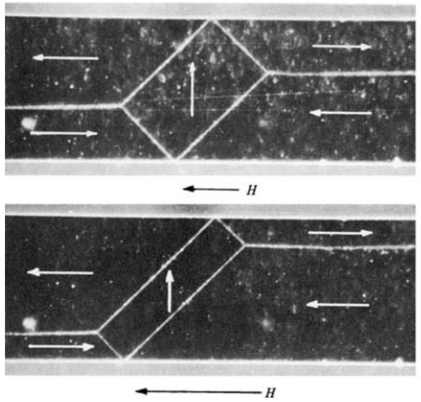

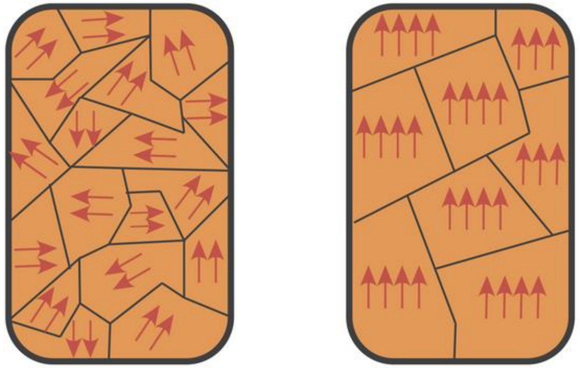

Magnetization rotation

Cullity, *Introduction to Magnetic Materials*, Wiley

Magnetization loop

Saturation magnetization Ms

Chemical property (no influence of microstructure)

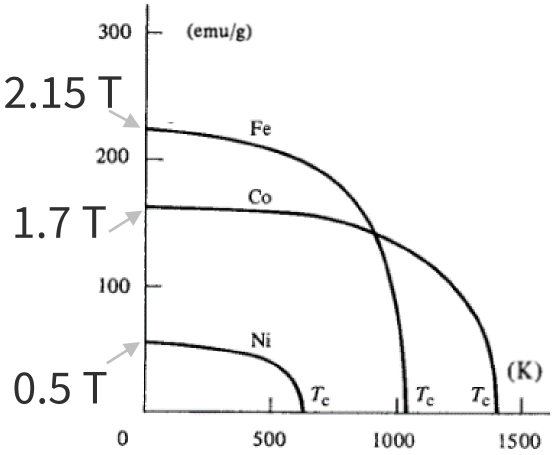

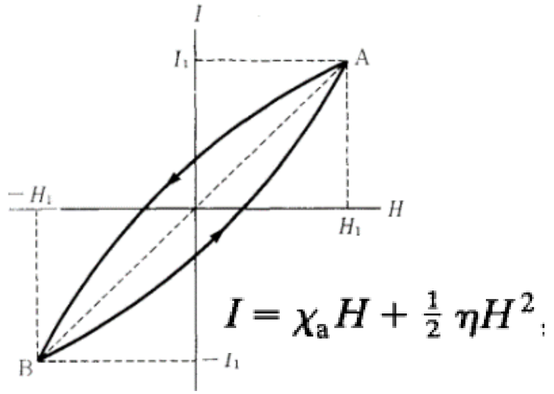

$$I = \chi_a H + \tfrac{1}{2}\eta H^2;$$

Rayleigh regime

±3 A/m: Reversible linear magnetization

χ_a ≈100~200, increases with T (Hopkinson effect)

Major hysteresis loop

reaches full saturation

shape does not depend upon how it is approached

$$M \approx M_s\left(1 - \frac{a}{H} - \frac{b}{H^2} + \cdots\right)$$

Approach to saturation

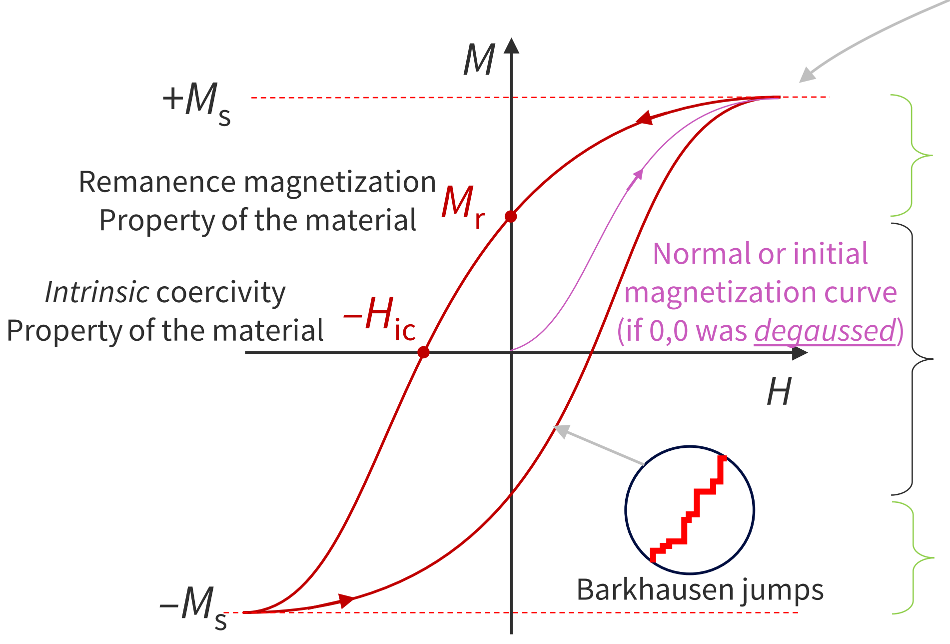

Remanence magnetization
Property of the material

Intrinsic coercivity
Property of the material

Normal or initial magnetization curve (if 0,0 was *degaussed*)

Barkhausen jumps

Reversible magnetization rotation

small Barkhausen jumps

χ depends upon on magnetic anisotropy

Irreversible domain wall movement

large Barkhausen jumps

χ strongly dependent on composition and microstructure (wall mobility)

$$M \approx \chi(H)H$$

Susceptibility χ strongly depends on microstructure
decreases with T and cold work

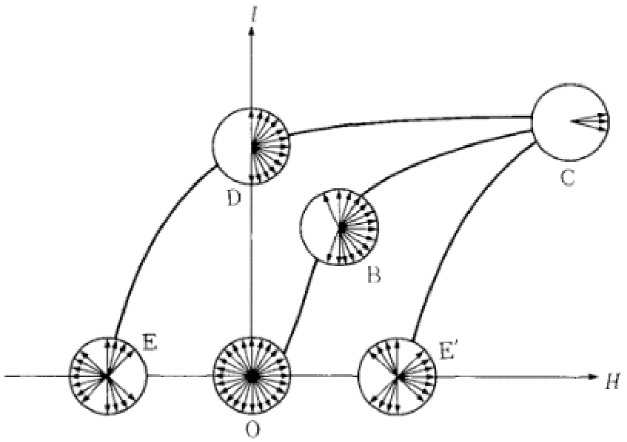

Distribution of domain magnetization
Cullity, *Introduction to Magnetic Materials*, Wiley

Magnetic induction loop

Relative permeability

$$B = \mu_0(H+M) = \mu_0\big(1+\chi(H)\big)H = \mu_0\,\mu_\mathrm{r}(H)H$$

Major (symmetric) induction hysteresis loop

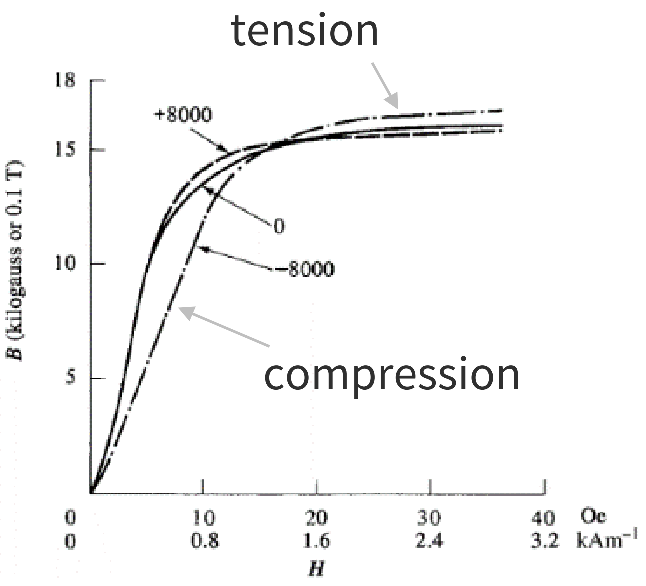

Strain dependence

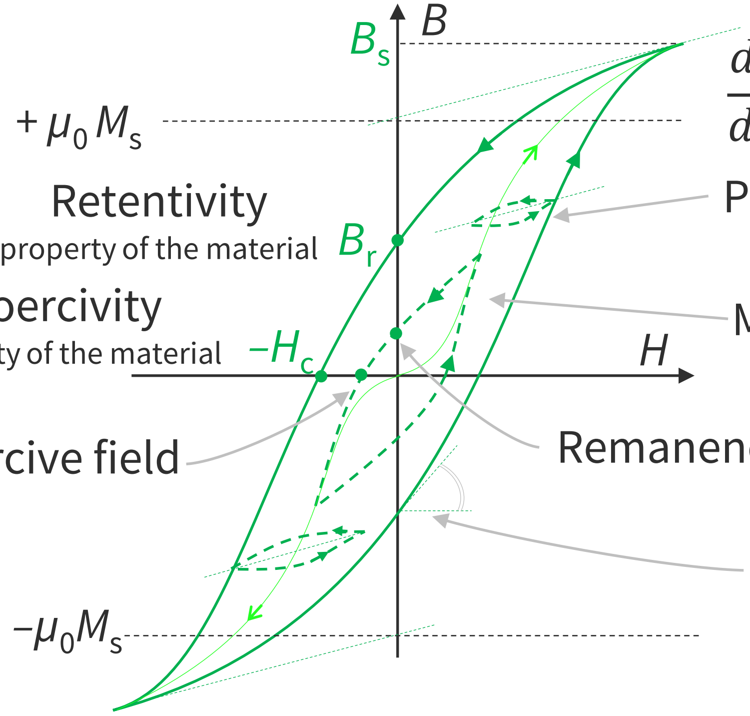

$$\frac{dB}{dH} = \mu_0$$

Retentivity
property of the material

Coercivity
Property of the material

Parasitic (asymmetric) hysteresis loop

Minor (symmetric) hysteresis loop

Coercive field

Remanence

Differential permeability

$$\frac{1}{\mu_0}\frac{dB}{dH} = \mu_r + \frac{d\mu_r}{dH}H$$

Other time-dependent effects 1/2

Magnetic after-effect (viscosity)

- Magnetization delay on top of eddy currents, equivalent to a time-dependent permeability
- Dominant mechanism in magnetic steel: irreversible diffusion of impurities (Richter) → strong T dependence
- For low-C steel:
  - — $\xi \approx 30\%$ in the initial permeability range
  - — 1~2% at high field.
- Effect does not depend upon shape / excitation rate (unlike eddy currents)

$$\Delta M = \chi_0 \Delta H \left(1 + \xi \left(1 - e^{-t/\tau_\mathrm{v}}\right)\right)$$

$$\Delta M = \xi \chi_1 \Delta H$$

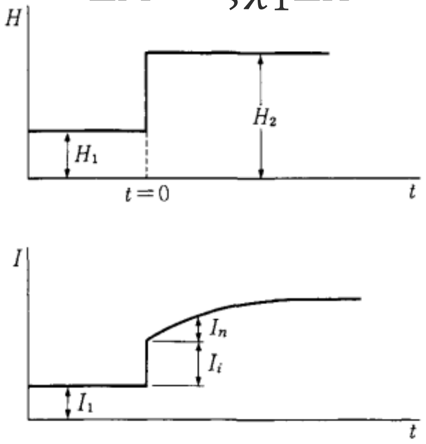

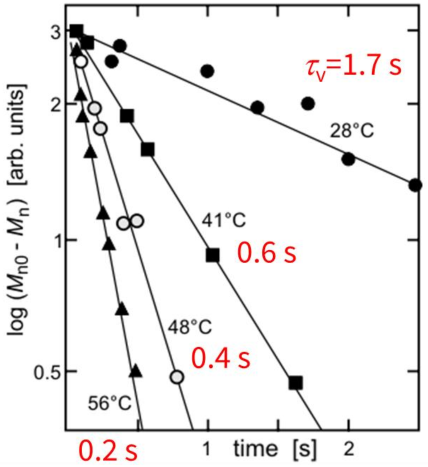

T dependence

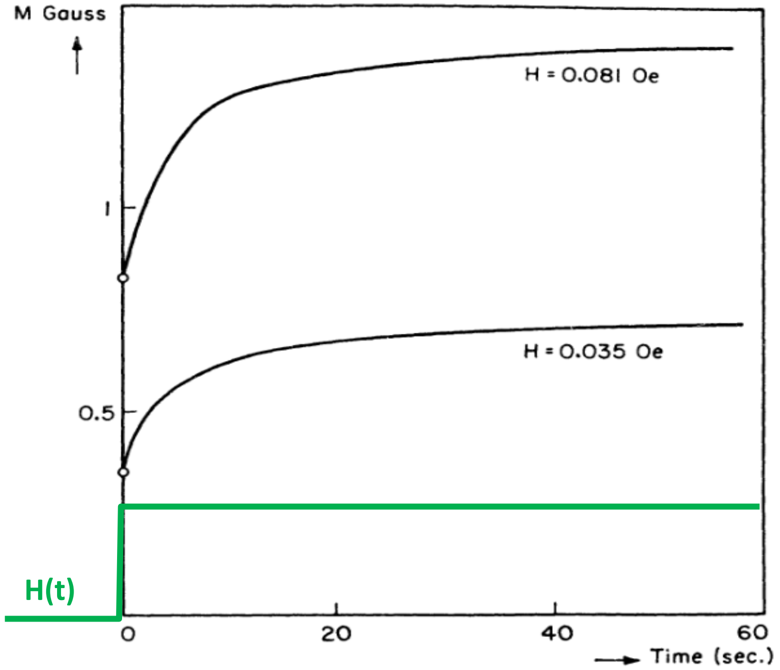

Fig. 1—Magnetic Viscosity As Measured on a Wire of Wrought Iron. Demagnetization ended at t = o. (After Ewing)

$$\Delta M \propto k_B T \log t$$

Distribution of τ → approx. logarithmic behavior at intermediate time scales

Chikazumi, Physics of Ferromagnetism, Oxford University Press, 1996

Other time-dependent effects 2/2

Accommodation

- Repetitive minor loops apparently drift toward an equilibrium loop
- Rate-independent effect, triggered by a change in applied field.
- Sometimes confused with after-effect

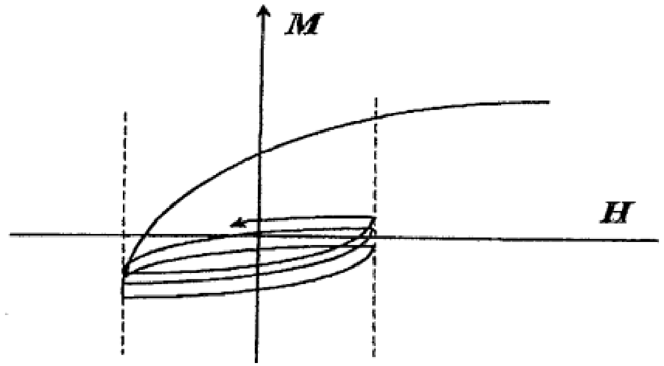

Disaccommodation

- Gradual drop of permeability after the application of field/mech, stress
- Due to thermally induced diffusion of impurities C/N
- Negligible in pure Fe
- Up to -50% in Mn-Zn ferrites over several years (electronic inductors!)

Ageing

- irreversible changes due metallurgical phenomena: precipitation, diffusion, phase transition
- Long time scale (at RT)

Mathematical modelling of saturation and hysteresis

Semi-empirical models

- Typically apply to initial magnetization curve
- **Langevin**: $\mathcal{L}(s) = \dfrac{1}{\tanh s} - s, \quad s = \dfrac{\langle m \rangle \mu_0}{k_B T} H$
  classical model of paramagnetism
- **Wlodarski**: $M(H) = M_s \mathcal{L}\left(\dfrac{H}{a}\right) + (1 - M_s) \tanh \dfrac{H}{a} \mathcal{L}\left(\dfrac{H}{b}\right)$
- Home-made best-fit: (0.5% RMS error)

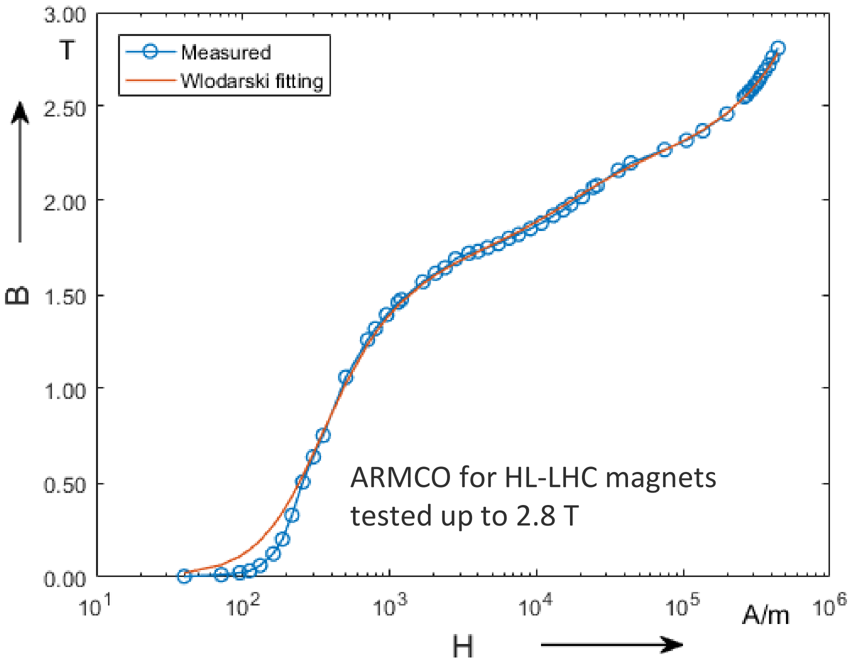

ARMCO for HL-LHC magnets tested up to 2.8 T

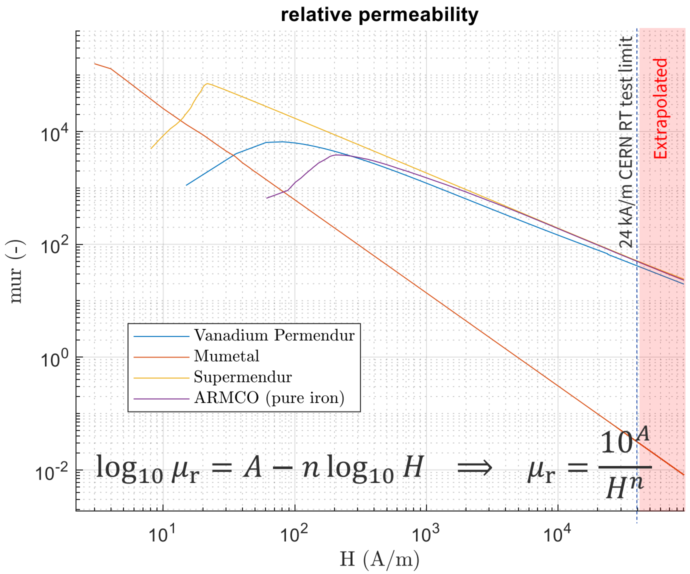

$$\log_{10} \mu_r = A - n \log_{10} H \quad \Longrightarrow \quad \mu_r = \frac{10^A}{H^n}$$

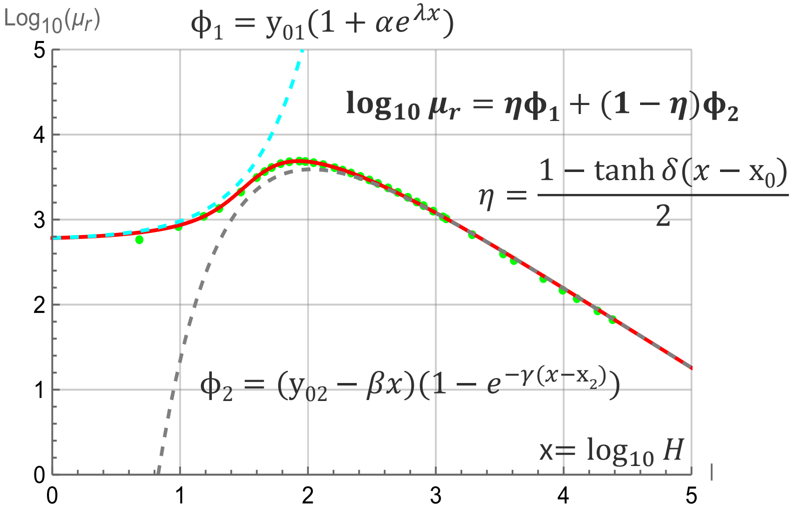

$$\phi_1 = y_{01}(1 + \alpha e^{\lambda x})$$

$$\log_{10} \boldsymbol{\mu_r} = \boldsymbol{\eta \phi_1} + (\mathbf{1} - \boldsymbol{\eta})\boldsymbol{\phi_2}$$

$$\eta = \frac{1 - \tanh \delta (x - x_0)}{2}$$

$$\phi_2 = (y_{02} - \beta x)(1 - e^{-\gamma(x - x_2)})$$

$$x = \log_{10} H$$

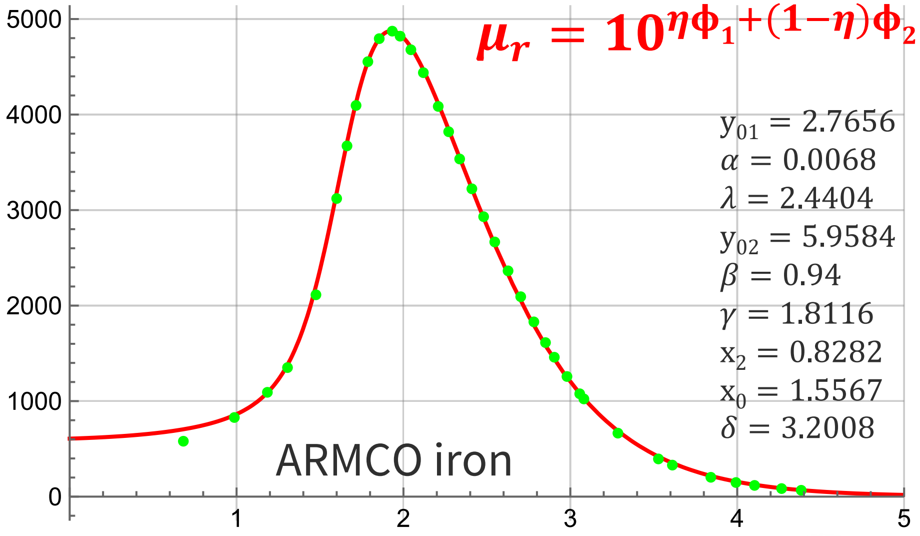

$$\boldsymbol{\mu_r = 10^{\eta\phi_1 + (1-\eta)\phi_2}}$$

$y_{01} = 2.7656$
$\alpha = 0.0068$
$\lambda = 2.4404$
$y_{02} = 5.9584$
$\beta = 0.94$
$\gamma = 1.8116$
$x_2 = 0.8282$
$x_0 = 1.5567$
$\delta = 3.2008$

ARMCO iron

Differential models

Jiles-Atherton

- Vast family of physics-based, ODE models
- Decomposition of M in anhysteretic, reversible and irreversible components with physically-derived parameters
- Notoriously unable to follow minor loops
- Large number of ad-hoc variations published

Parameter	Property
α	Linked to domain interaction
a	Linked to the shape of M_{an}
k	Linked to hysteresis losses
c	Reversibility coefficient
M_s	Saturation magnetization

$$\frac{\mathrm{d}M}{\mathrm{d}H} = \frac{(1-c)(\mathrm{d}M_{\mathrm{irr}}/\mathrm{d}H_{\mathrm{e}}) + c(\mathrm{d}M_{\mathrm{an}}/\mathrm{d}H_{\mathrm{e}})}{1-\alpha(1-c)(\mathrm{d}M_{\mathrm{irr}}/\mathrm{d}H_{\mathrm{e}}) - \alpha c(\mathrm{d}M_{\mathrm{an}}/\mathrm{d}H_{\mathrm{e}})}.$$

$$M_{\mathrm{an}} = M_{\mathrm{s}}\left[\coth\left(\frac{H_{\mathrm{e}}}{a}\right) - \frac{a}{H_{\mathrm{e}}}\right] \qquad \frac{\mathrm{d}M_{\mathrm{irr}}}{\mathrm{d}H_{\mathrm{e}}} = \frac{M_{\mathrm{an}} - M_{\mathrm{irr}}}{k\delta}$$

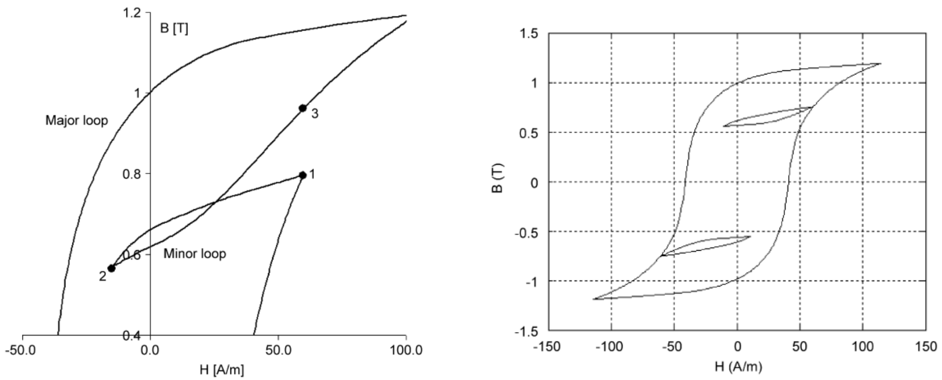

Benaboua, J. Magnetism and Magn. Mat. 320 (2008)

Flatley

- Lesser-known phenomenological model
- μ_{diff} interpolation based on distance from opposite branch
- Easy to implement
- Also struggles to get minor loops right …

$$\frac{dB}{dH} = B_1(q_0 - (1-q_0)f^p)$$

$$B_1 = \frac{2}{\pi}kB_s\cos^2\theta$$

$$\theta = \frac{\pi}{2}\frac{B}{B_s} \qquad H_L = \frac{\tan\theta}{k} - H_c$$

$$f = \begin{cases} \frac{dH}{dt}>0 & \frac{H-H_L}{2H_c} \\ \frac{dH}{dt}<0 & 1-\frac{H-H_L}{2H_c} \end{cases}$$

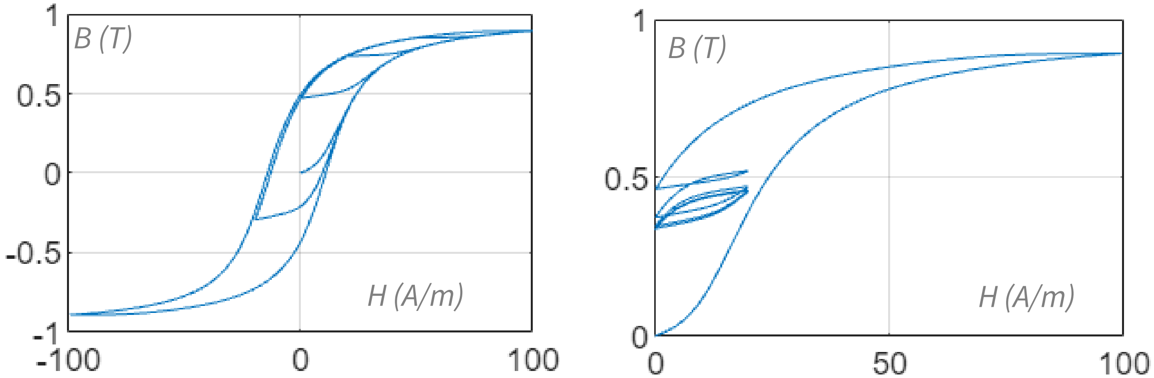

Flatley, NASA N95-27801 320 (1995)

Preisach models

- Popular phenomenological model class
- response integrated over distribution of abstract elementary hysteretic units
- Challenge: identification of model parameters
- Some distinctive properties:

H De Gersem
CAS Greece 2018

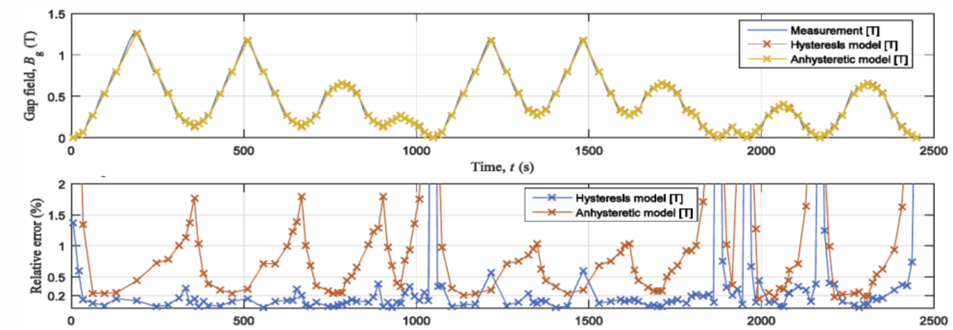

Best result to date at CERN: ~2% error on PS U17 cycles
(V. Pricop, Hysteresis Effects In Particle Accelerator Magnets, PhD Thesis,2016)

Non-locality

- system state ≠ (B,H), is determined by succession of local extrema
- observed in ferromagnets
- → simple ODEs cannot work !

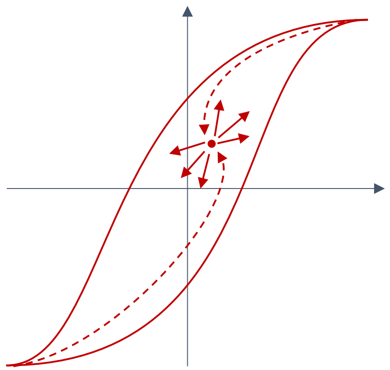

Congruency

- shape of minor loops depends only upon the extrema of input
- Not always physical

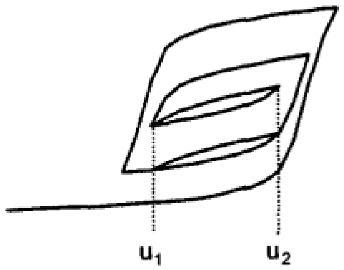

Wiping-out

- Any local extremum at *B* wipes out memory of previous extrema < |*B*|
- Not always physical (holds for saturation in ferromagnets)

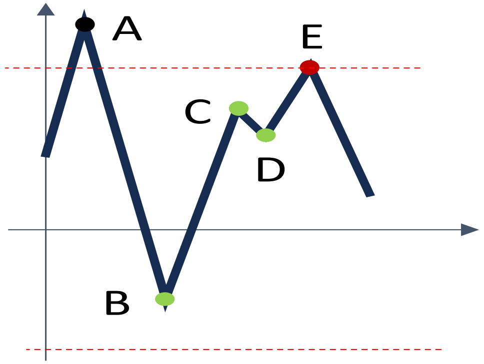

Preisach-Recurrent Neural Network Model

- Vast literature of ANN on their own/in combination addressing rate-independent hysteresis
- Example: model where the Preisach density function is represented by a Recurring Neural Network

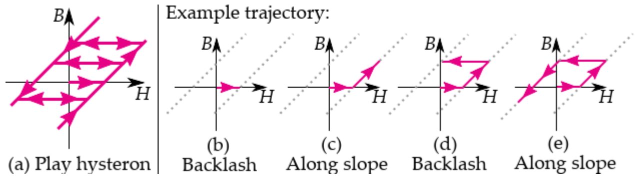

$$\hat{y}(t) = \int_0^{+\infty} g(r, P[u(t)])\,\mathrm{d}r = \sum_{j=1}^{n} \phi_j P_j[u](t)$$

discretized Preisach model

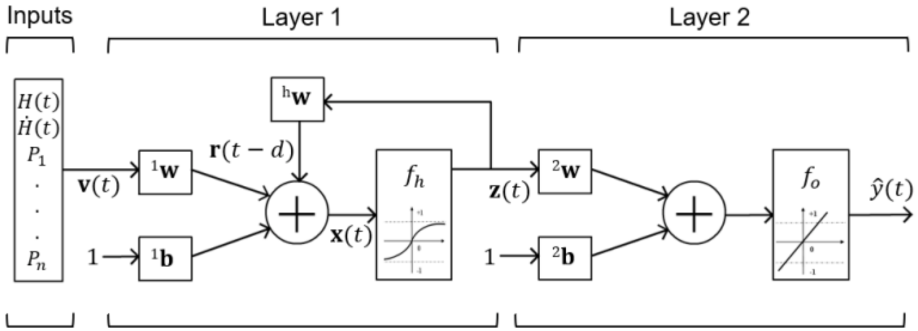

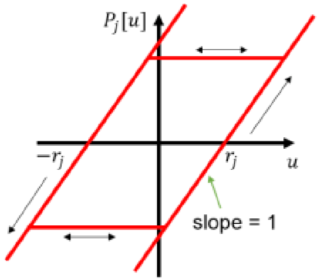

hysteron = Play operator

$$\mathbf{z}(t) = f_h[{}^1\mathbf{w}(\mathbf{v}(t) + {}^1\mathbf{b}) + {}^h\mathbf{w}(\mathbf{z}(t-d))]$$

$$f_h(x) = \frac{2}{1+e^{-2x}} - 1 \qquad \hat{y}(t) = f_o[{}^2\mathbf{w}(\mathbf{z}(t) + {}^2\mathbf{b})]$$

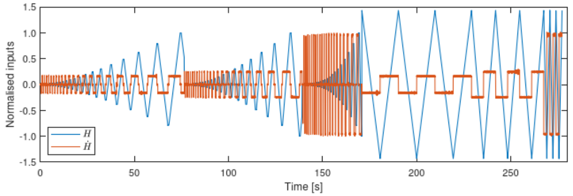

Figure 5. Magnetic field data and its derivative used for training, validation and testing the model.

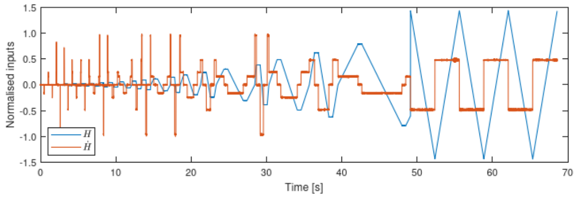

Figure 6. Magnetic field data and its derivative used for evaluating the model.

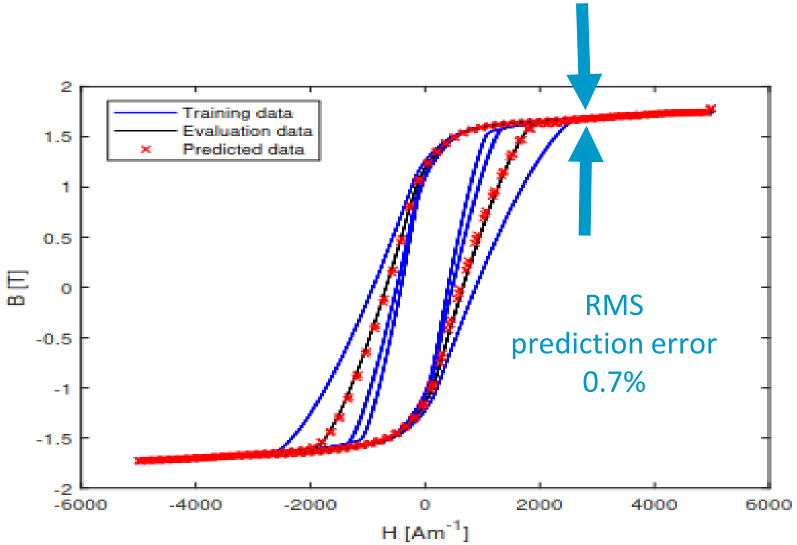

RMS prediction error 0.7%

(C Grech, M Pentella, “Dynamic Ferromagnetic Hysteresis Modelling using a Preisach-Recurrent Neural Network Model”, Materials 2020, 13(11), 2561

Measurement of material properties

Magnetic material measurements methods

- Goal: specific values (Hc,χ,M) or curves (B(H), μ_r(H))
- Few instruments commercially available
- IEC-standard measurements (e.g. rings) from electrical metrology institutes
- Major method classes:
  - — **Force-based**
  - — **Fluxmetric**: generator ($\nabla\Phi$) or transformer ($\partial\Phi/\partial t$) principle
  - — **Flux distortion**
- Choice depends upon sample type, size and shape; range of permeability, temperature, dB/dt …

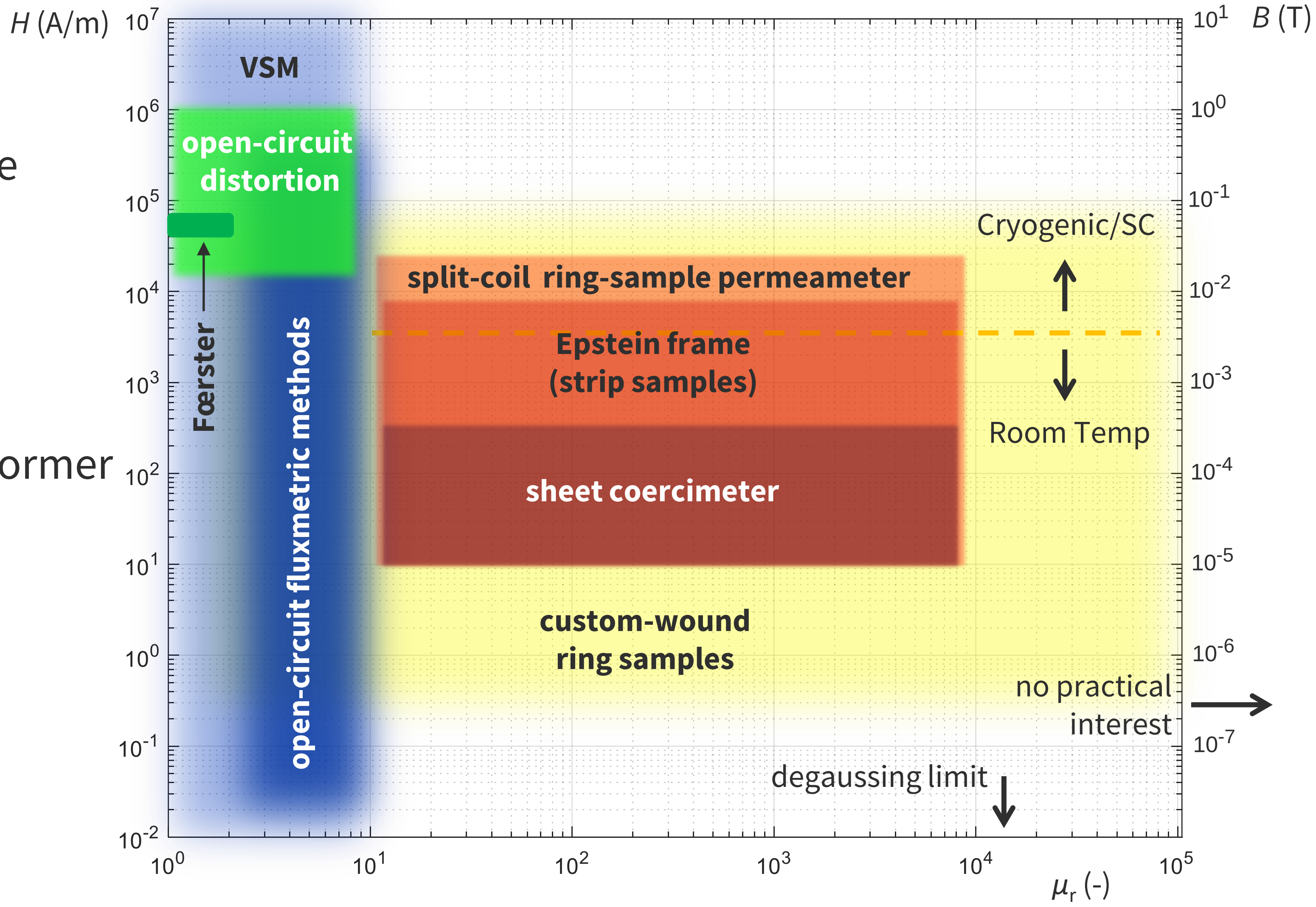

Mariano Pentella, Characterization of magnetic materials at extreme ranges of field, temperature, and permeability, PhD Thesis, Politecnico di Torino, 2022

Demagnetization factors

- sample magnetized by external field $H_{\text{ext}} \rightarrow$ surface pole density $-\nabla \cdot \boldsymbol{M} \rightarrow$ demagnetizing field H_{d}
- in general: non-uniform, non-parallel $\boldsymbol{B}, \boldsymbol{H}$ (nontrivial correction = shearing transformation)
- only exceptions: ellipsoids; prismatic bars and tori when aspect ratio $\rightarrow \infty$

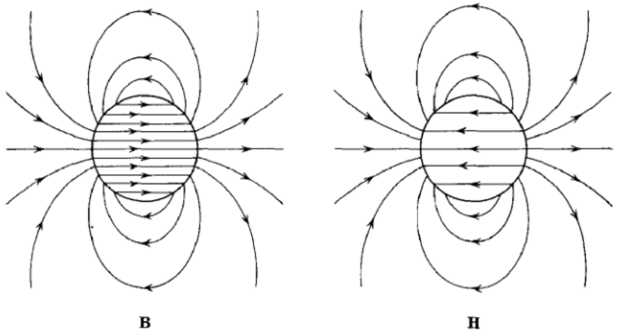

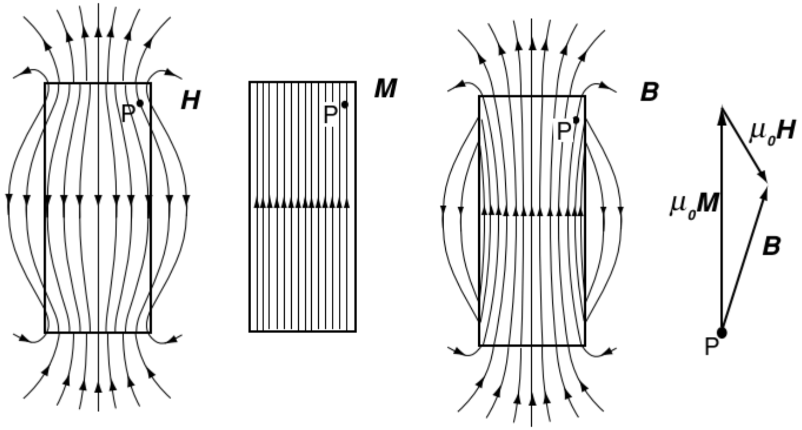

$$\boldsymbol{H} = \boldsymbol{H}_{\text{ext}} + \boldsymbol{H}_{\text{d}} \qquad \boldsymbol{H}_{\text{d}} = -N\boldsymbol{M}$$

$$\boldsymbol{B} = \mu_0(\boldsymbol{H} + \boldsymbol{M}) = \mu_0(\boldsymbol{H}_{\text{ext}} + (1 - N)\boldsymbol{M})$$

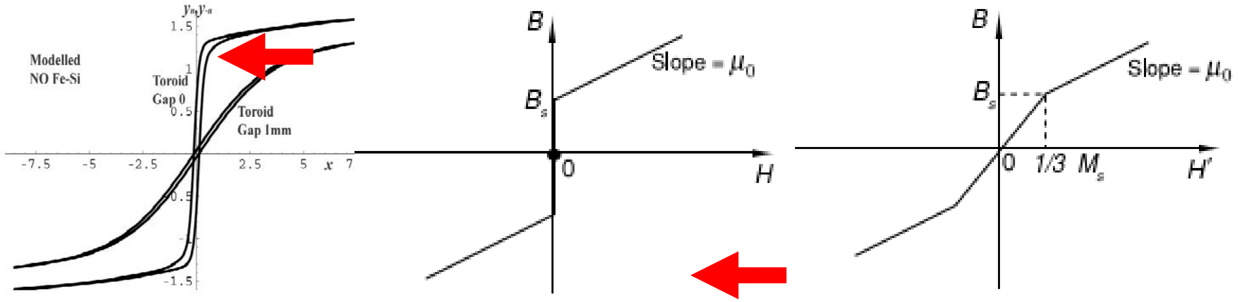

Open-circuit measurements

magnetometric

e.g. ring-sample permeameter

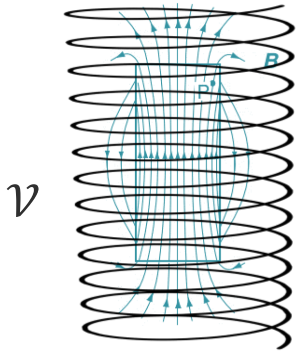

$$N_\mathrm{m} = -\frac{\iiint_\mathcal{V} \boldsymbol{H}_\mathrm{d}\, d\mathcal{V}}{\iiint_\mathcal{V} \boldsymbol{M}\, d\mathcal{V}}$$

N_m <= 5% for $\gamma>10$
$dN_\mathrm{m}/d\mu_r < 0$

fluxmetric

e.g. cylindric samples

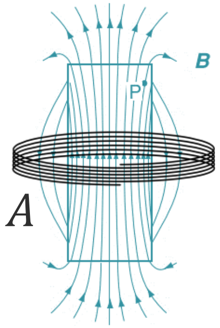

$$N_\mathrm{f} = -\frac{\iint_\mathcal{A} \boldsymbol{H}_\mathrm{d}\, d\mathcal{A}}{\iint_\mathcal{A} \boldsymbol{M}\, d\mathcal{A}}$$

N_f <= 1% for $\mu_r < 10$, $\gamma>10$
dN_f<$d\mu_r > 0$

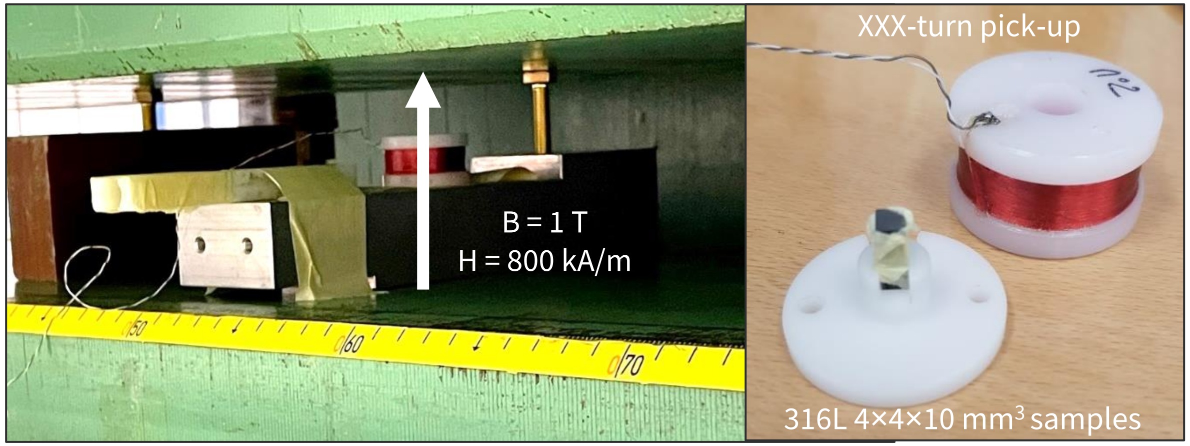

Example:
magnetometric measurement

- smallest sample capability
- 100 ppm resolution
- wide test field range when immersed in a background field (for μ_0)
- excitation coils not possible

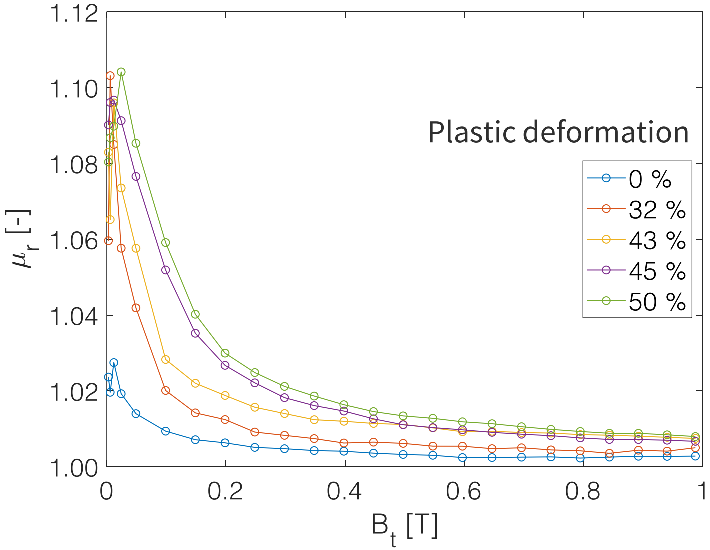

D.X. Chen, *Demagnetizing factors for cylinders*, 1991

Courtesy Mariano Pentella, CERN

Vibrating Sample Magnetometer

- Fluxmetric method widely accepted as reference
- Precision ~10 ppm for background B = 0 ~ 13 T and T =1.9 ~ 300 K
- Best for low-permeability samples (negligible demagnetization)
- Mechanical constraints → very small samples (careful preparation !)

$$\begin{cases} \Phi(t) = k\mu_0(1-N)M\mathcal{V}A_c y(t) \\ \Phi_{\text{ref}}(t) = k\mu_0(1-N)M_{\text{ref}}\mathcal{V}A_c y(t) \end{cases}$$

$$M = M_{\text{ref}}\frac{V_{\text{c}}}{V_{\text{ref}}}$$

$$\begin{cases} V_{\text{c}} = \frac{\partial \Phi}{\partial t} = k\mu_0(1-N)M\mathcal{V}A_c\frac{\partial y}{\partial t} \\ V_{\text{ref}} = \frac{\partial \Phi_{\text{ref}}}{\partial t} = k\mu_0(1-N)M_{\text{ref}}\mathcal{V}A_c\frac{\partial y}{\partial t} \end{cases}$$

$$\mu_r - 1 = \mu_0\frac{M}{B}$$

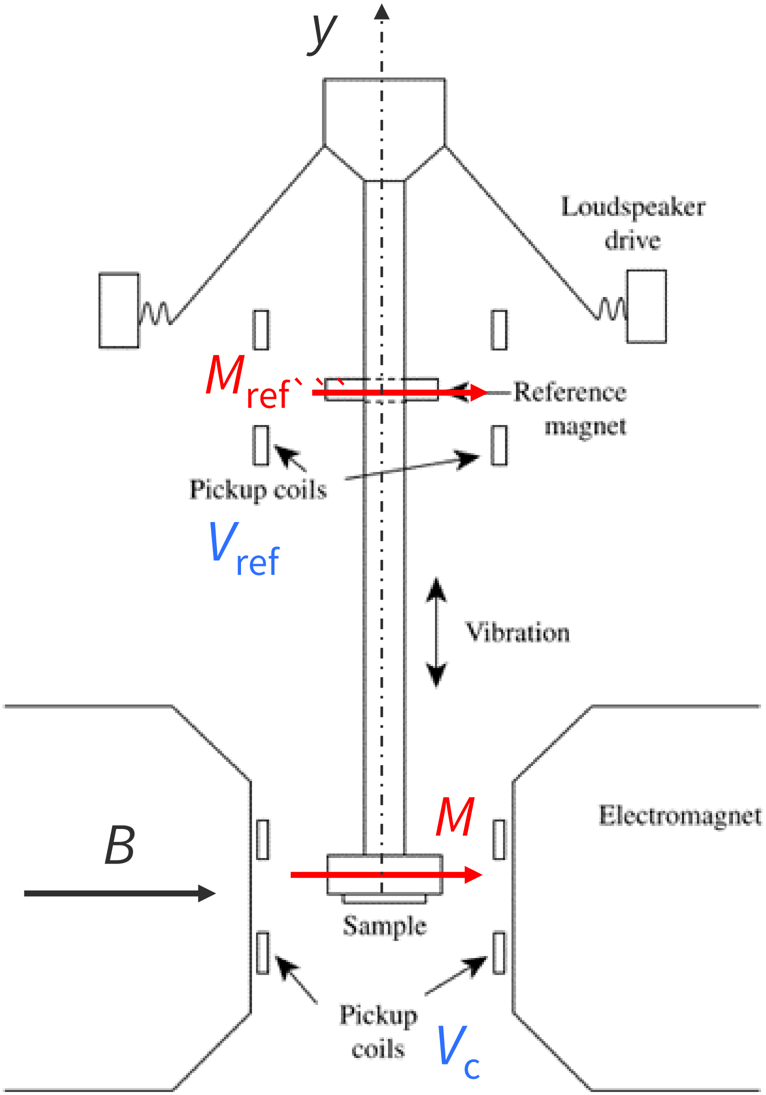

Courtesy Mariano Pentella, CERN

Ring-sample measurements

- Reference fluxmetric method for isotropic-material samples
- Limitations: too small samples; laborious setup; low current control, thermal dissipation; eddy currents

$$H(r) = H_0 \frac{r_0}{r}, B(r) \approx B_0 \frac{r_0}{r} \qquad r_0 = \frac{r_{\mathrm{out}} - r_{\mathrm{in}}}{\ln(r_2/r_1)}$$

$$\bar{H}(t) = \frac{1}{r_{\mathrm{out}} - r_{\mathrm{in}}} \int_{r_{\mathrm{in}}}^{r_{\mathrm{out}}} \frac{N_e I(t)}{2\pi r} dr = \frac{N_e I(t)}{2\pi r_0}$$

excitation turns

$$\int_0^t V(\tau) d\tau$$

$$\bar{B}(t) = \frac{1}{A_s}\left(\frac{\Phi(t)}{N_m} - \mu_0 \bar{H} A_0\right)$$

$$\mu_r = \frac{1}{\mu_0}\frac{\bar{B}}{\bar{H}}$$

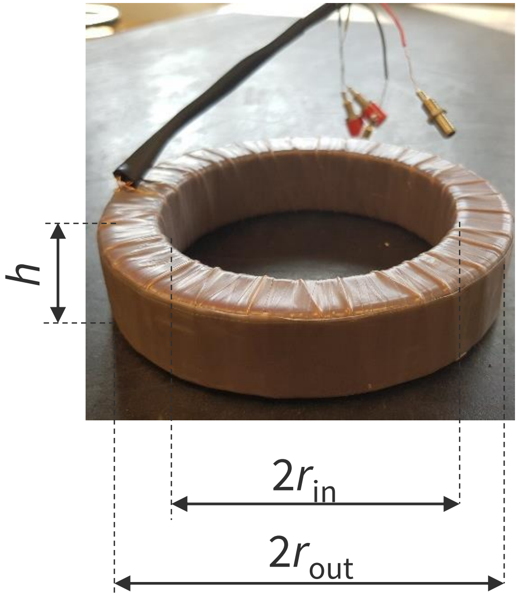

calibration of air cross-section A_0 at *saturation*

$$\frac{dB}{dH} = \mu_0 = \frac{1}{(A_s + A_0)N_m}\frac{d\Phi}{dH}$$

sample cross-section

measurement turns

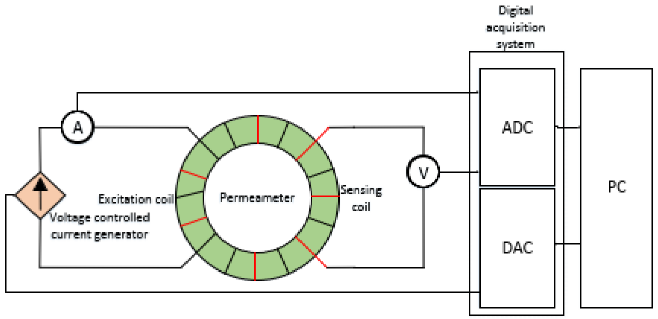

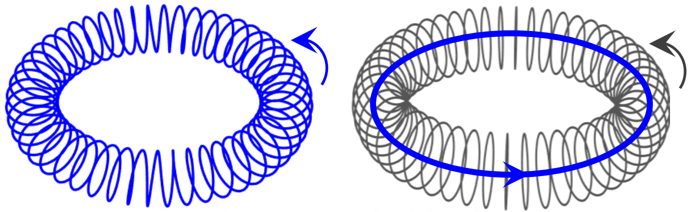

NB: there is one hidden loop !

Ring sample test procedures

Dynamic measurement

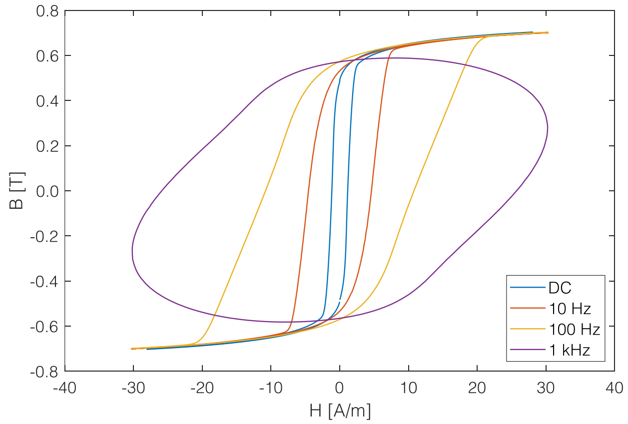

eddy currents in solid sample !

Stepwise major loop

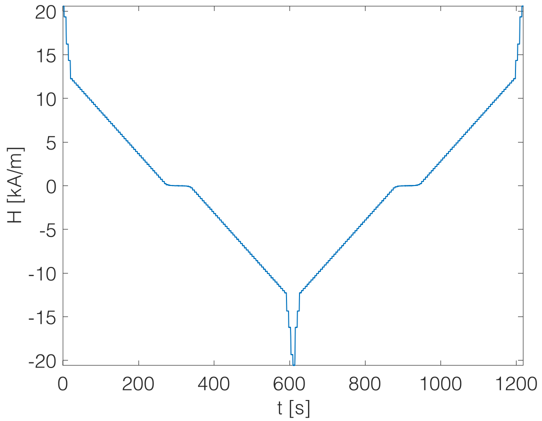

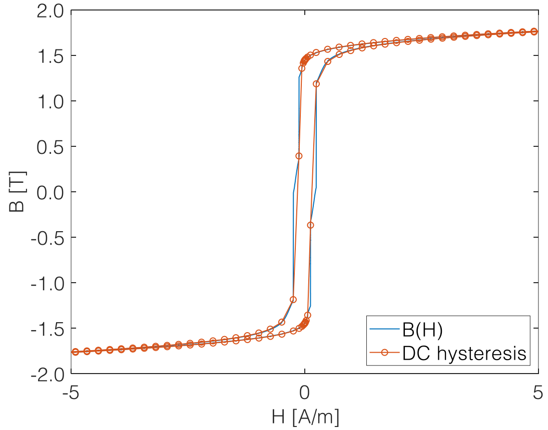

Stepwise initial magnetization curve

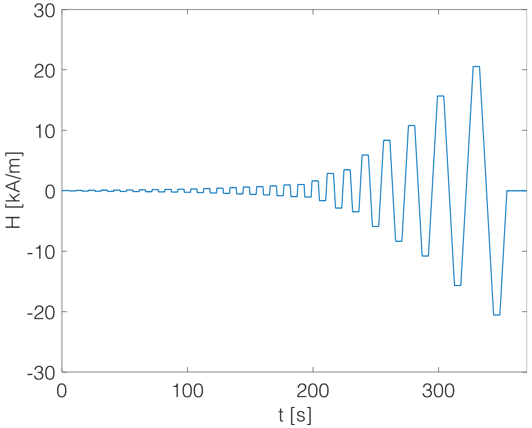

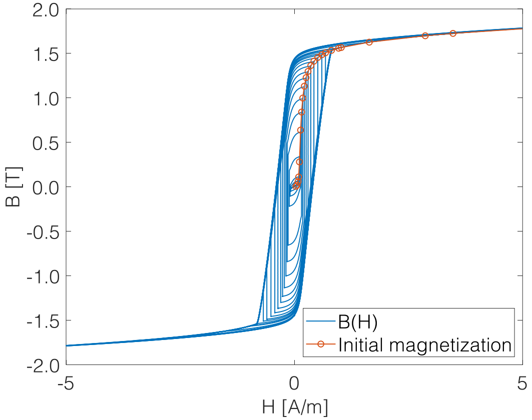

Anhysteretic magnetization curve

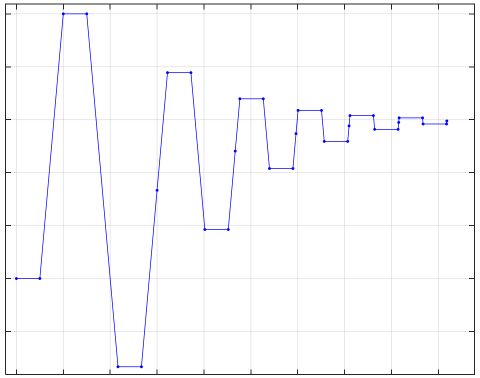

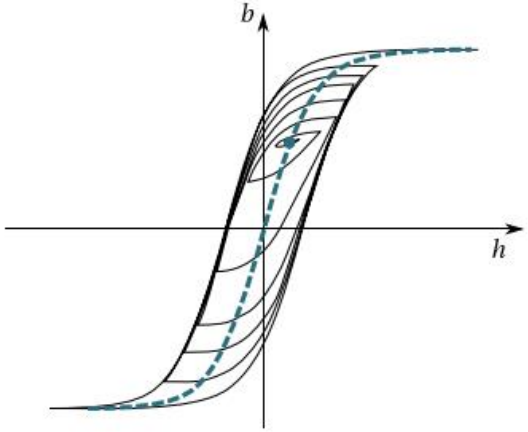

≈ “symmetry axis” of major loop

CERN ring-sample permeameters

Split-coil permeameter

- 2×90-turn excitation + 1×90-turn measurement coils
- 24 kA/m DC (60°C), 30 min for 1st curve
- 0.1% uncertainty
- ~10 Hz with laminated samples
- High μ_r accuracy 10%: limited by low-current control
- Low μ_r accuracy 5%: limited by low output S/N

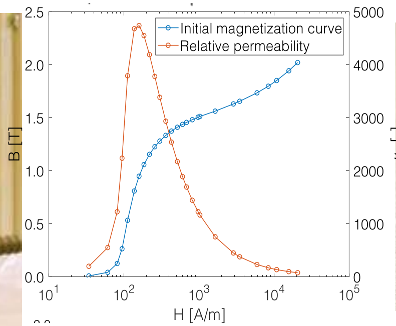

- originally developed by K. Henrichsen (1965)
- recently upgraded with new 24-bit DAQ and software
- IEC 60404 standard test specimen:
  $\varnothing_{out}$=114 mm, $\varnothing_{in}$=105 mm, h=15 mm

Cryogenic permeameter

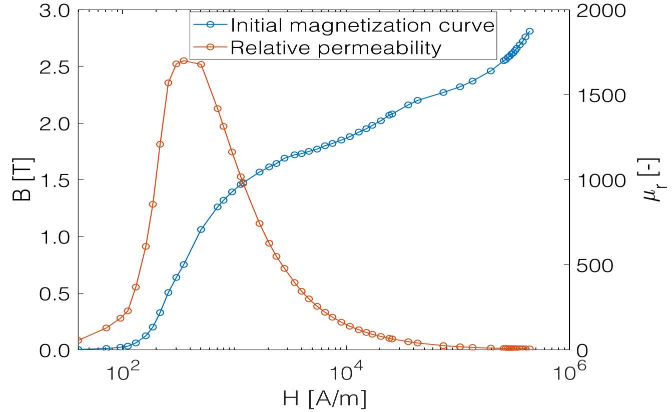

- 77 K (LN) and 4.2 K (LHe) poured on the specimen
- Holder made of 3D printed bluestone (10^{-4}/K thermal contraction)
- 3200-turn Furukawa 0.5 mm NbTi cable, 2830 × 10 µm filaments, Ic=666 A, Tc=9 K
- **300 kA/m → 2.8 T** in ARMCO @ 1.9 K

Rotating sample magnetometer (3D Helmholtz coils)

- Widely used measurement system for permanent magnets **based on the fluxmetric method**
- Recently **fully automatized** for large series measurements. 5 min = 30 reps per PM block.
- Giant coil area ~100 m^2 determines high sensitivity
- Accuracy: **||M||** 0.1 % **,** vector direction 3 mrad. No dynamic measurement (hysteresis loop)

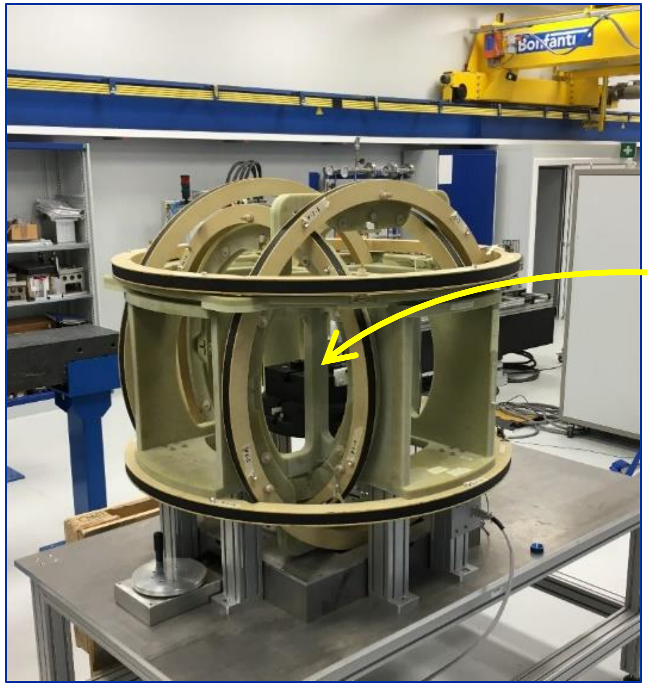

6× ~2000-turn, ∅1 m

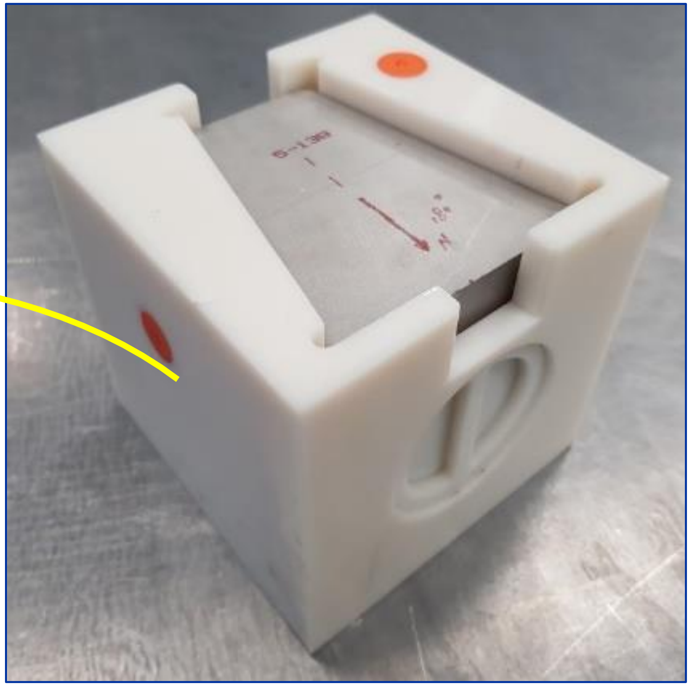

Credit: Olaf Dunkel, Mariano Pentella, CERN

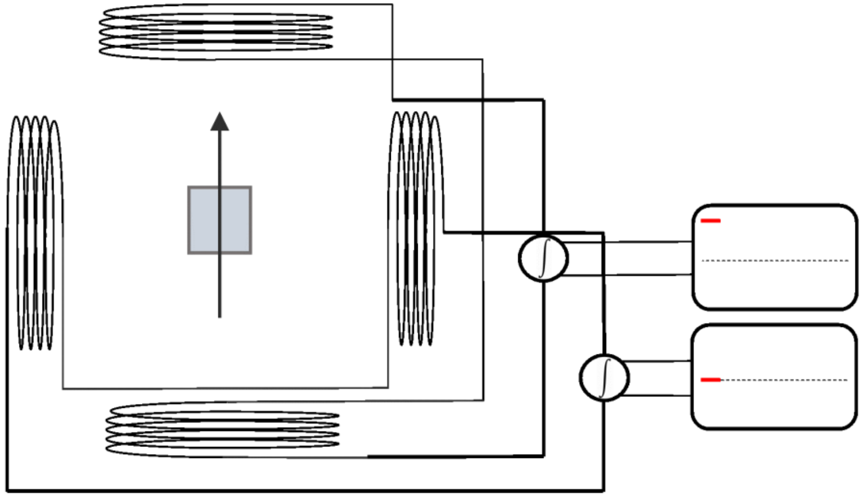

$$\Delta\Phi_j = 2k\mu_0 M_j$$

Open-circuit, low-permeability measurement

- Flux distortion method for very low μ_r (→ high field) @ room temperature
- Analytical treatment possible for simple geometries; arbitrary samples need FE simulations
- Typical accuracy 100 ppm, repeatability 10 ppm
  (best result: $\mu_r = 1.00085$ of a W alloy sample, validated by vibrating sample)

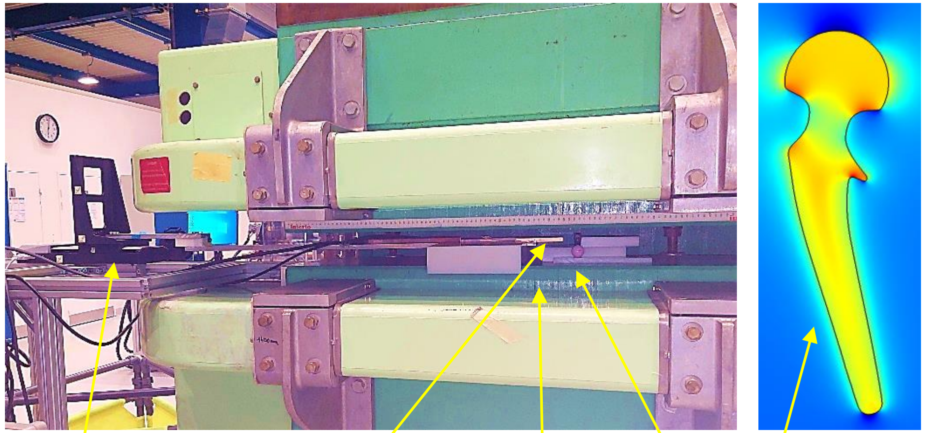

Translation stage

Moving NMR probe (5 ppm accuracy)

Sample: Ti hip prosthesis

1 T dipole, high uniformity background field

Credit: M. Pentella

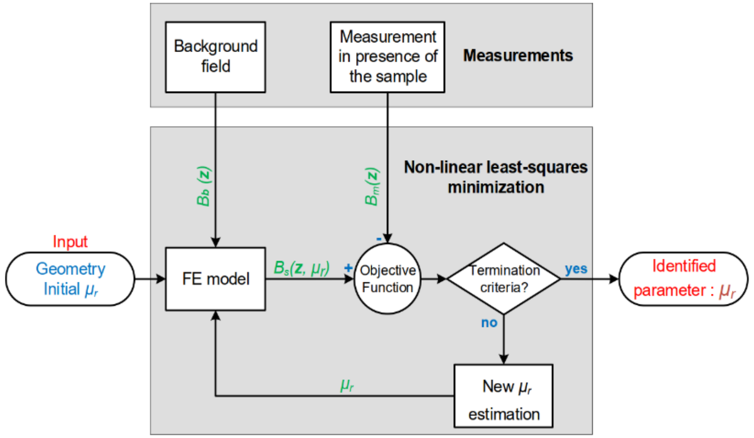

Background field

Measurement in presence of the sample

Measurements

$B_b(z)$

$B_m(z)$

Non-linear least-squares minimization

Input

Geometry

Initial μ_r

FE model

$B_s(z, \mu_r)$

+

-

Objective Function

Termination criteria?

yes

no

Identified parameter : μ_r

New μ_r estimation

μ_r

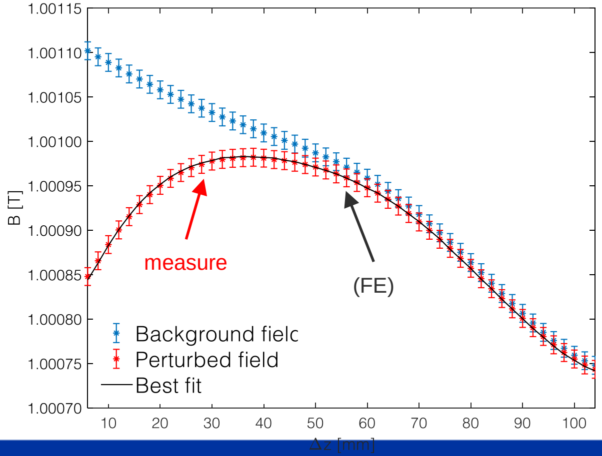

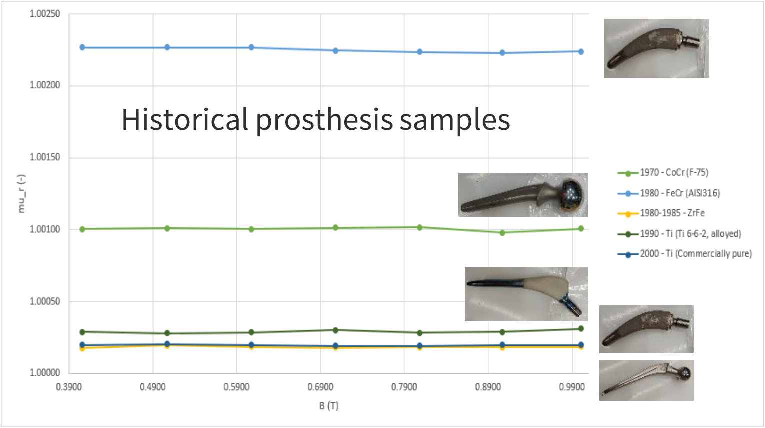

Historical prosthesis samples

$$\frac{F_{\text{magnetic}}}{mg} = (1 - \mu_r)\frac{B\nabla B}{\mu_0 g \rho}$$

Worst-case (Fe-Cr prosthesis): $\mathbf{\mu_r = 1.0023}$

$F_m \approx mg$ for $B\nabla B \approx 42$ T/m^2 (i.e. ~ 20 T MRI magnet!)

Færster™ permeameter

- **Only** portable instrument available
- Based on flux distortion method **IEC 60404-15** (relative measurement)
- Best suited for in-situ QA of material batches
- χ range from 10^{-5} to 1 @ 80 kA/m (100 mT)
- Min. sample volume 35 × 35 × 25 mm^3

Stefano Sgobba
this CAS

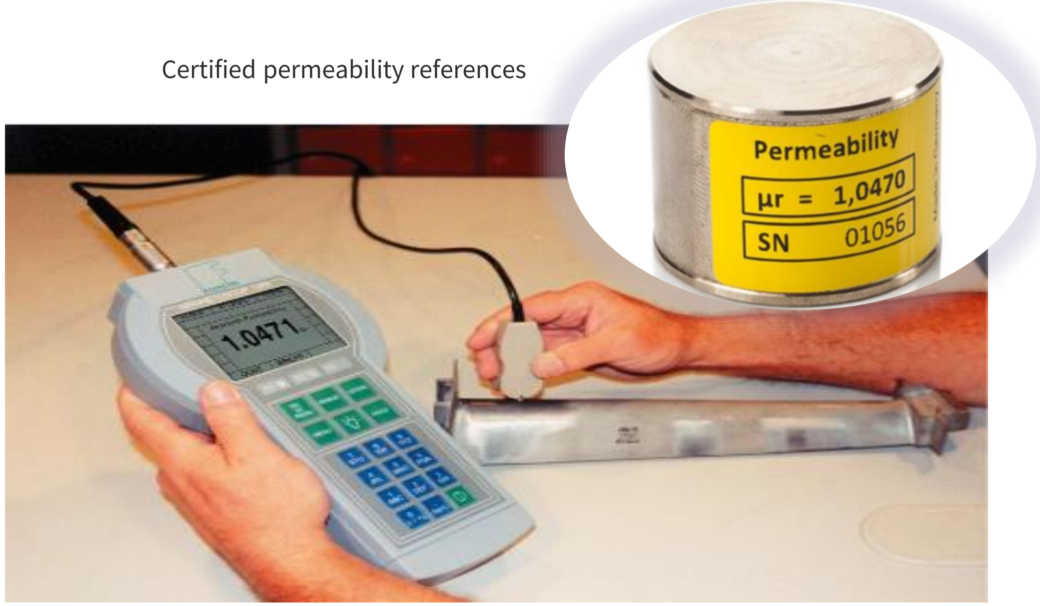

Certified permeability references

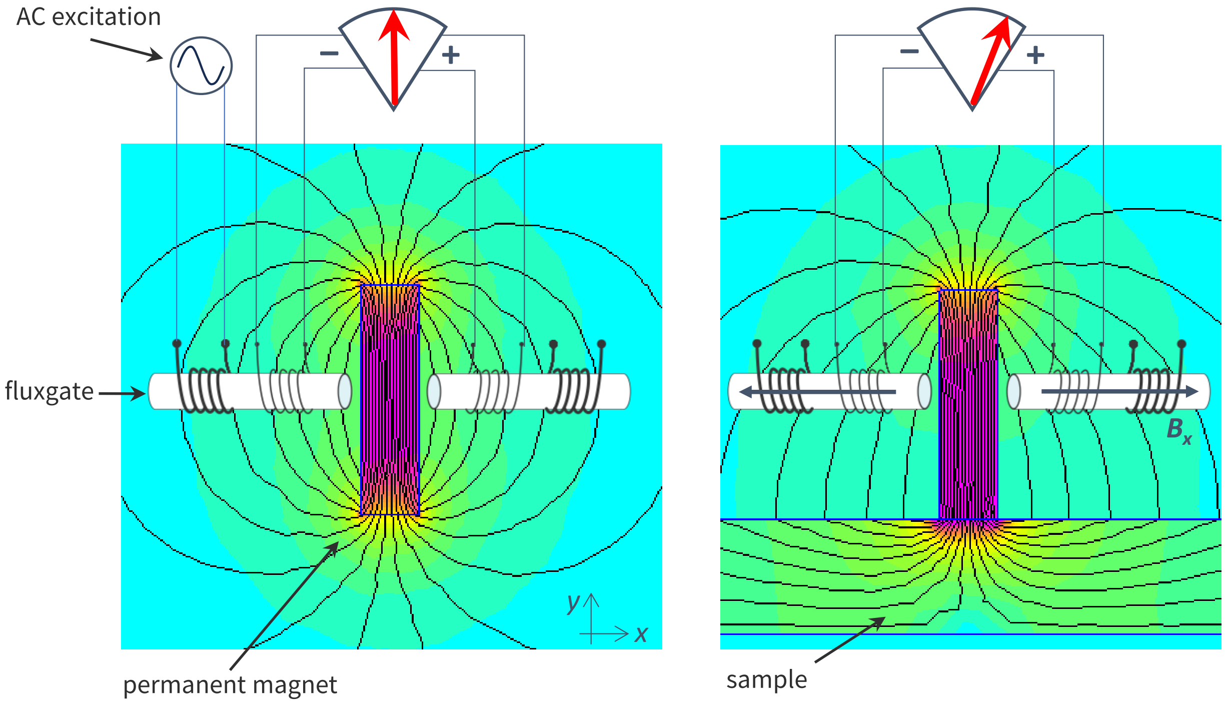

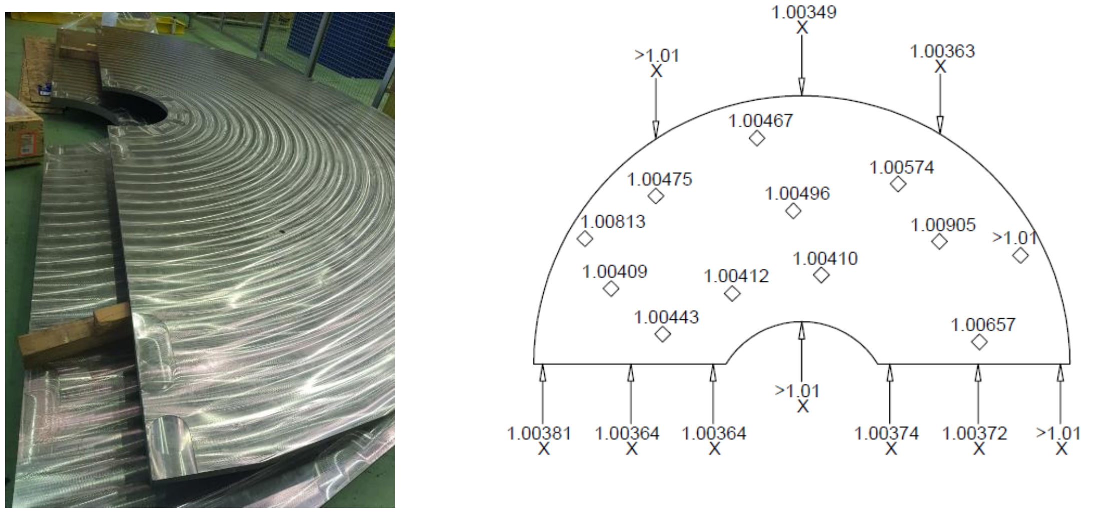

Example: HGCAL plate (304L) inspection for CMS

Part II – Dynamic phenomena in magnets

Phenomenology and modelling from material to devices

Eddy currents in magnets

Eddy currents in iron-dominated magnets

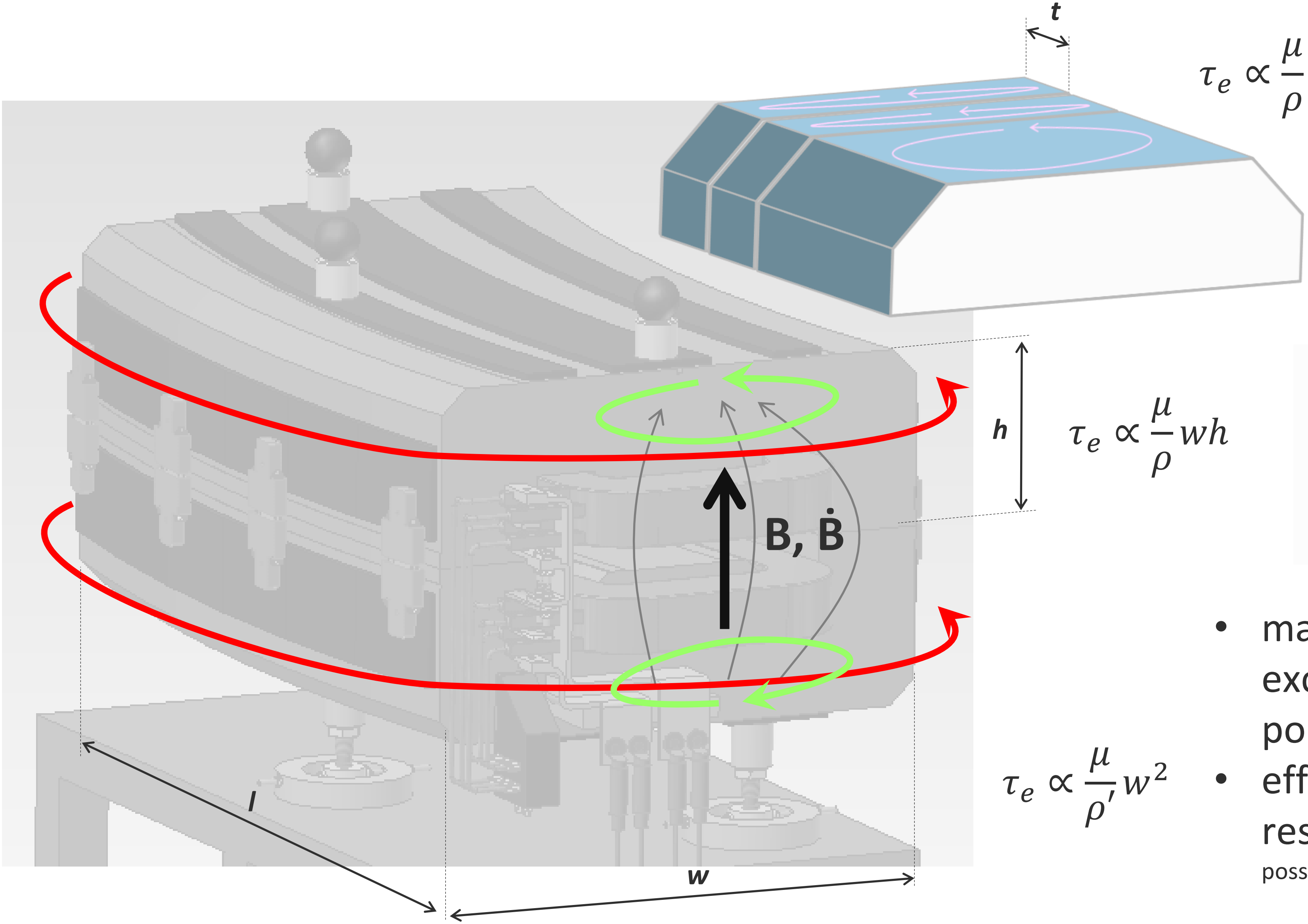

$$\tau_e \propto \frac{\mu}{\rho} t^2$$

- eddy currents in the laminations (normally negligible)
- NB: integral shielding of end plates $\propto t^2$ (local attenuation + fraction of length)

$$\tau_e \propto \frac{\mu}{\rho} wh$$

- eddy currents in-plane of the end laminations, due to the leaking normal field component
- dominant in short magnets

$$\tau_e \propto \frac{\mu}{\rho'} w^2$$

- main eddy current circuit || to main excitation coils (path through magnet poles and/or yoke)
- effect dominated by inter-lamination resistance (factors: chemical composition, surface state, possible shorts due to fasteners or burrs)

Circuital model – linear ramp

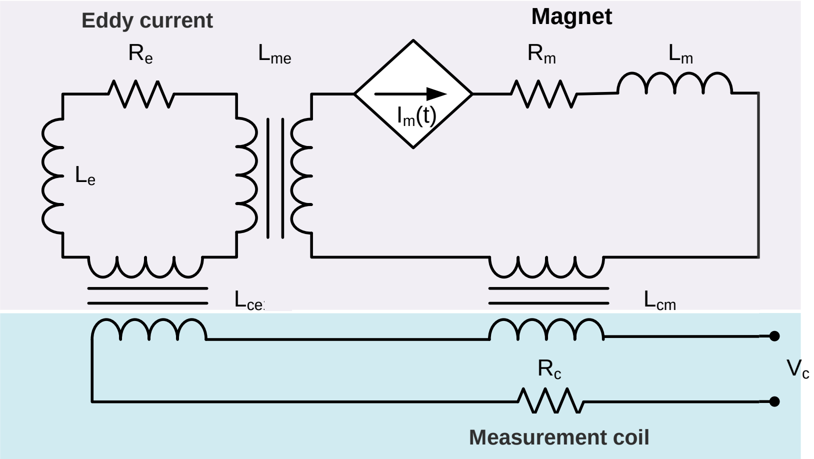

Assume: I_m measured, linear magnet and coil

$$\begin{cases} L_e \dfrac{dI_e}{dt} + R_e I_e + L_{em}\dfrac{dI_m}{dt} = 0 \\ B = \dfrac{1}{A_c}\left(L_{cm}I_m + L_{ce}I_e\right) \end{cases}$$

$$\begin{cases} \tau_e \dfrac{dI_e}{dt} + I_e = -\tau_{em}\dfrac{dI_m}{dt} \\ B = \dfrac{L_{cm}}{A_c}\underbrace{\left(I_m + \dfrac{L_{ce}}{L_{cm}}I_e\right)}_{I^*} \end{cases}$$

Analytical solution on a linear current ramp

$$I_e(t_2) = 0 \quad \Longrightarrow \quad I^*(t_2) = I_m(t_2) = \frac{A_c}{L_{cm}}B(t_2)$$

$$I_e = -\tau_{em}\dot{I}_m \qquad \Delta B = \frac{L_{ce}}{A_c}\tau_{em}\dot{I}_m \qquad \Delta t = \frac{L_{ce}}{L_{cm}}\tau_{em}$$

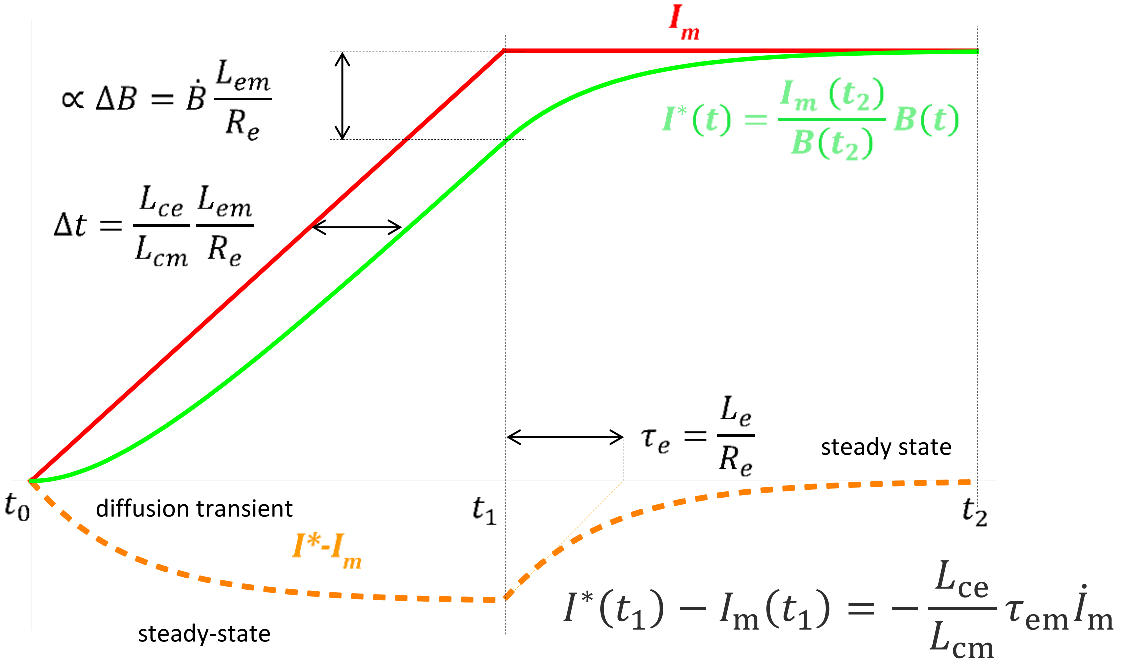

Eddy currents in ITER TF coils

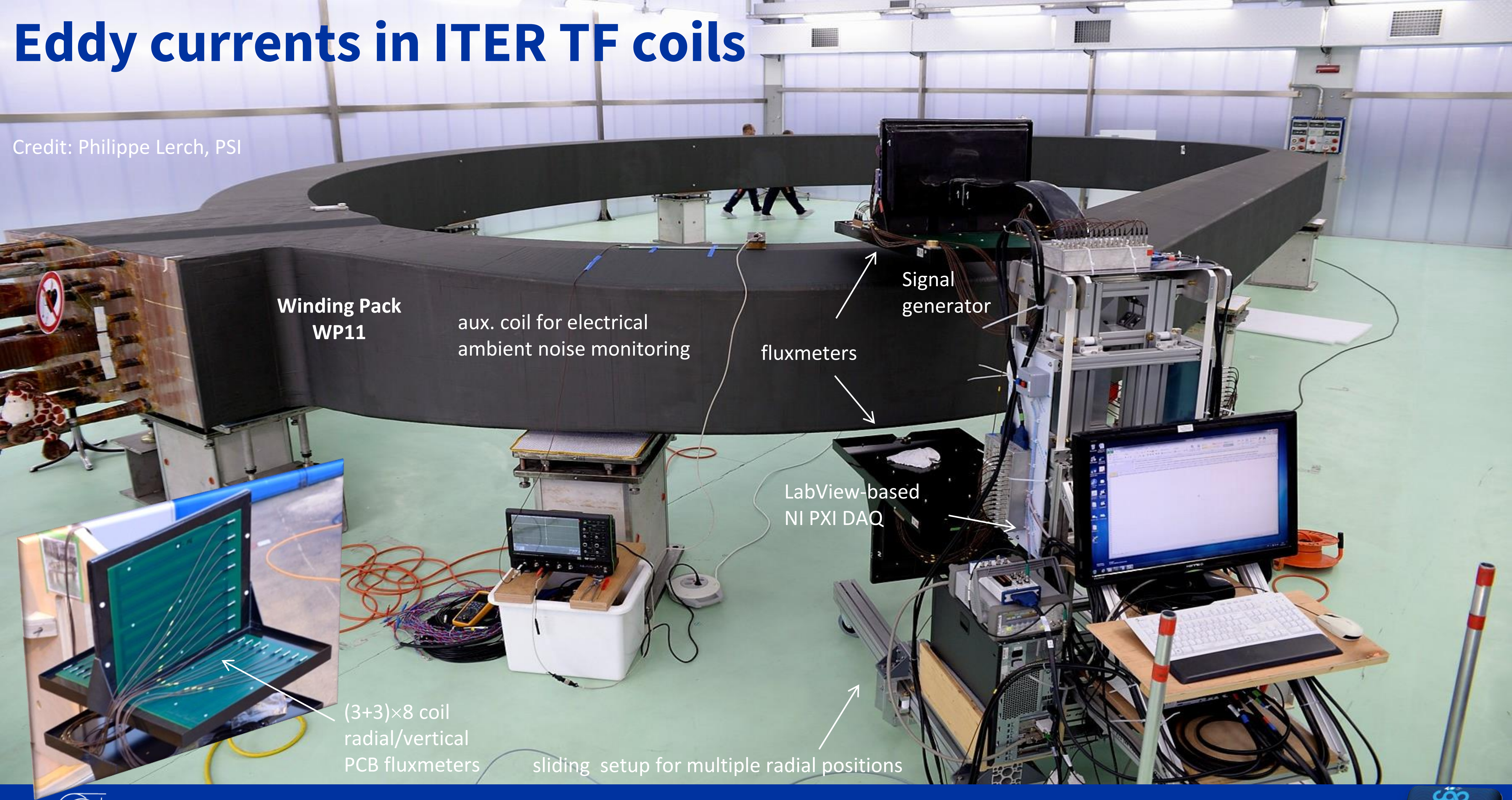

Credit: Philippe Lerch, PSI

Winding Pack WP11

aux. coil for electrical ambient noise monitoring

Signal generator

fluxmeters

LabView-based NI PXI DAQ

(3+3)×8 coil radial/vertical PCB fluxmeters

sliding setup for multiple radial positions

Eddy currents in ITER TF coils

- Final objective: regularized best-fit of coil center line to external magnetic field measurements
- Method: extrapolation of low-current AC measurements to DC conditions

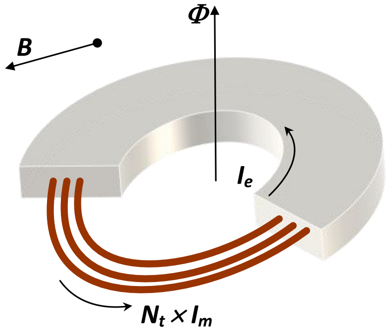

$$\frac{V_c}{I_m}(s) = A_c k_m s \frac{1+\varepsilon s\tau_e}{1+s\tau_e}$$

$$\frac{B}{I_m}(s) = k_m \frac{1+\varepsilon s\tau_e}{1+s\tau_e}$$

$$\begin{cases} L_{em}\dfrac{dI_m}{dt} + L_e\dfrac{dI_e}{dt} + R_e I_e = \\ B = k_m I_m + k_e I_e \\ V_c = A_c\dfrac{dB}{dt} \end{cases}$$

$$\frac{I_e}{I_m}(s) = -\eta N_t \frac{s\,\tau_e}{1+s\tau_e}$$

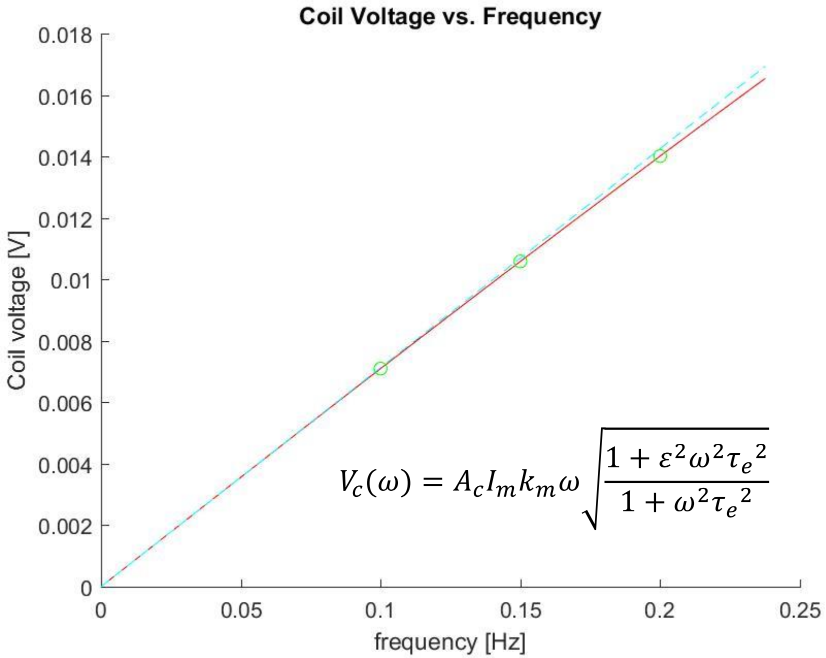

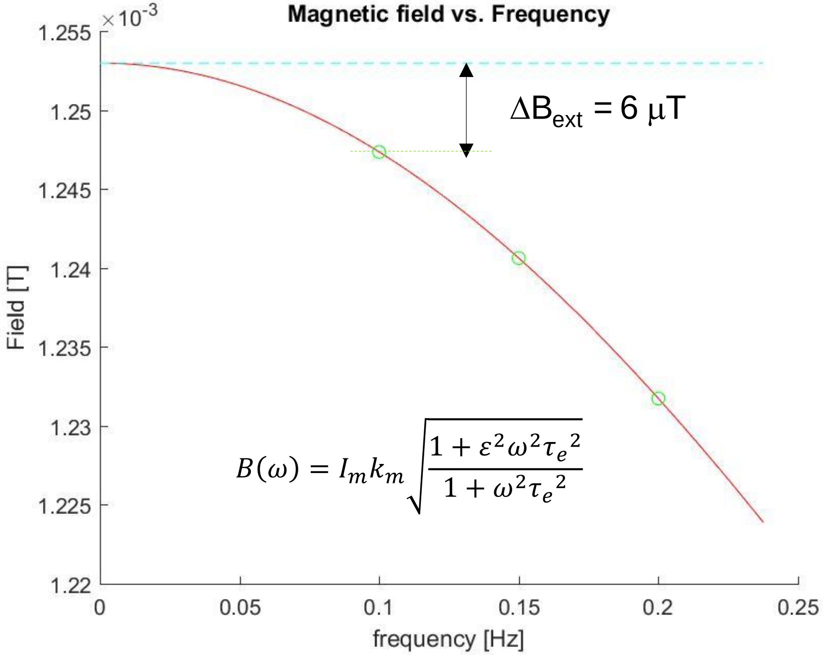

Saturation and Hysteresis effects in Magnets

Impact of permeability on gap field

- Assume: simple 1D magnetic circuit, no leakage
- Impact of permeability strongly limited by circuit aspect ratio

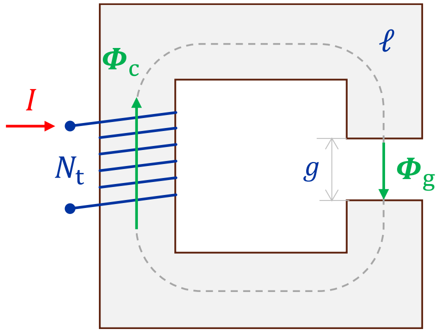

$$B = \frac{\mu_0 \mu_r N_t I}{\ell + \mu_r g} = \frac{1}{\frac{1}{\mu_r} + \frac{g}{\ell}} \frac{\mu_0 N_t I}{\ell} = \begin{cases} \dfrac{\mu_0 N_t I}{g} & \mu_r \gg \dfrac{\ell}{g} \gg 1 \text{ (low field)} \\ \dfrac{\mu_0 \mu_r N_t I}{\ell} & \mu_r \ll \dfrac{\ell}{g} \text{ (saturation)} \end{cases}$$

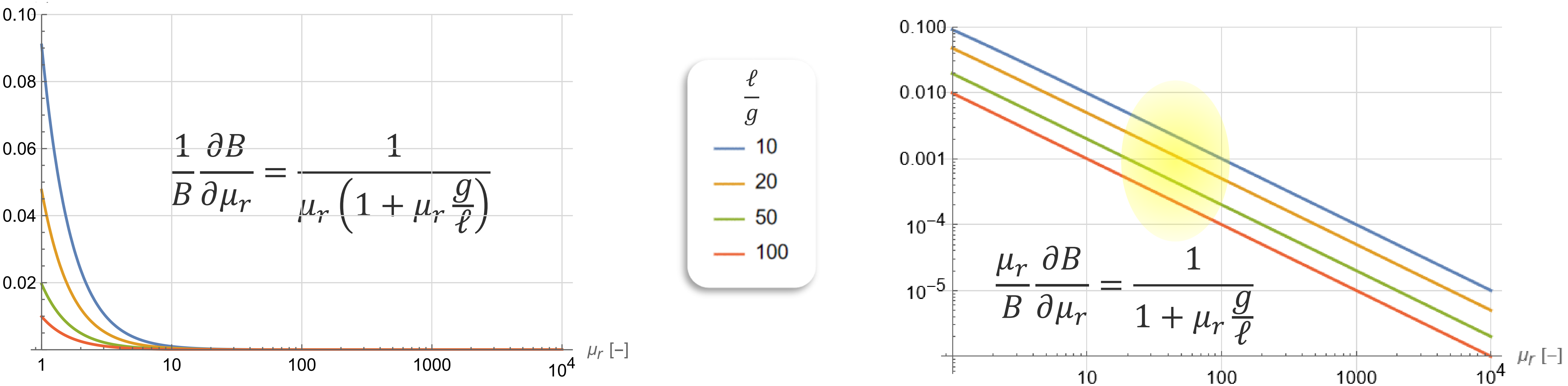

$$\frac{1}{B}\frac{\partial B}{\partial \mu_r} = \frac{1}{\mu_r\left(1 + \mu_r \frac{g}{\ell}\right)}$$

$$\frac{\mu_r}{B}\frac{\partial B}{\partial \mu_r} = \frac{1}{1 + \mu_r \frac{g}{\ell}}$$

Current-to-field transfer function

- Non-linearity best represented by plotting field transfer function B/I
- Low-field regime dominated by B_r, depends upon excitation history → large variability → difficult to control
- High-field regime dominated by saturation, depends upon chemical composition, T → memory reset

$$\frac{B}{I} \approx \frac{B_r}{I} + \frac{\mu_0 N_t}{g}$$

$$\frac{B}{I} \approx \frac{\mu_0 \mu_\mathrm{r}(H(I)) N_\mathrm{t}}{\ell}$$

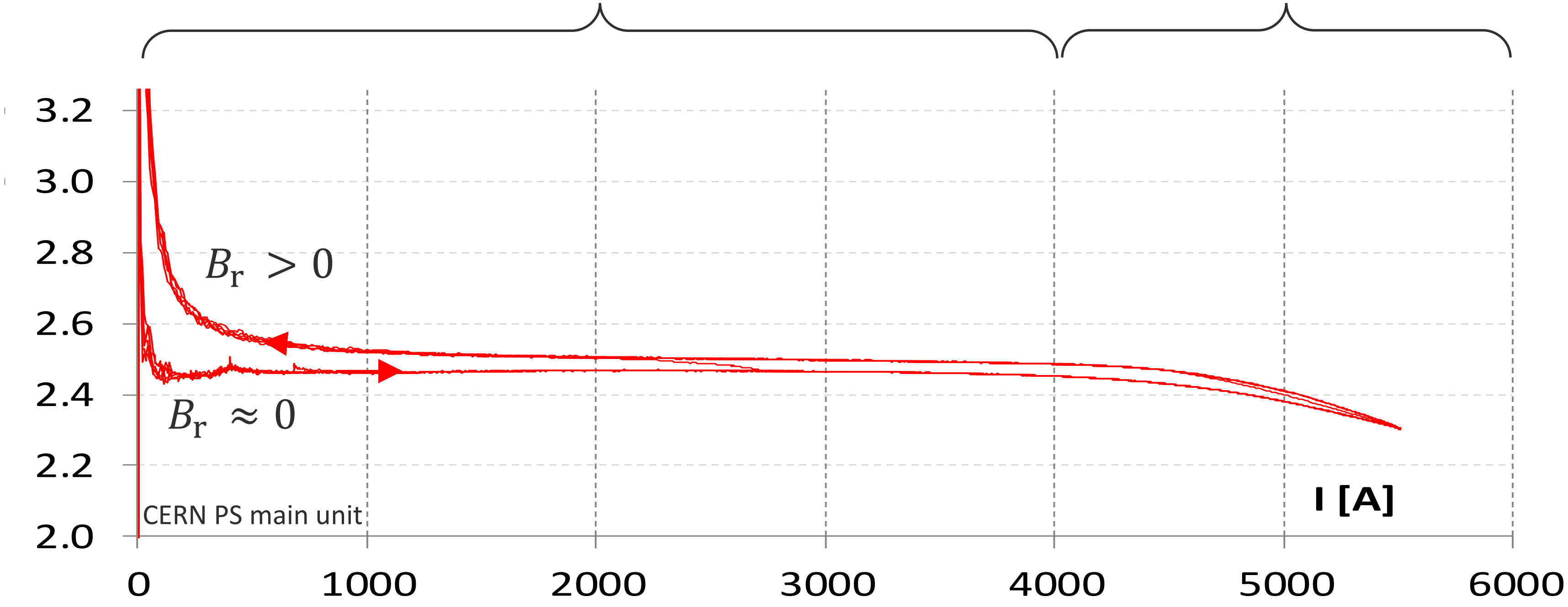

apparent *negative* saturation
due to mechanical coupling
(data from PS main units):

$$p = \frac{B^2}{2\mu_0} \approx 40\ \mathrm{bar}$$

$$g \approx g_0\left(1 - \epsilon \frac{I^2}{I_{\max}^2}\right)$$

$$\epsilon = \frac{0.16\ \mathrm{mm}}{70\ \mathrm{mm}} = \mathbf{0.2\%}\ @\ I\mathrm{max}$$

Credit: Anthony Beaumont

Eddy currents + saturation in a dipole

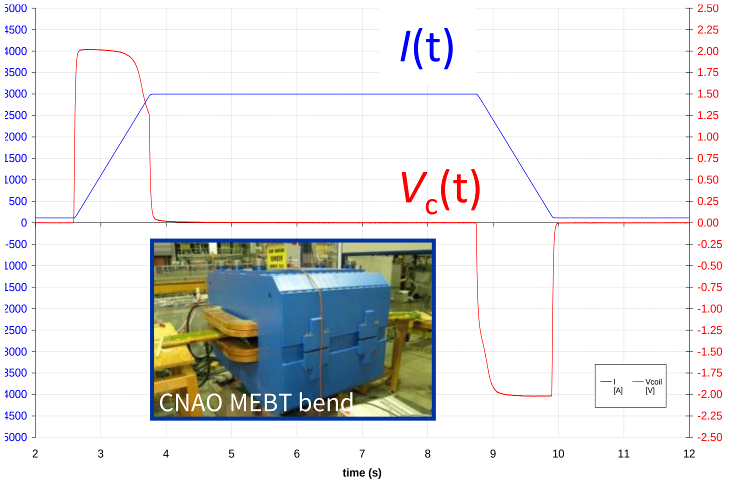

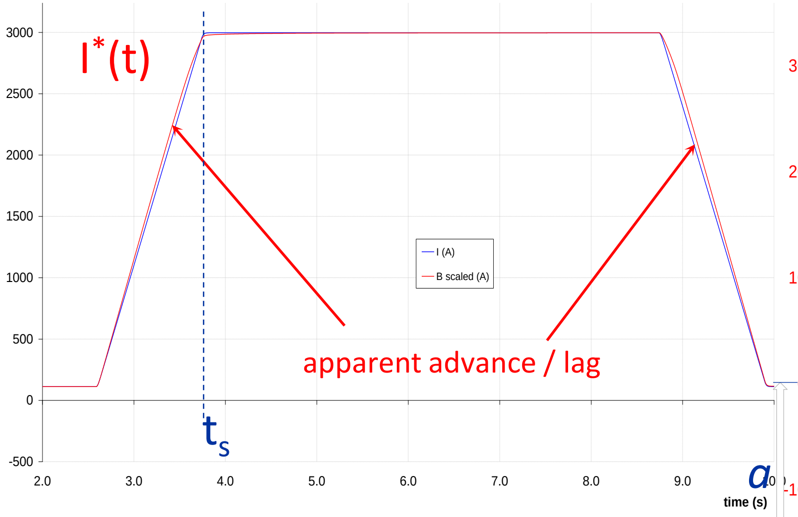

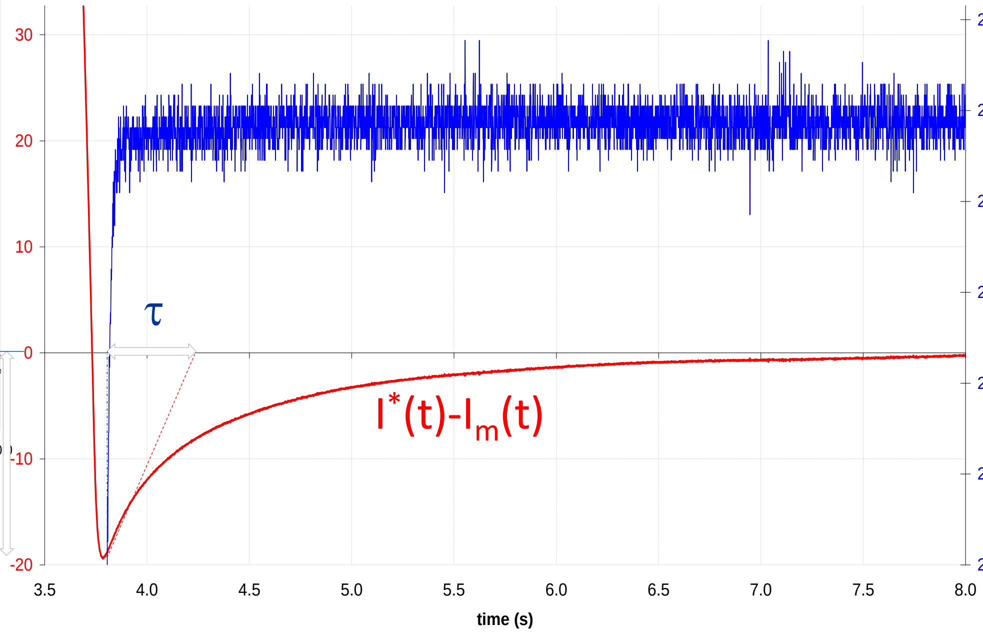

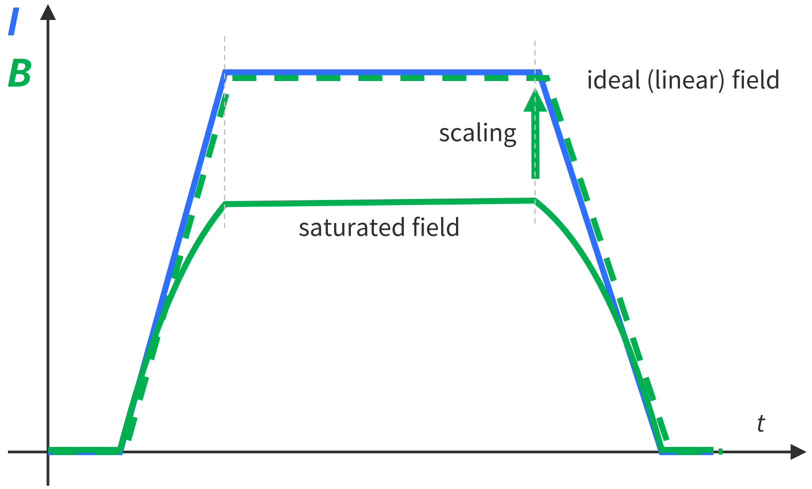

- apparent field advance/lag on ramps = artifact of scaling B ⟶ I*
- overlaps with eddy current's advance/lag
- End of ramp: field *seems* to converge from above
- time of start of the exponential decay needed to derive ΔB
- further complication: rounded corner/overshoots

Eddy currents + saturation in a ring sample

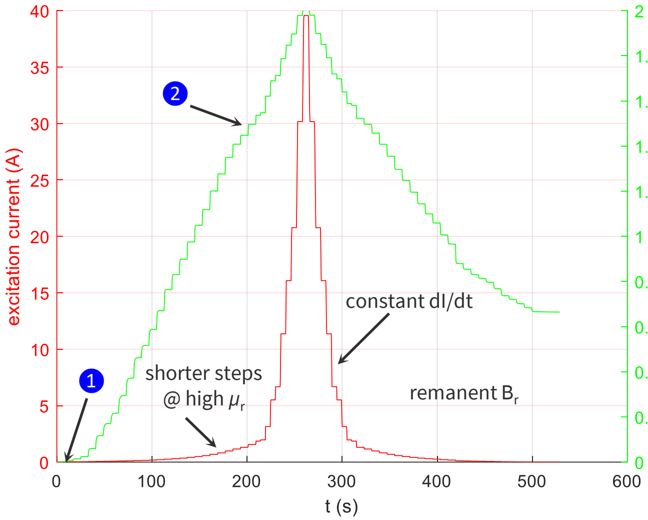

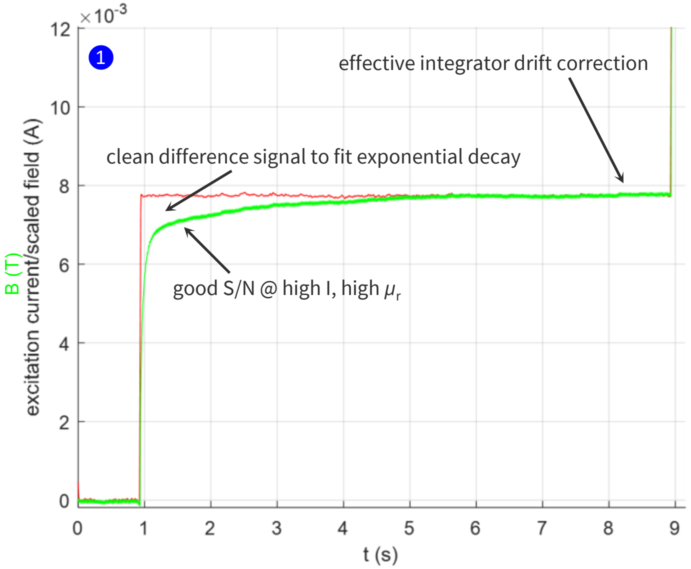

- stepwise magnetization in a ring for easier identification of $\tau_E(H)$ dependency
- one eddy current circuit; no impact of gap
- imperfect but clear result $\boldsymbol{\tau_E \propto \mu_d}$

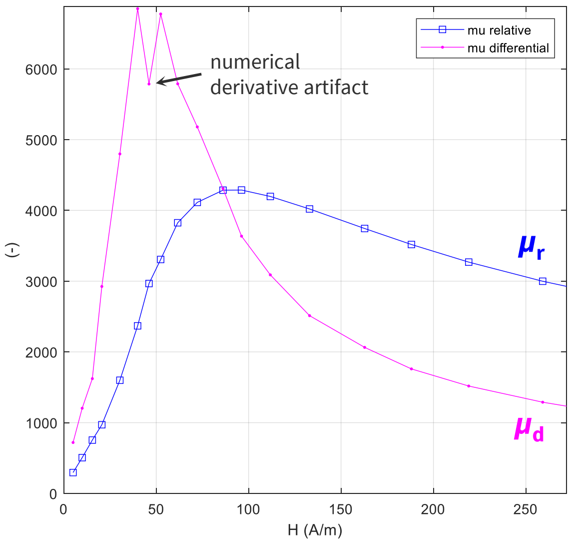

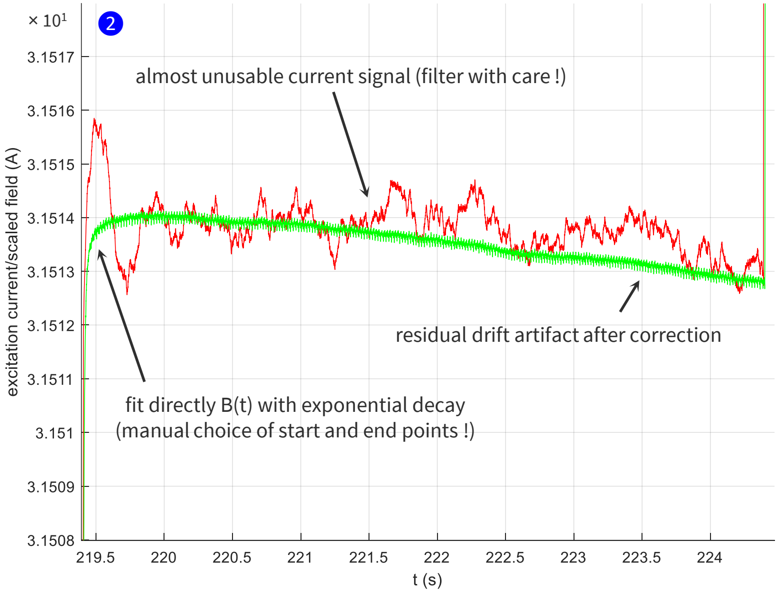

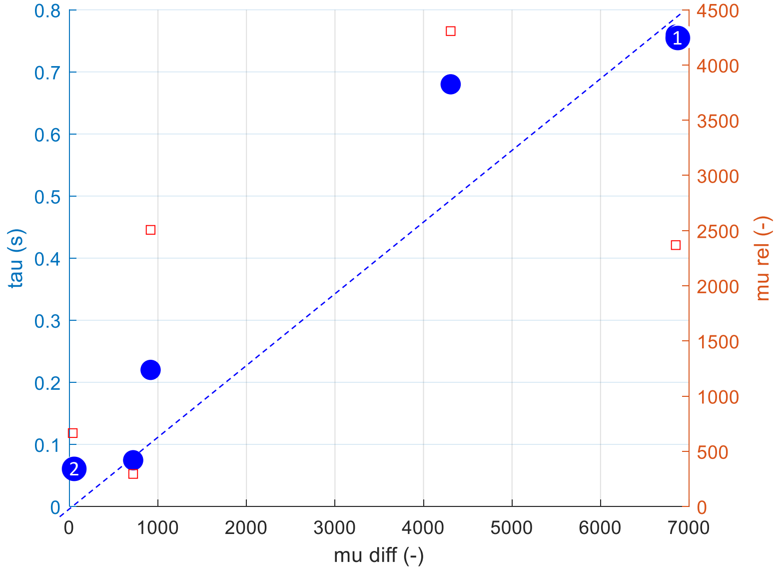

Eddy currents + hysteresis in a fast-pulsed bumper

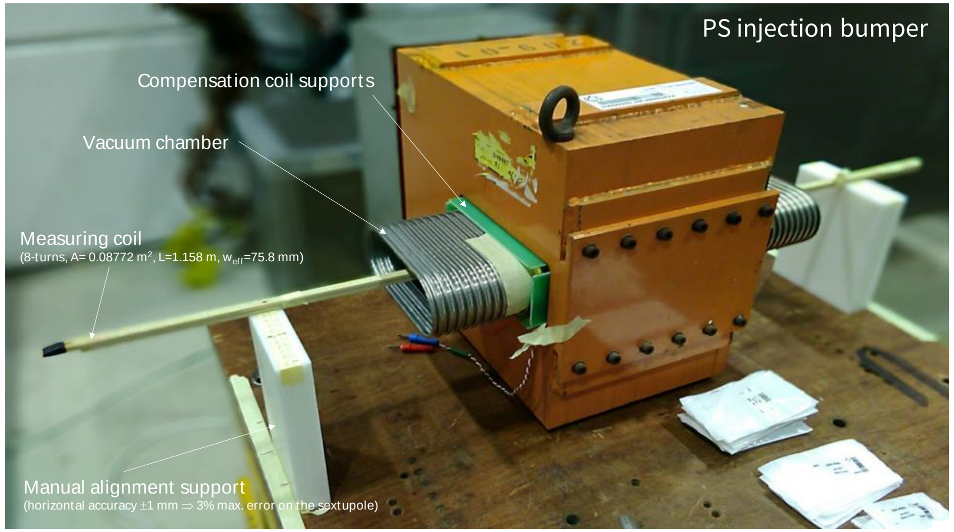

- high dB/dt≈200 T/s → high impact of vacuum chamber, even if corrugated
- free degaussing ! Really a gift ?

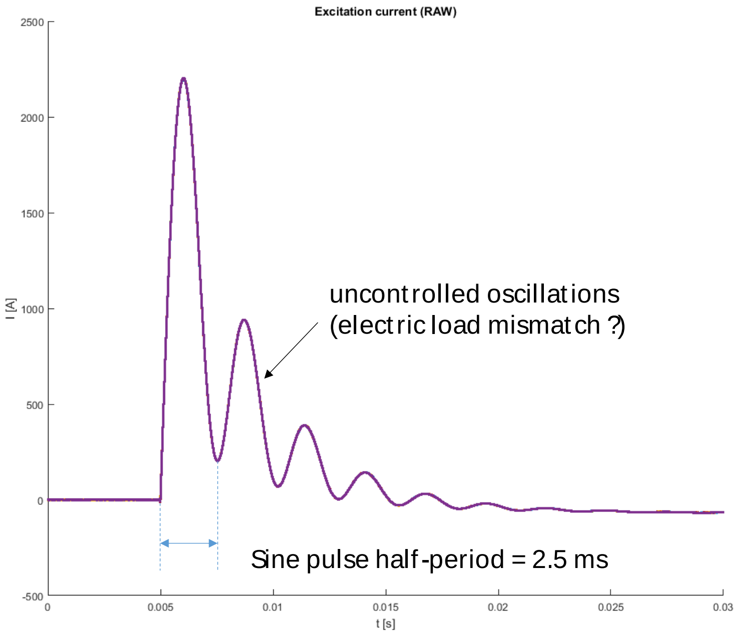

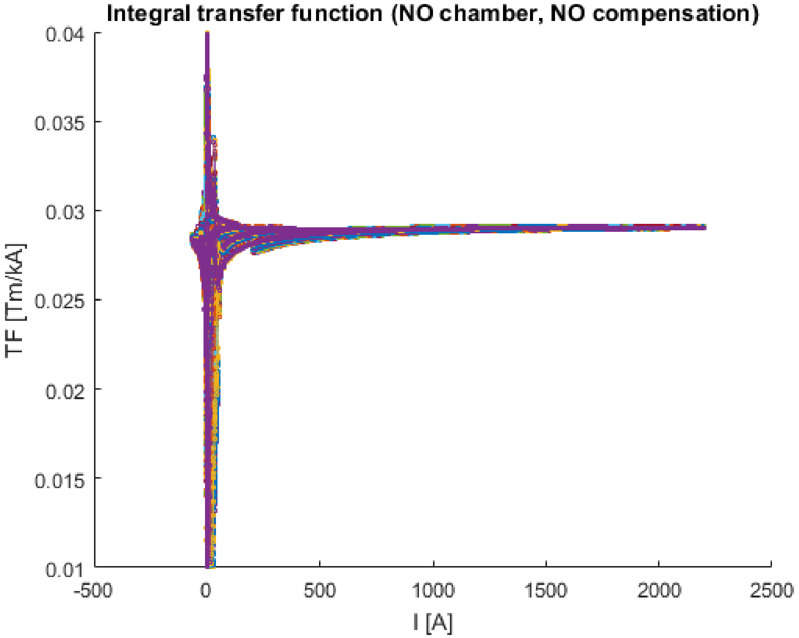

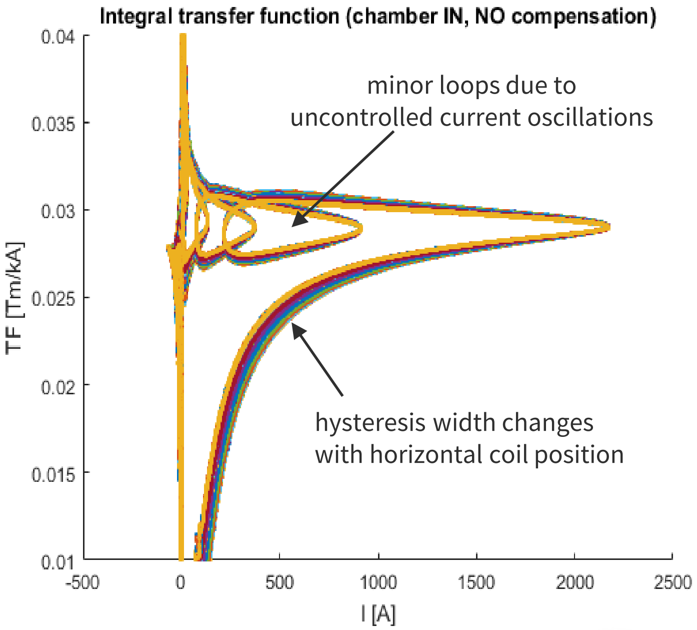

Eddy currents + hysteresis: impact on field profile

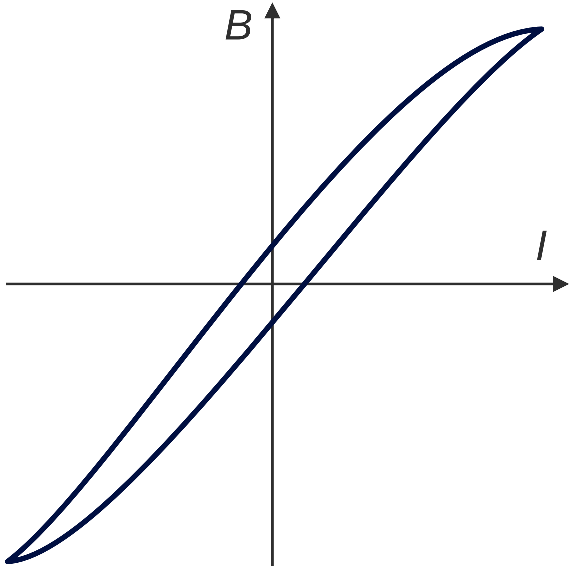

Iron yoke, central region

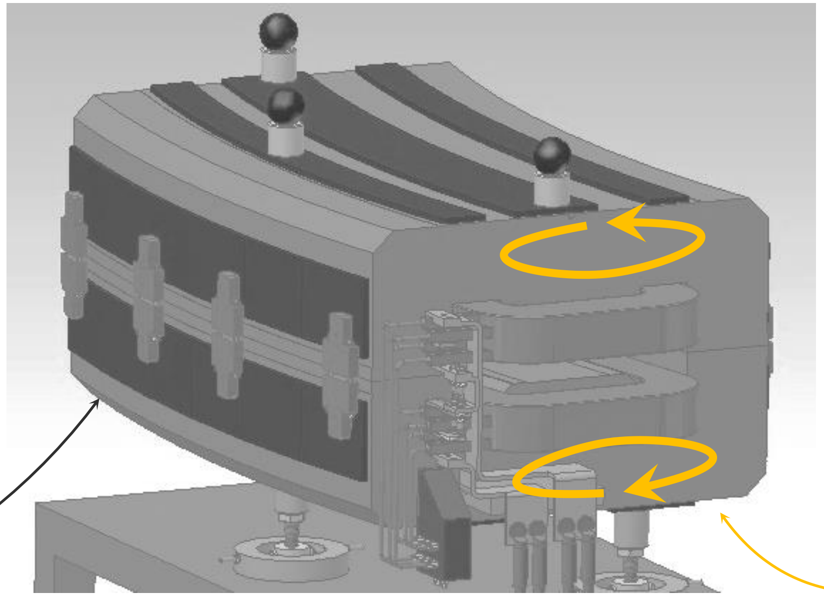

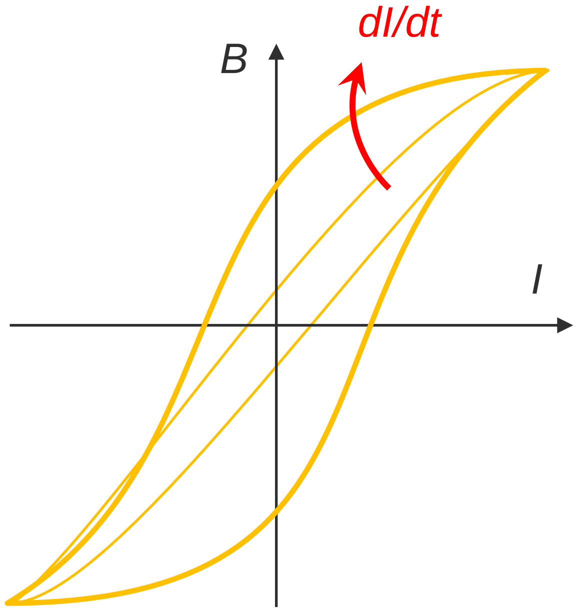

End plates

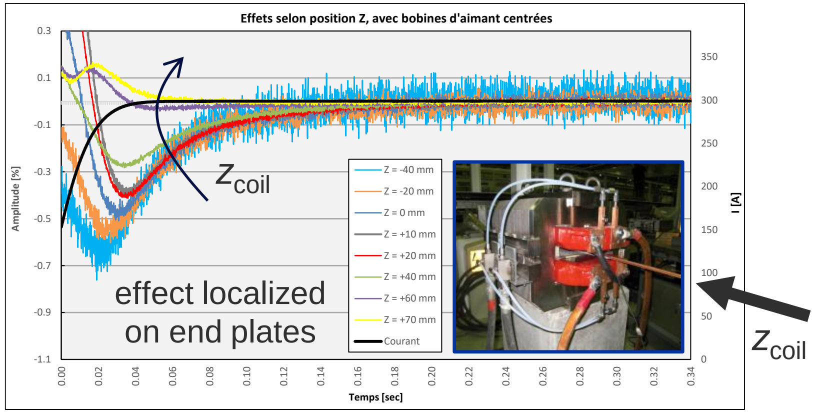

- Localized screening effect ∝ d*I*/dt
- *B*(*z*) profile changes
- Integral field *B*=*B*(I,dI/dt)

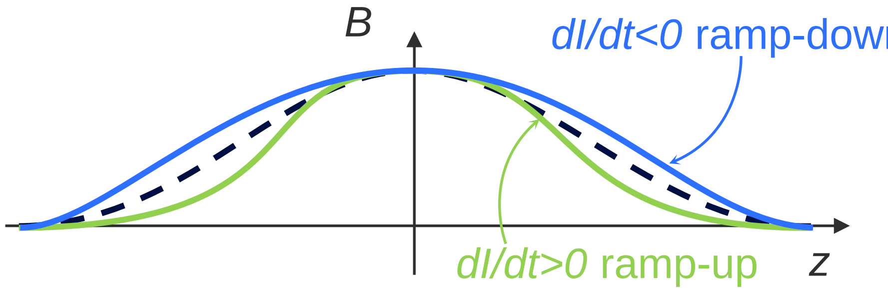

Eddy currents + hysteresis: loop switching

different major loops, B_r

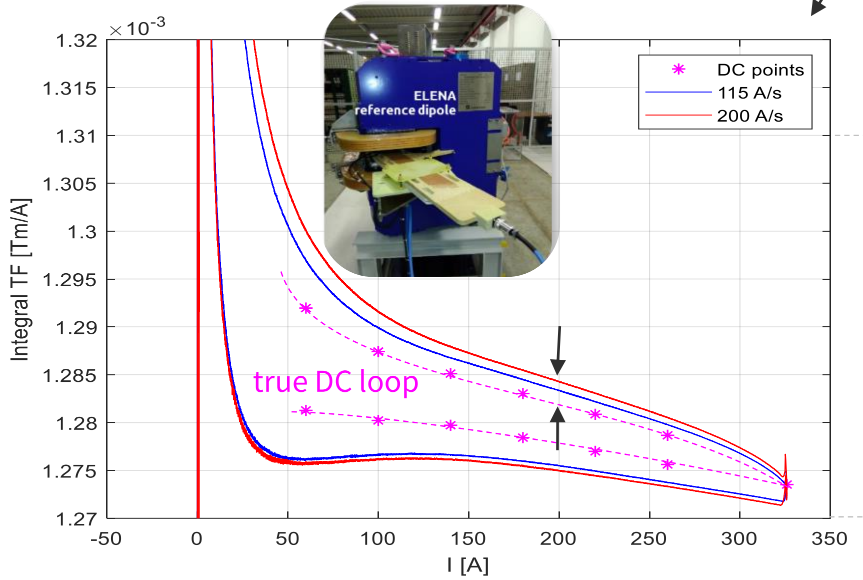

Losses / Δ(B/I not necessarily proportional to dI/dt
Extrapolation to DC not trivial

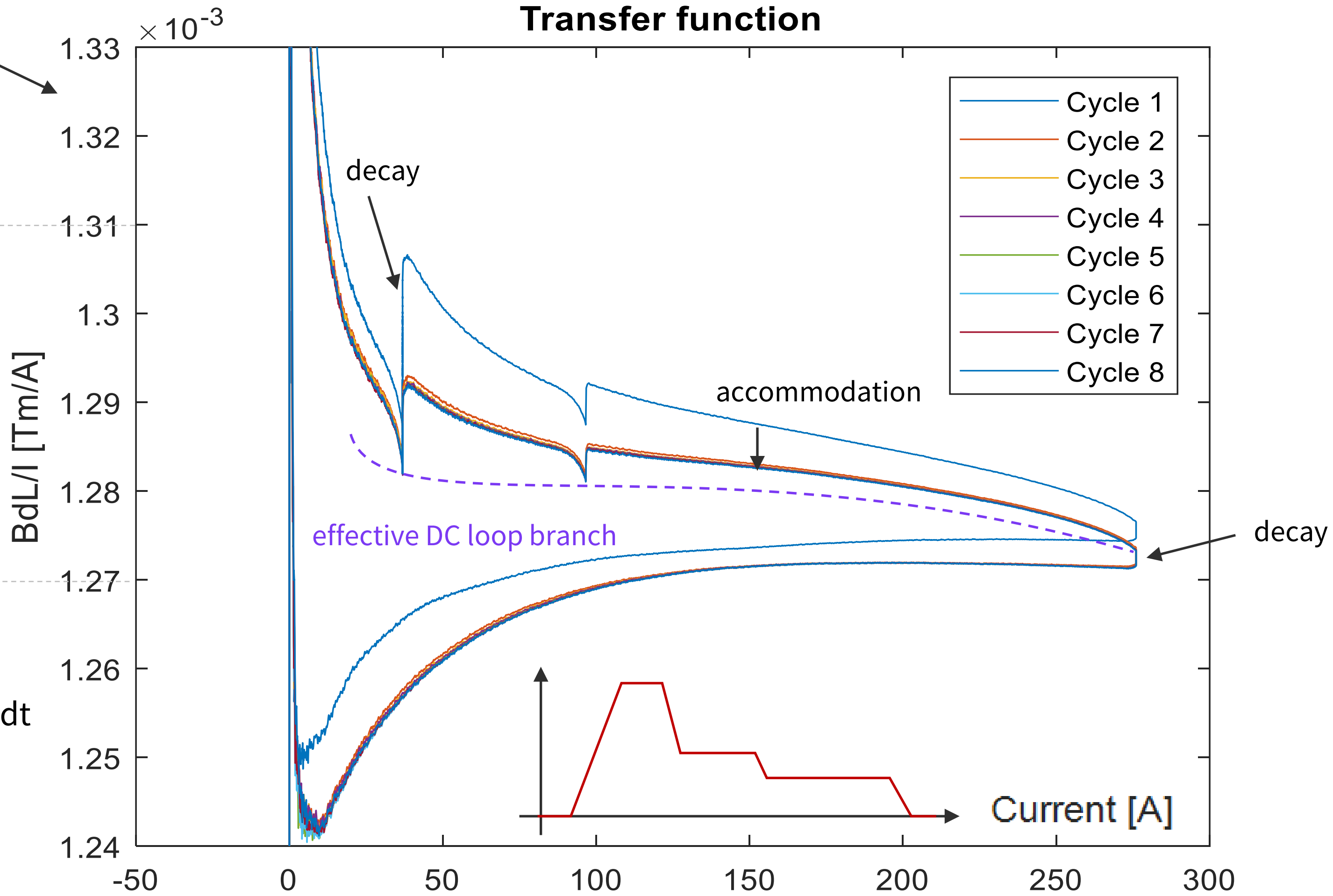

- sequence of ramps and plateaux → switch between different hysteresis loops
- for best reproducibility, always work at constant dI/dt

Eddy currents + hysteresis: impact of timing

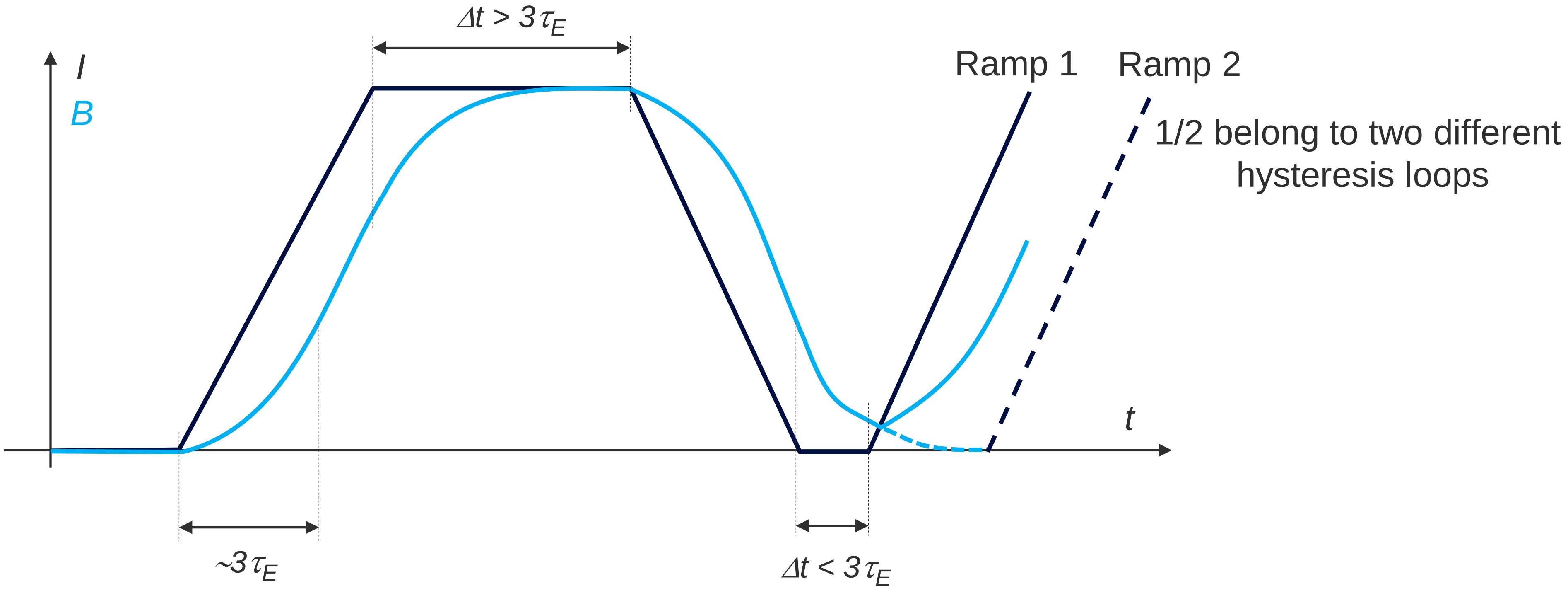

- Assumptions: – characteristic time of eddy current τ_E constant; effects negligible after $\sim 3\tau_E$
  – current ramps > $3\tau_E$ (steady-state reached during the ramp)
- Eddy current decay may be cut short, if plateau is too short
- ***B*/*I* relationship depends also upon the durations of the previous ramps/plateaux**
- In practice cycles are not made of straight segments→ fully functional dependence of $B(t)$ upon $I(t)$ (important for Machine Learning modelling/training)

Magnet self-inductance

Self-Inductance modelling 1/3

Samer Yammine
this CAS

- Observation of inductance drop in power converter controller at high field
- Apparent L drop seemingly unrelated to observed field drop
- Several L definitions possible, with different nonlinear behavior

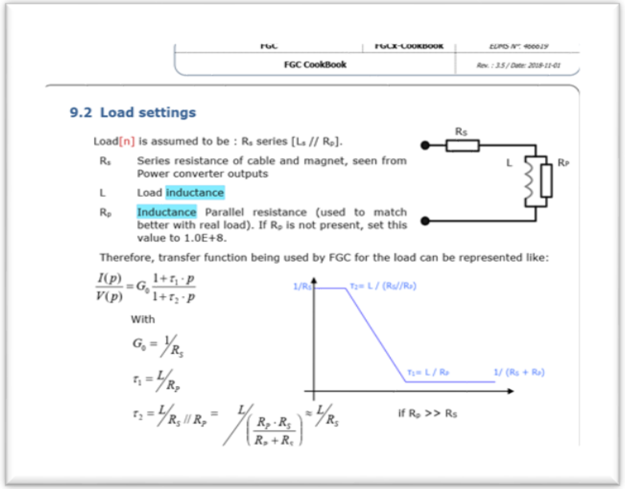

FGC CookBook

Rev. : 3.5 / Date: 2018-11-01

9.2 Load settings

Load[n] is assumed to be : Rₛ series [Lₛ // Rₚ].

Rₛ	Series resistance of cable and magnet, seen from Power converter outputs
L	Load inductance
Rₚ	Inductance Parallel resistance (used to match better with real load). If Rₚ is not present, set this value to 1.0E+8.

Therefore, transfer function being used by FGC for the load can be represented like:

$$\frac{I(p)}{V(p)} = G_0 \frac{1+\tau_1 \cdot p}{1+\tau_2 \cdot p}$$

With

$$G_0 = {}^{1}\!/_{R_S}$$

$$\tau_1 = {}^{L}\!/_{R_P}$$

$$\tau_2 = {}^{L}\!/_{R_S /\!/ R_P} = {}^{L}\!/_{\left(\frac{R_P \cdot R_S}{R_P + R_S}\right)} \approx {}^{L}\!/_{R_S}$$

If Rₚ >> Rs

$$L_t = \frac{\Phi_t}{I}$$

Apparent/secant
self-inductance of one turn

flux self-linked by the coil

$$\Phi_c = LI = N_t^2\,\Phi_t(1-\lambda_c)$$

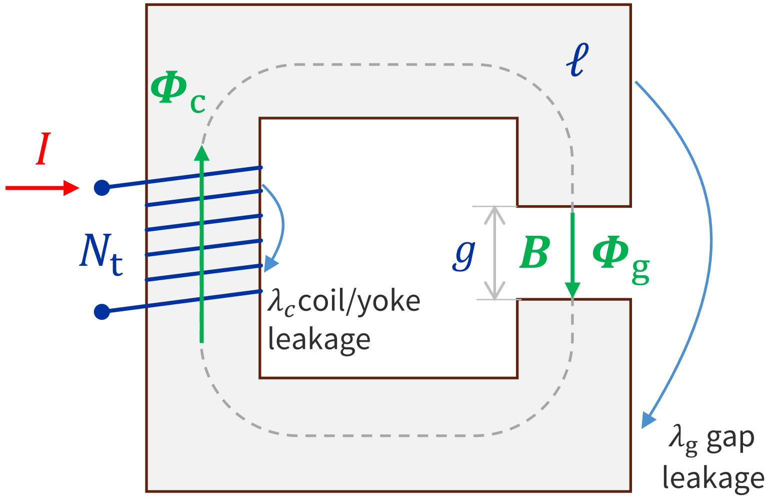

$$\Phi_g = BA = N_t\,\Phi_t(1-\lambda_g)$$

link to field in magnet

Total apparent self-inductance

$$L = N_t A \frac{B}{I}\frac{1-\lambda_c}{1-\lambda_g}$$

$$\frac{\Delta L}{L} \approx \frac{\Delta B}{B} - \Delta\lambda_c + \Delta\lambda_g$$

high aspect ratio
yoke leakage dominates

low aspect ratio
coil leakage dominates

$$\begin{cases} \frac{\ell}{g} \gg 1 & \frac{\Delta L}{L} > \frac{\Delta B}{B} \\ \frac{\ell}{g} \approx 1 & \frac{\Delta L}{L} < \frac{\Delta B}{B} \end{cases}$$

Measurement of the inductance of resistive magnets: two case studies, CERN ATS Note 2011/047

Self-inductance modelling 2/3

- Model based qualitatively on the anhysteretic *B*(*I*) transfer function
- Simple analytical expressions, intended for inner-loop power converter control

Apparent/secant inductance

$$L(I) = \frac{\Phi}{I} = L_0\left(1 - \left(\frac{I}{I^*}\right)^n\right)$$

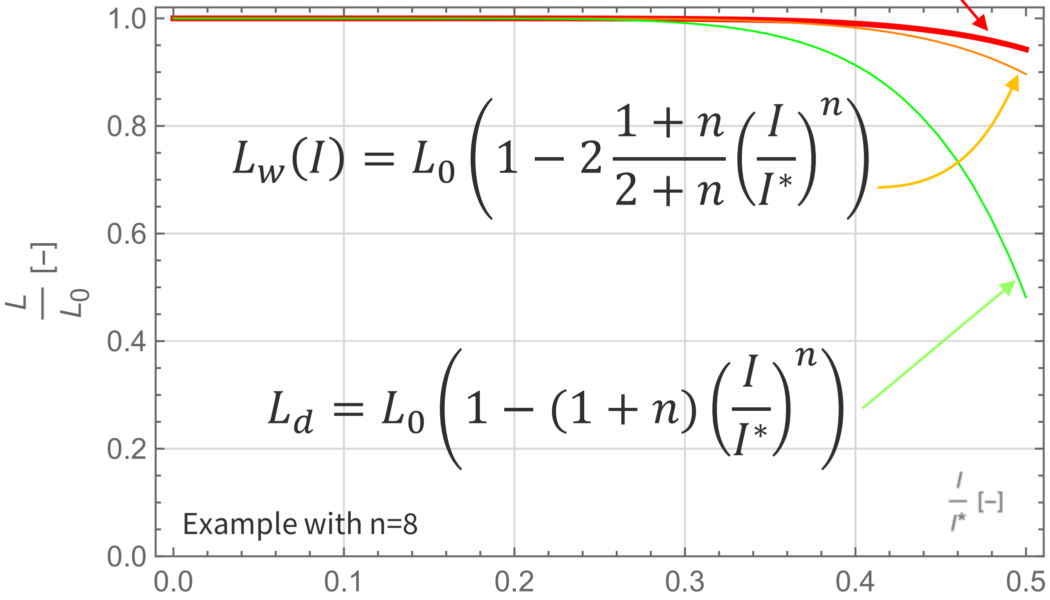

$$L_w(I) = L_0\left(1 - 2\,\frac{1+n}{2+n}\left(\frac{I}{I^*}\right)^n\right)$$

$$L_d = L_0\left(1 - (1+n)\left(\frac{I}{I^*}\right)^n\right)$$

Example with n=8

$$V = RI + \frac{d\Phi}{dt} = \mathrm{RI} + \frac{d}{dt}(LI) = RI + L_d\frac{dI}{dt}$$

differential inductance
(seen by power converter)

$$L_d = \frac{V - RI}{\frac{dI}{dt}} = L + I\frac{dL}{dI}$$

energy-equivalent/
dynamic inductance

$$W = \iiint_{\mathcal{V}} \frac{B^2}{2\mu}dV = \frac{1}{2}L_w I^2$$

$$L_w = \frac{2}{I^2}\int_0^t (V - RI)I dt \approx \begin{cases} \text{dipole} & \frac{1}{\mu_0}\left(\frac{B}{I}\right)^2 g a l_m \approx \mu_0 {N_t}^2 \frac{a}{g} l_m \\ \text{quad} & \frac{\pi}{16\mu_0}\left(\frac{G}{I}\right)^2 \emptyset^4 l_m \approx 8\pi\mu_0 {N_p}^2 l_m \end{cases}$$

Self-inductance 3/3 – Measurement examples

- Measurements of apparent inductance drop qualitatively consistent with expectations for high/low aspect ratio magnets
- Measurements of differential inductance drop qualitatively consistent with polynomial model

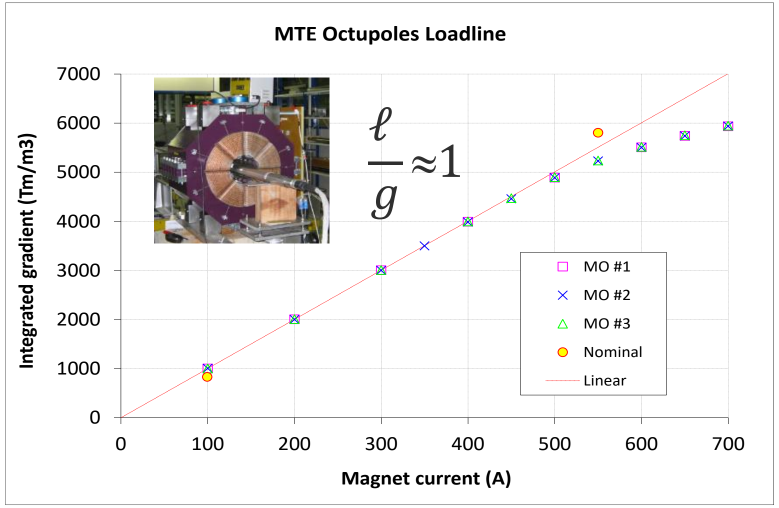
MTE Octupoles Loadline

$\frac{\ell}{g} \approx 1$

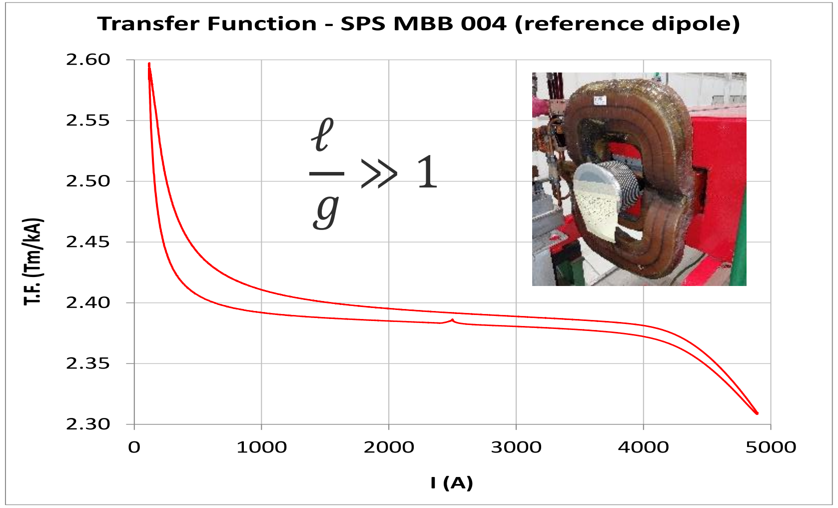
Transfer Function - SPS MBB 004 (reference dipole)

$\frac{\ell}{g} \gg 1$

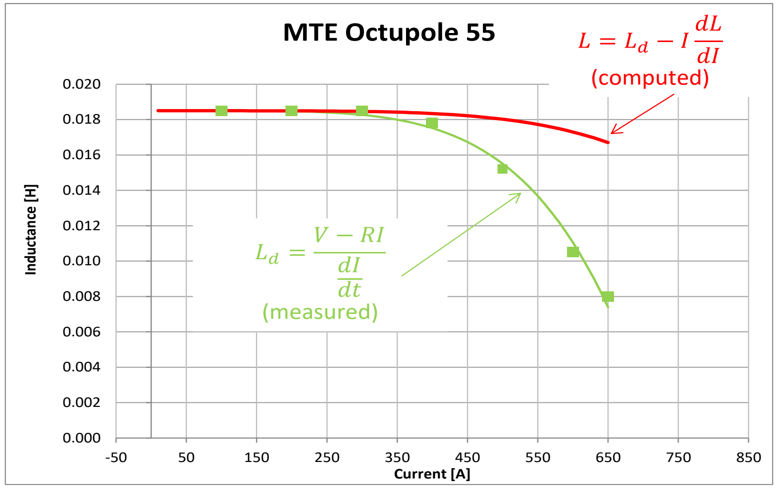
MTE Octupole 55

$L = L_d - I\frac{dL}{dI}$ (computed)

$L_d = \frac{V - RI}{\frac{dI}{dt}}$ (measured)

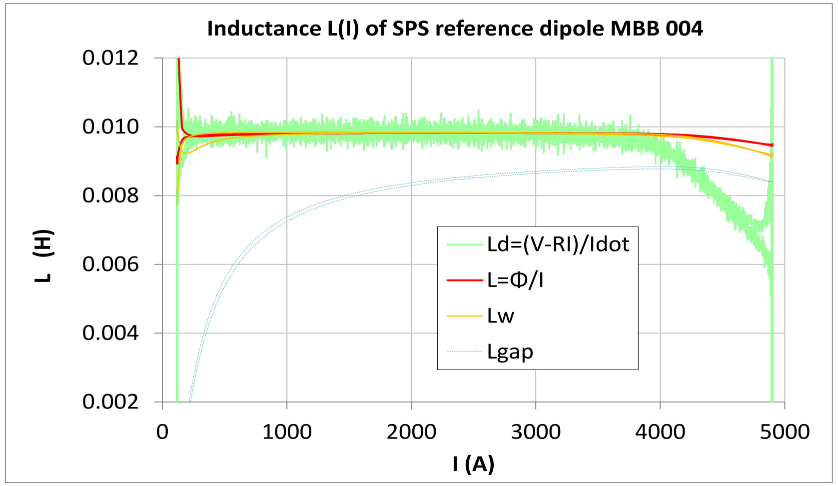
Inductance L(I) of SPS reference dipole MBB 004

$$\frac{\Delta L_d}{L_d} = -60\% \quad \frac{|\Delta B|}{B} = 4.9\% > \frac{|\Delta L|}{L} = 4.2\%$$

$$\frac{\Delta L_d}{L_d} = -39\% \quad \frac{|\Delta B|}{B} = 3.4\% < \frac{|\Delta L|}{L} = 4.0\%$$

Measurement techniques

Instrumentation for dynamic measurements

- no specific instrumentation required for eddy currents and hysteresis
- always acquire the excitation current synchronously to plot transfer function
- main limitation: sensor bandwidth

Hall-effect probes

- intrinsic limitations e.g. dielectric relaxation > MHz
- spinning-current technique for offset compensation, limit at f_{spin}
- practical limitations e.g. inductive loops in the wiring
- typical BW of good-quality commercial units in the 10+ kHz range

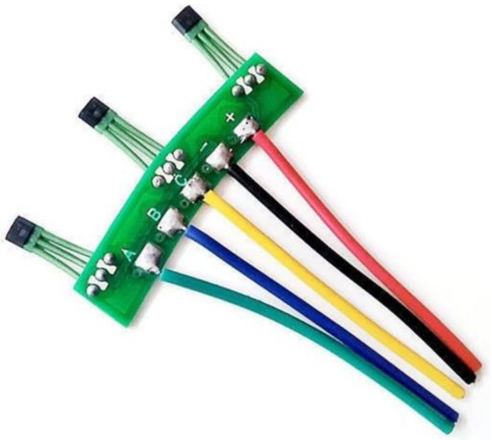

Induction coils

- linear vs field level and BW over wide range
- Unavoidable, due to thermocouple voltages, discrete and integrate component imbalance, noise rectification …
- Take care of connections, grounding and shielding

$$L = N_t{}^2 \frac{\mu_0}{\pi} \ell \left(2\frac{w}{d} + \frac{1}{4} - \frac{w}{\ell}\right), \qquad R = \frac{8}{\pi} N_t \rho_{\mathrm{Cu}} \frac{\ell}{d^2}$$

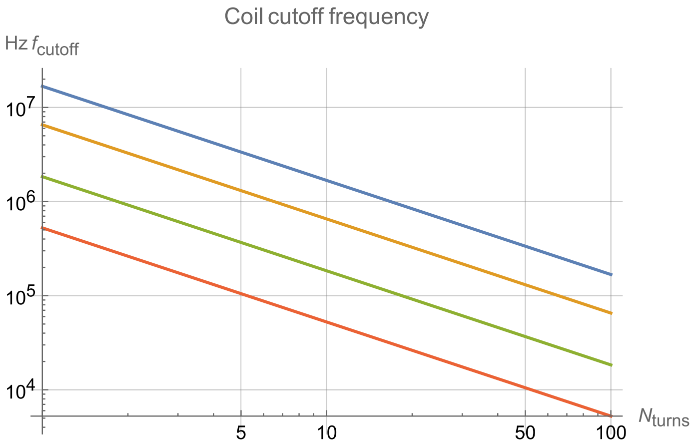

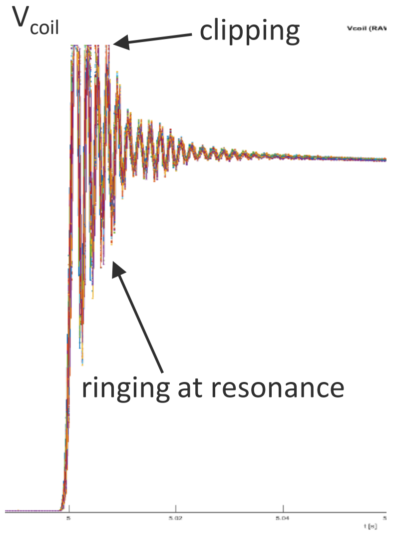

Voltage integrator drift correction

- bumper measurements 1 ms pulse with capacitive discharge converter
- acquisition with 16-bit, 2 MS/s (as fast as practical !)
- harmonic measurements require judicious choice of reference interval for drift correction

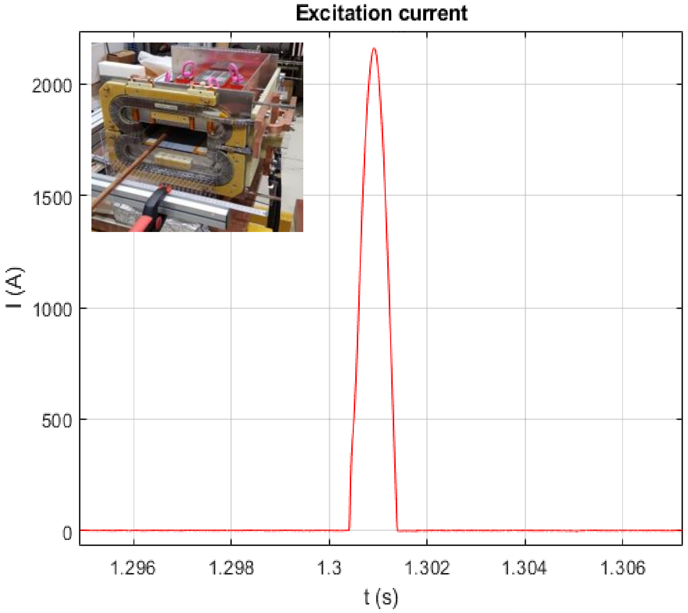

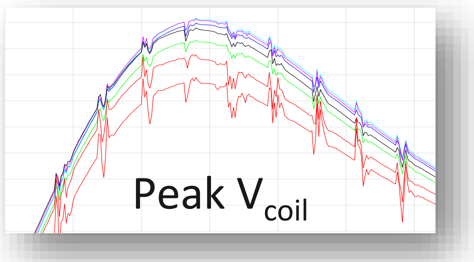
Peak V_{coil}

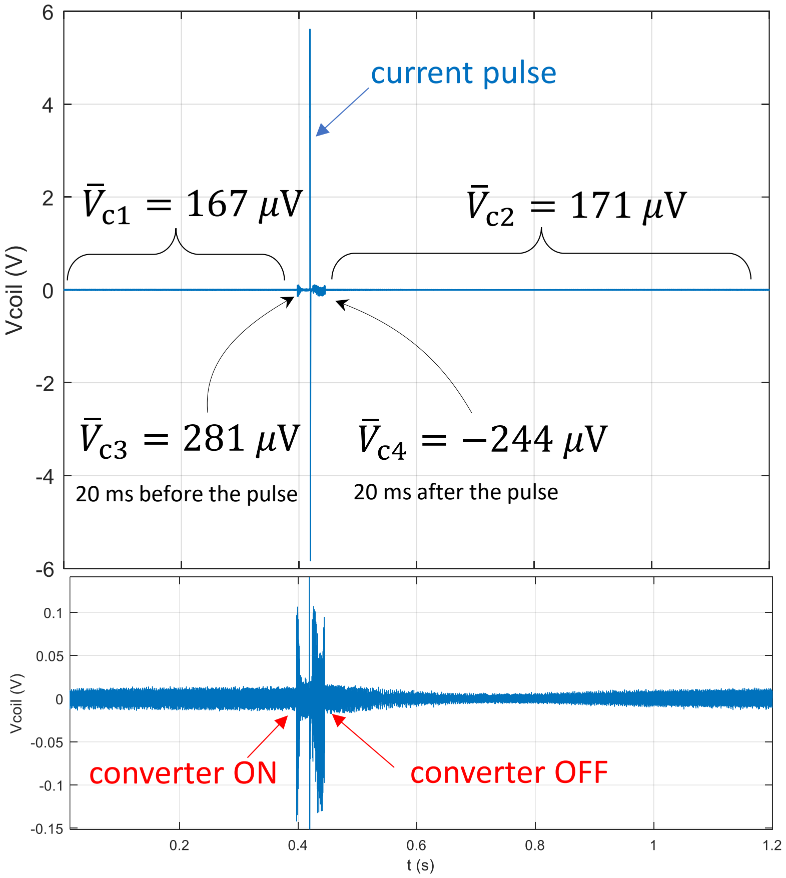

current pulse

$\bar{V}_{c1} = 167\ \mu\mathrm{V}$

$\bar{V}_{c2} = 171\ \mu\mathrm{V}$

$\bar{V}_{c3} = 281\ \mu\mathrm{V}$

20 ms before the pulse

$\bar{V}_{c4} = -244\ \mu\mathrm{V}$

20 ms after the pulse

converter ON

converter OFF

$\Delta\Phi$ =0.3 μVs ($1.8\cdot10^{-4}$)

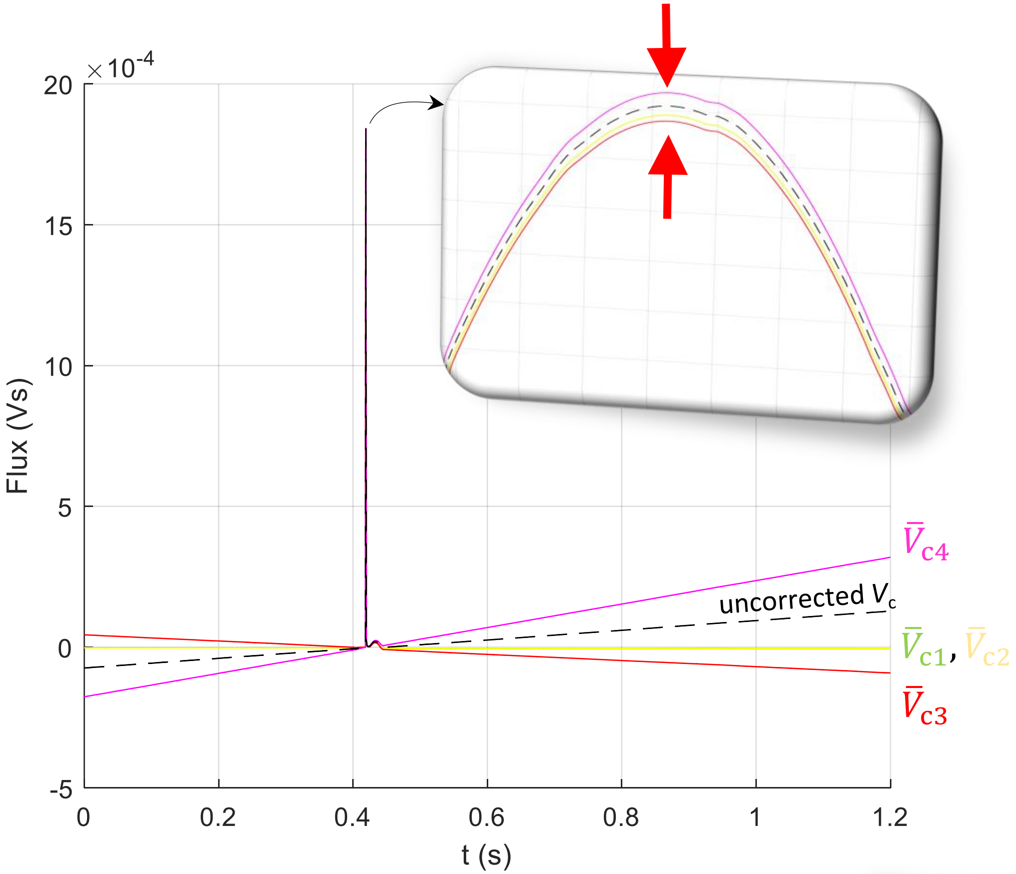

Drift correction – Kalman data fusion

- Problem: fixed-coil voltage integrator drift
- Kalman filtering: optimal estimation of the field in the presence of model (voltage offset V0) + measurement noise
- Combining coil/Hall probe → three orders of magnitude improvement

Field = hidden state

Coil voltage = input variable

State-space model
$$x_k = B_k = B_{k-1} + \frac{1}{A_c}\frac{(v_k + v_{k-1})}{2}T_s$$

Case I: measurement = Hall probe

$$z_k = B_{H,k} = B_k + q_k$$

Case II: measurement = excitation current

$$z_k = \frac{I_k}{g} + q_k$$

Arepoc HHP-NP 2067 Hall Probe

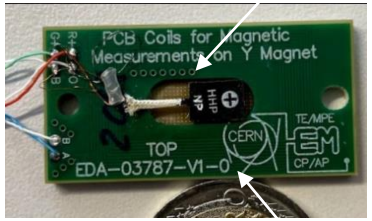

594 cm^2 160-turn 16-layer PCB coil

or

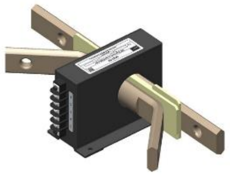

DCCT

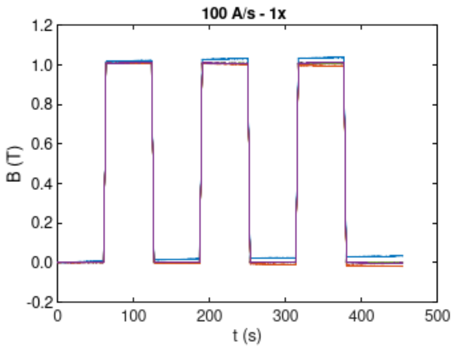

Stable (repeated) cycles

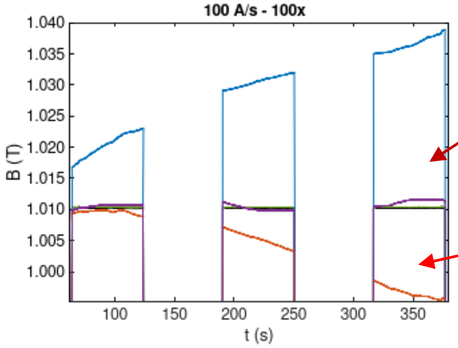

Uncorrected drift 60 ppm/s

V$_0$ updated on each plateau 3 ppm/s

V$_0$ estimated on first plateau 53 ppm/s

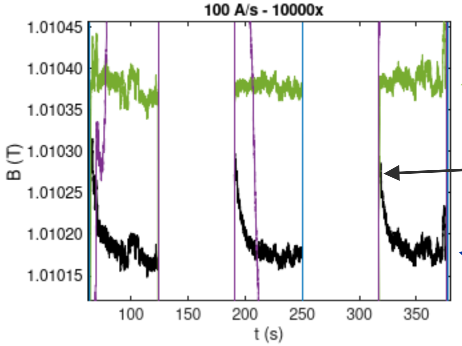

Kalman + exc. current 0.08 ppm/s

Actual eddy current decay transient

Kalman + Hall probe 0.03 ppm/s

V. Di Capua, M. Pentella *et al.*, *"Drift-free integration in magnetic measurements achieved by data fusion ", Sensors 2022, 22, 18*

Part III – Magnet control: open loop

Techniques to improve cycle stability and reproducibility

Open-loop control of eddy currents

Flat-top stabilization with current overshoot

- A current overshoot at the end of ramp-up can compensate, in part or completely, eddy currents
- Linear case: perfect compensation takes ~**1.5**$\boldsymbol{\tau_e}$ (vs. exponential decay 3~4 τ_e)
- Drawbacks:
  – power converter needs high dV/dt
  – higher peak working point
  – move onto higher-saturation hysteresis loop branch

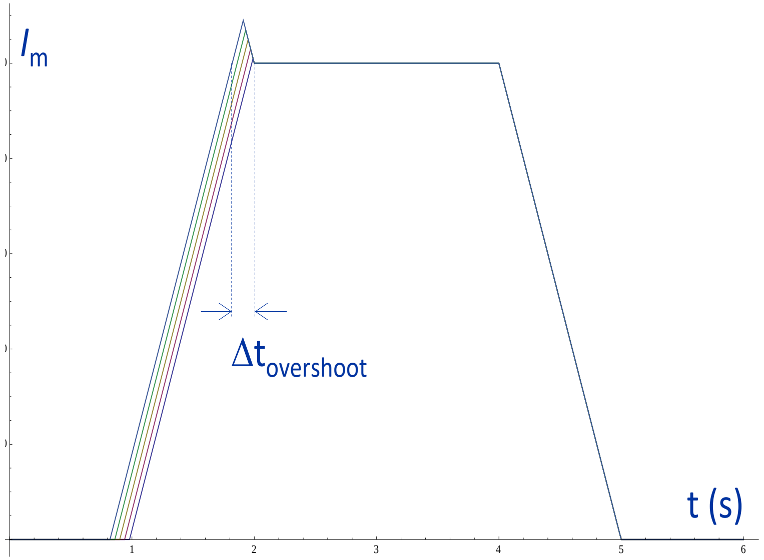

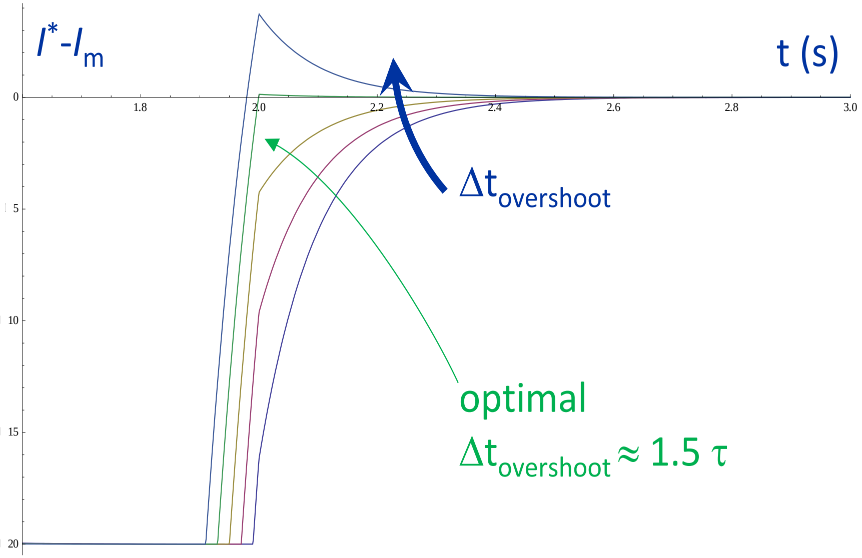

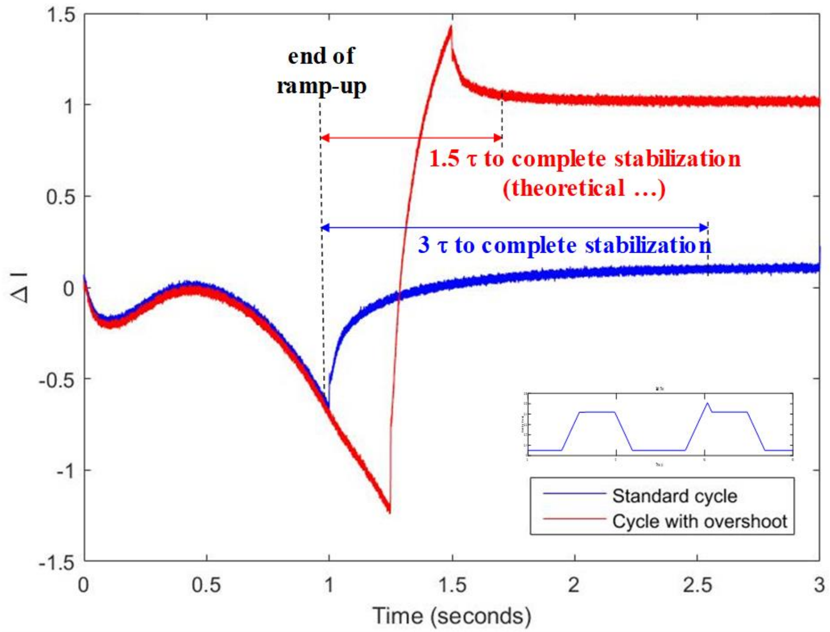

Flat-top stabilization – example

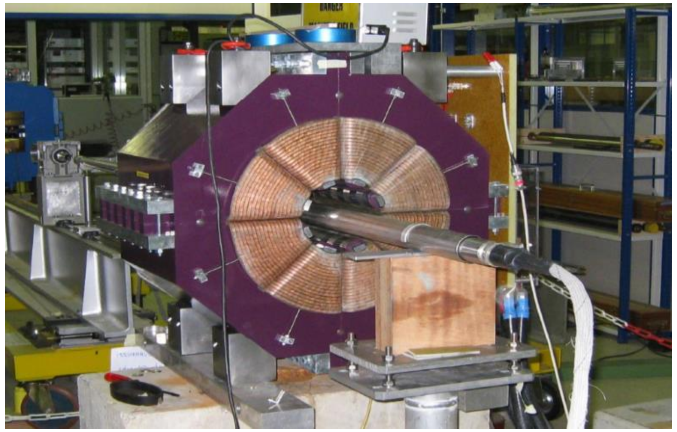

CERN PS MTE multi-turn extraction octupole

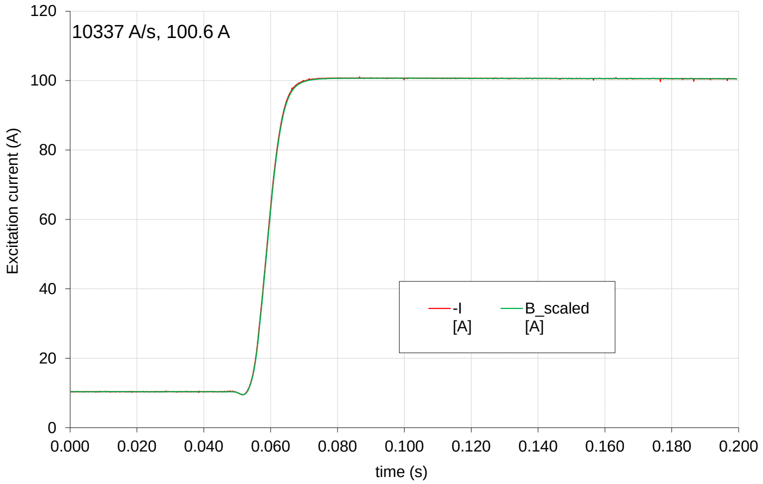

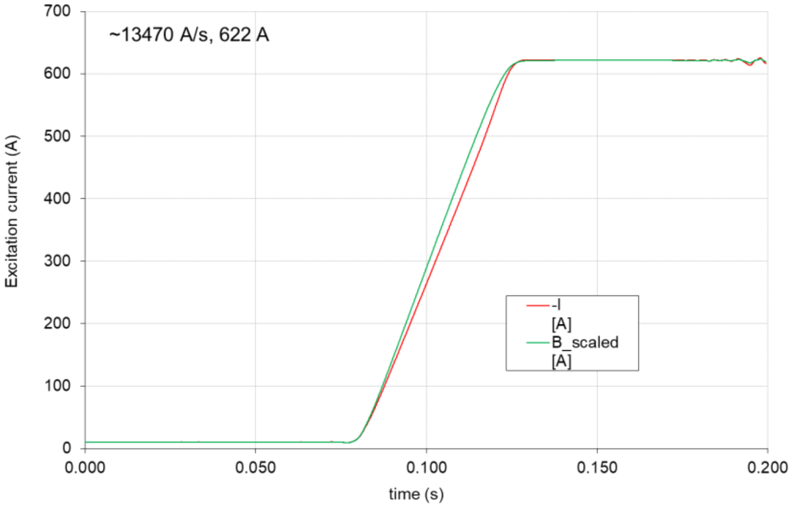

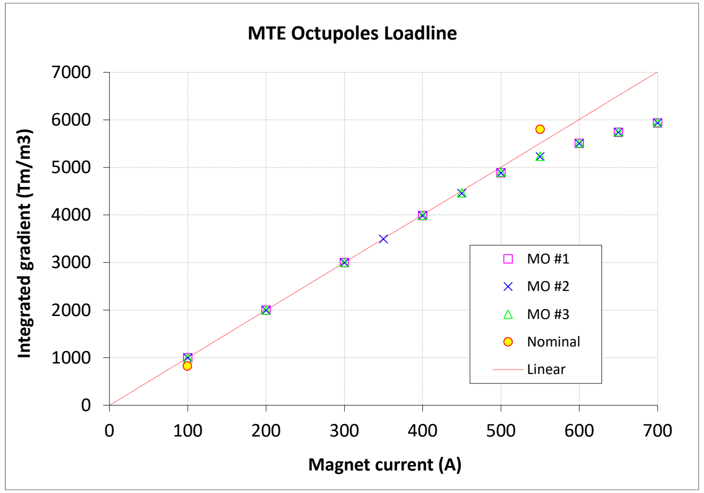

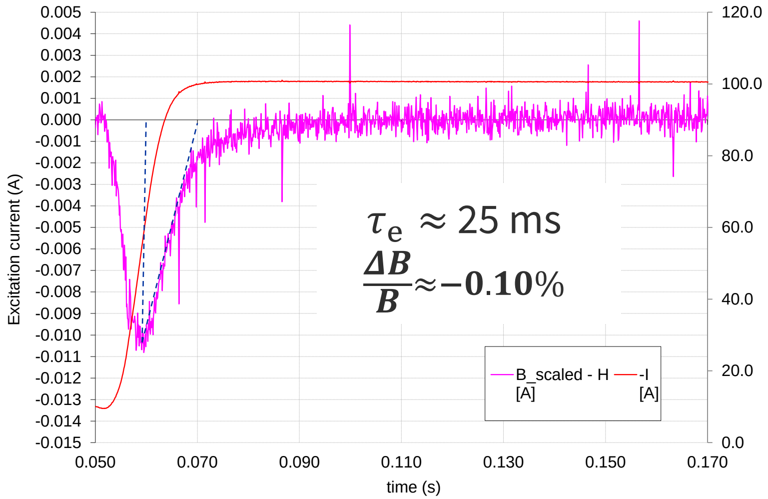

$\tau_e \approx 25$ ms

$\frac{\boldsymbol{\Delta B}}{\boldsymbol{B}} \approx \mathbf{-0.10\%}$

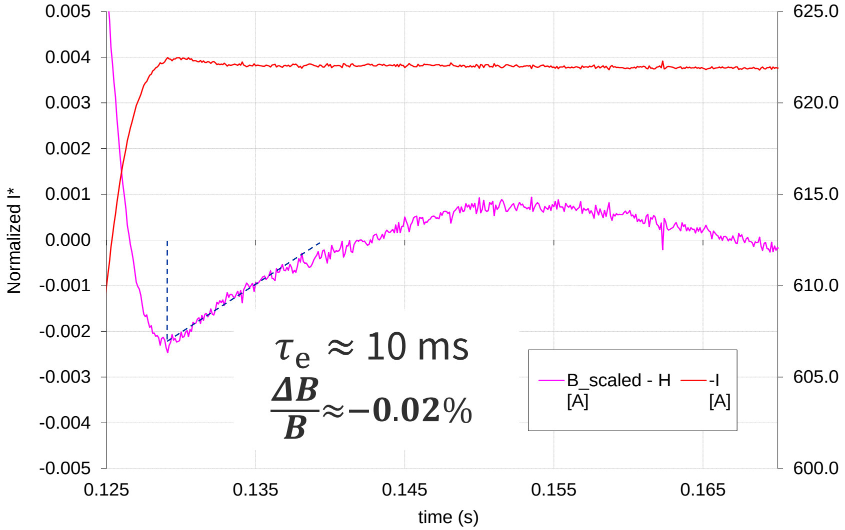

$\tau_e \approx 10$ ms

$\frac{\boldsymbol{\Delta B}}{\boldsymbol{B}} \approx \mathbf{-0.02\%}$

Passive attenuation of B_3 in CERN PS bumpers 1/3

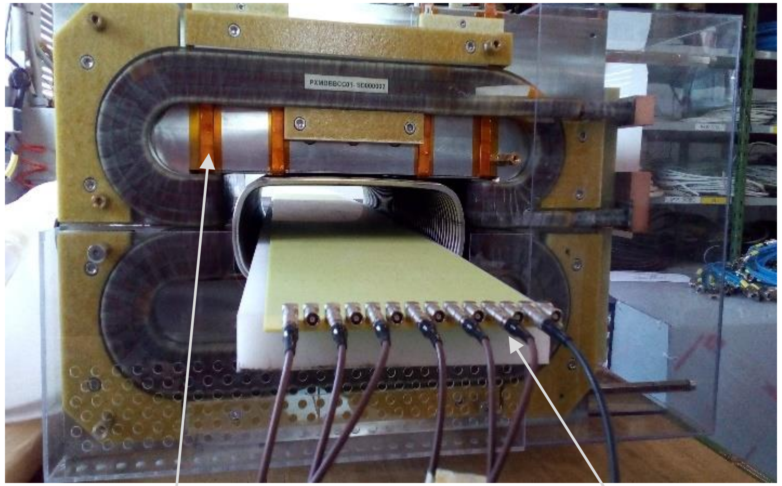

2 (top) + 2 (bottom) passive loops
open-circuit R_0=2 mΩ

Integral measurement coil array

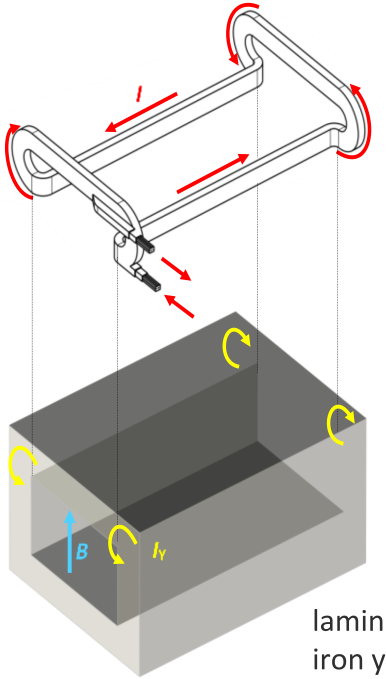

1-turn bedstead
excitation coils

laminated
iron yoke circuit

Vacuum chamber circuit

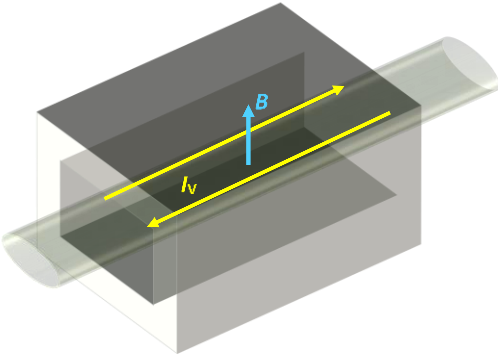

Passive loop circuit

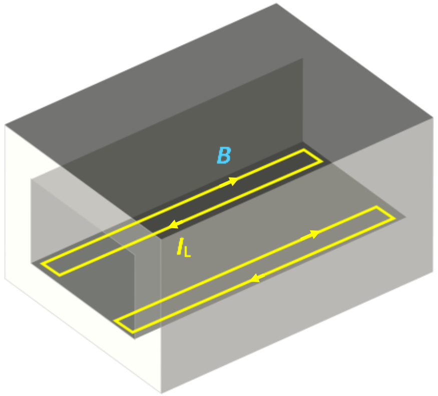

- “Simpler” problem: just compensate B_3 attenuation
- Difficult calculation: ~200 T/s, corrugated vacuum chamber → experimental approach

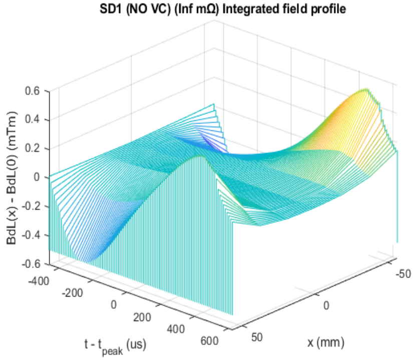

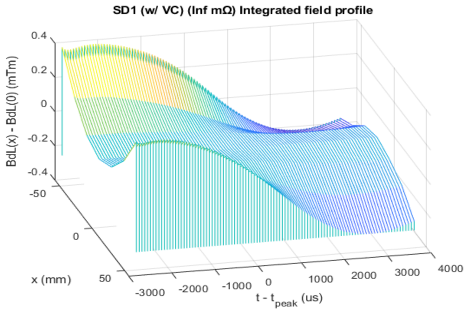

$$\begin{cases} L_Y \dfrac{dI_Y}{dt} + R_Y I_Y + M_Y \dfrac{dI}{dt} = 0 \\ L_V \dfrac{dI_V}{dt} + R_V I_V + M_V \dfrac{dI}{dt} = 0 \\ L_L \dfrac{dI_L}{dt} + (R_0 + R_L) I_L + M_L \dfrac{dI}{dt} = 0 \end{cases}$$

3 eddy current circuits driven by dI/dt

Passive attenuation of B$_3$ in CERN PS bumpers 2/3

- Solve analytically for half-sine current pulse
- Re-parameterize and linearize B vs d*I*/*dt*

$$I = I_0 \sin\left(\pi \frac{t}{T}\right) \qquad \dot{I} = \frac{\pi}{T} I_0 \cos\left(\pi \frac{t}{T}\right)$$

$$I_{\mathrm{E}}(t) = -I_0 \frac{\tau_{\mathrm{EM}}}{T} \frac{\pi}{1+\pi^2 \frac{\tau_{\mathrm{E}}^2}{T^2}} \left[-e^{-\frac{t}{\tau_{\mathrm{E}}}} + \pi \frac{\tau_{\mathrm{E}}}{T} \sin\left(\pi \frac{t}{T}\right) + \cos\left(\pi \frac{t}{T}\right)\right]$$

$$\frac{B_n}{N_{\mathrm{t}} k I_0} = \gamma \frac{\tau_{\mathrm{EM}}}{T} e^{-\frac{t}{\tau_e}} + \left(1 - \pi\gamma \frac{\tau_{\mathrm{E}} \tau_{\mathrm{EM}}}{T^2}\right) \sin\left(\frac{\pi t}{T}\right) - \gamma \frac{\tau_{\mathrm{EM}}}{T} \cos\left(\frac{\pi t}{T}\right)$$

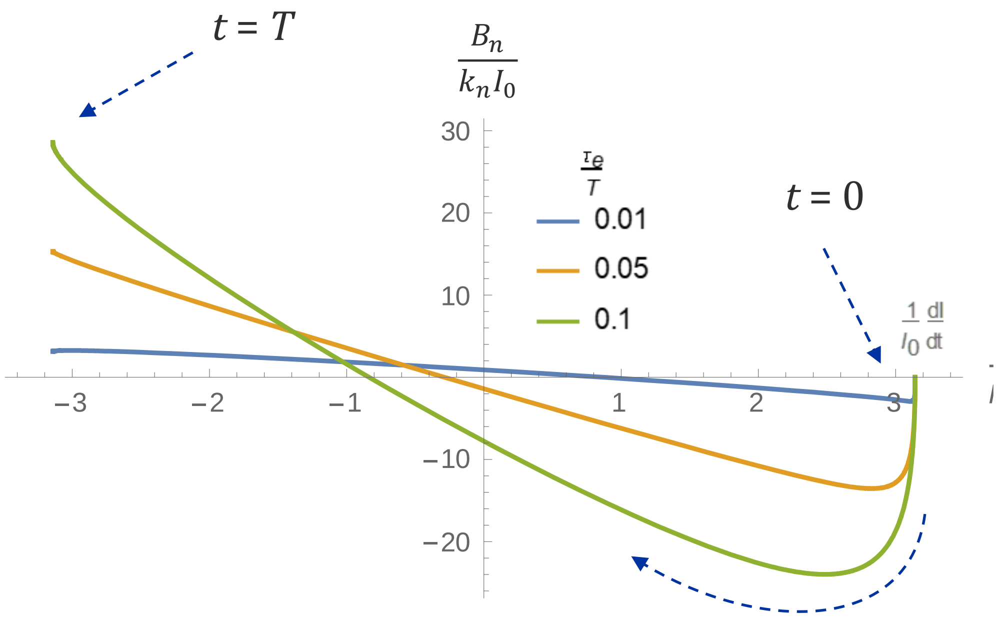

$$\lim_{\substack{R_{\mathrm{E}}\to\infty \\ \tau_{\mathrm{E}}\to 0 \\ \tau_{\mathrm{EM}}\to 0}} \left.\frac{\partial B_n}{\partial \dot{I}}\right|_{\dot{I}=0} = -k_{\mathrm{E}} \frac{M_{\mathrm{E}}}{R_{\mathrm{E}}}$$

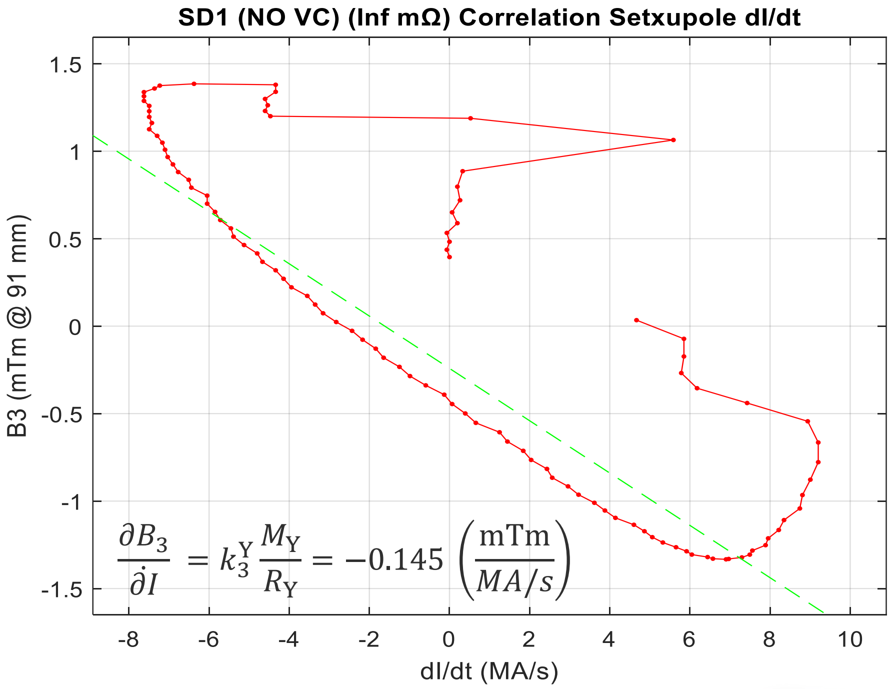

Passive attenuation of B_3 in CERN PS bumpers 3/3

Excitation current

Eddy currents

$$B_3 = k_3 I + k_{\mathrm{Y},3} I_{\mathrm{Y}} + k_{\mathrm{V},3} I_{\mathrm{V}} + k_{\mathrm{L},3} I_{\mathrm{L}} \approx k_3 I + \dot{I} \left.\frac{\partial B_3}{\partial \dot{I}}\right|_{\dot{I}=0}$$

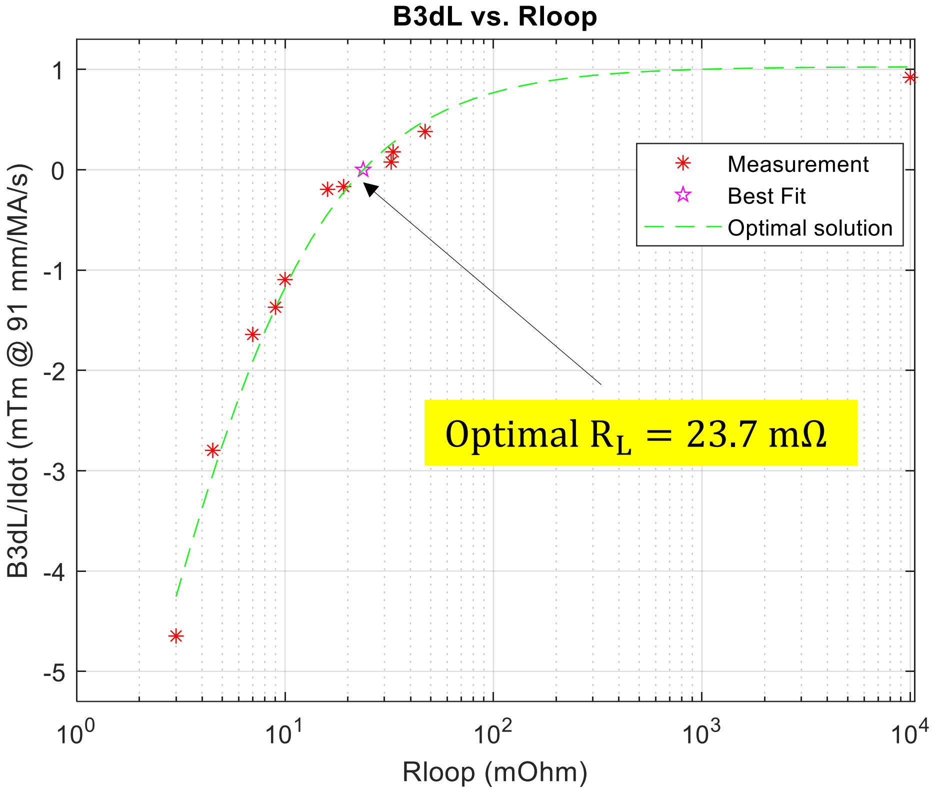

Optimal $\mathrm{R_L} = 23.7\ \mathrm{m\Omega}$

Best-fit results $1.0276 \quad -26.407$

$$\left.\frac{\partial B_3}{\partial \dot{I}}\right|_{\dot{I}=0} \approx -k_{\mathrm{Y},3}\frac{M_{\mathrm{Y}}}{R_{\mathrm{Y}}} - k_{\mathrm{V},3}\frac{M_{\mathrm{V}}}{R_{\mathrm{V}}} - k_{\mathrm{L},3}\frac{M_{\mathrm{L}}}{R_0 + R_{\mathrm{L}}} = a + \frac{b}{R_0 + R_{\mathrm{L}}}$$

$-0.145 \quad 1.066 \quad \begin{cases} R_{\mathrm{L}} \approx 0 & -22.3 \\ R_{\mathrm{L}} = \infty & 0 \end{cases} \quad \frac{\mathrm{mTm}}{M\,A/s}$

Individual measurement results (cross-check)

- The corrective capability of the passive loops is 5 × what is strictly necessary
- Reasonable fit, if not very precise around zero
- Optimal resistors being installed for 2024 run

Open-loop control of ripple effects

Ripple attenuation by eddy currents

- Observation in PS main magnet: ripple in measured field, current and beam radial position
- Assume: eddy current I_e through poles || I_m → same effect on field
- Nominal DC gain = **2.5 G/T** up to ~1 Hz
- Gain drops **to 1.5 G/A @ 27 Hz**, constant for > 100 Hz (magnet's L/R filtering effect already included)

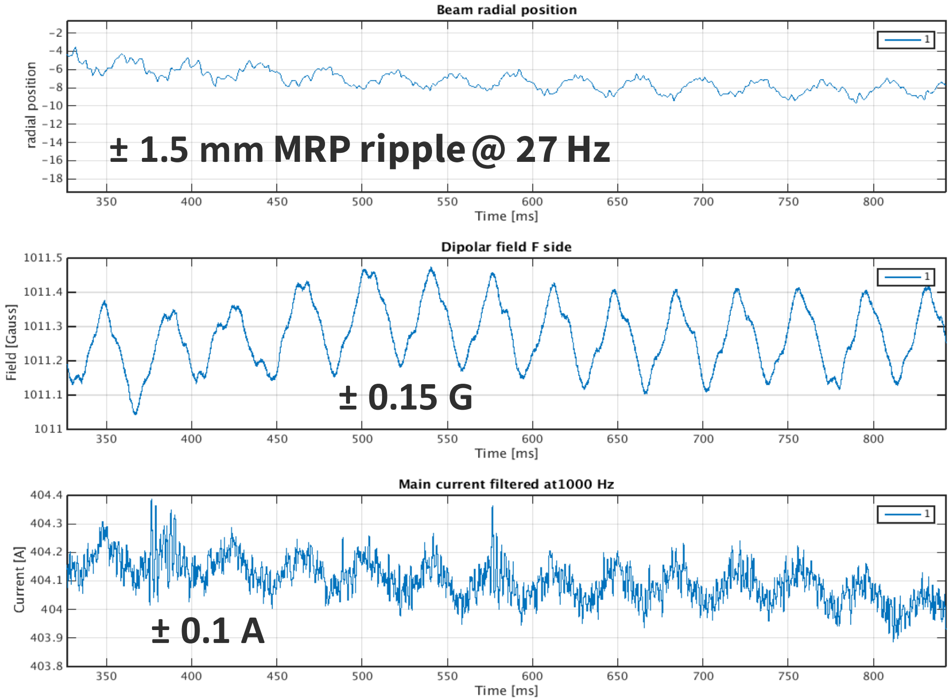

$$\begin{cases} I_\mathrm{e} + \tau_\mathrm{e}\dfrac{dI_\mathrm{e}}{dt} = \tau_\mathrm{em}\dfrac{dI_\mathrm{m}}{dt} \\ B = k(I_\mathrm{m} + I_\mathrm{e}) \end{cases}$$

$$\frac{B}{I_\mathrm{m}} = k\frac{1 + (1 - \frac{\tau_\mathrm{em}}{\tau_\mathrm{e}})\tau_\mathrm{e} s}{1 + \tau_\mathrm{e} s}$$

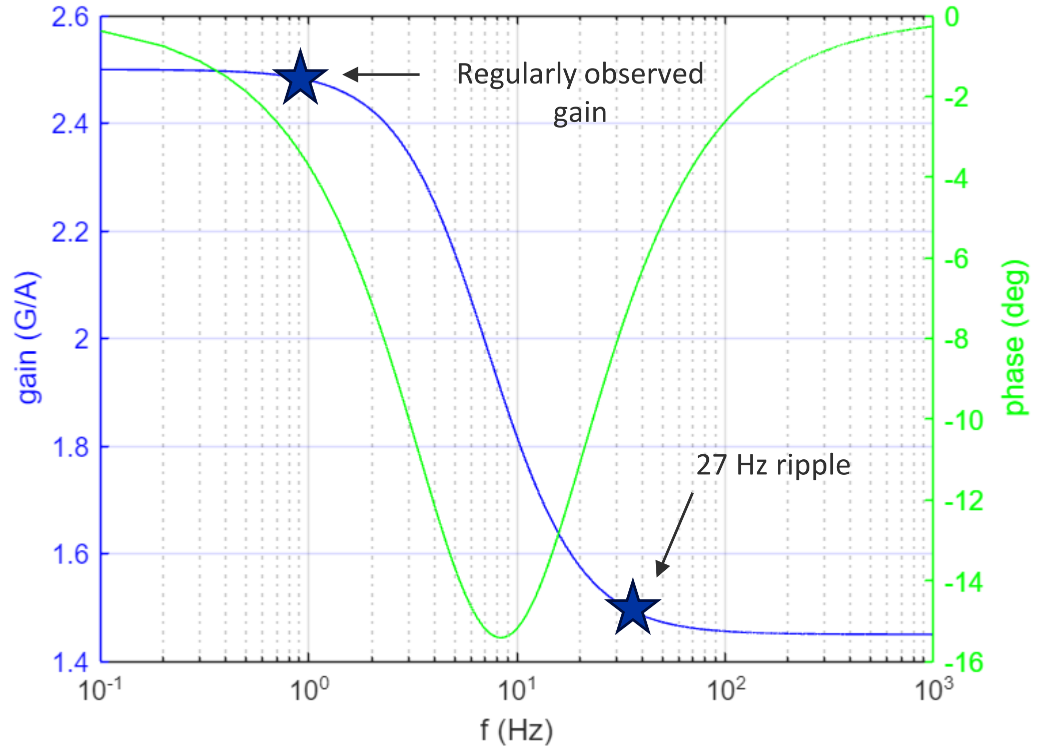

Ripple attenuation by shunt resistor

- Classic technique to damp high current frequencies: resistor in parallel with excitation coil
- Example: CERN SPS MBB: R_m=3.2 mΩ, L_m=7.7 mH

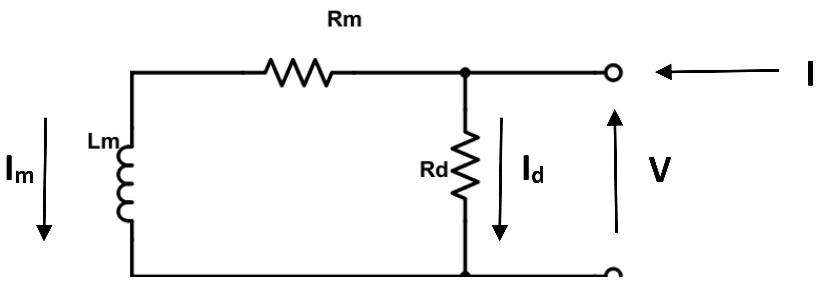

$$\frac{I_\mathrm{d}}{I} = \frac{R_\mathrm{m}}{R_\mathrm{d}} \frac{1 + i2\pi f\tau_\mathrm{m}}{1 + \frac{R_\mathrm{m}}{R_\mathrm{d}}(1 + i2\pi f\tau_\mathrm{m})}$$

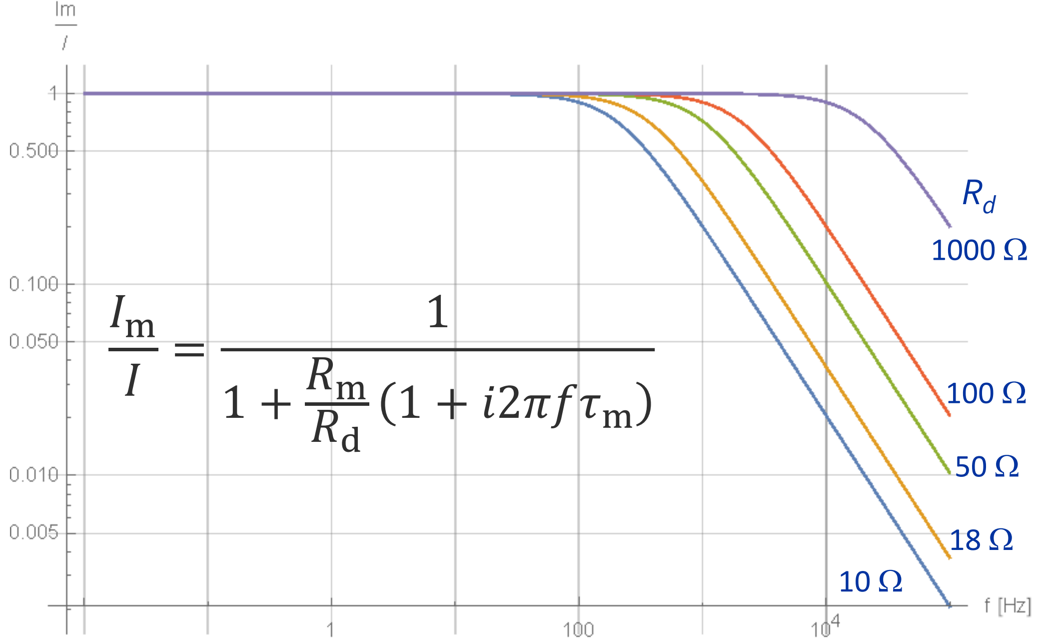

$$\frac{I_\mathrm{m}}{I} = \frac{1}{1 + \frac{R_\mathrm{m}}{R_\mathrm{d}}(1 + i2\pi f\tau_\mathrm{m})}$$

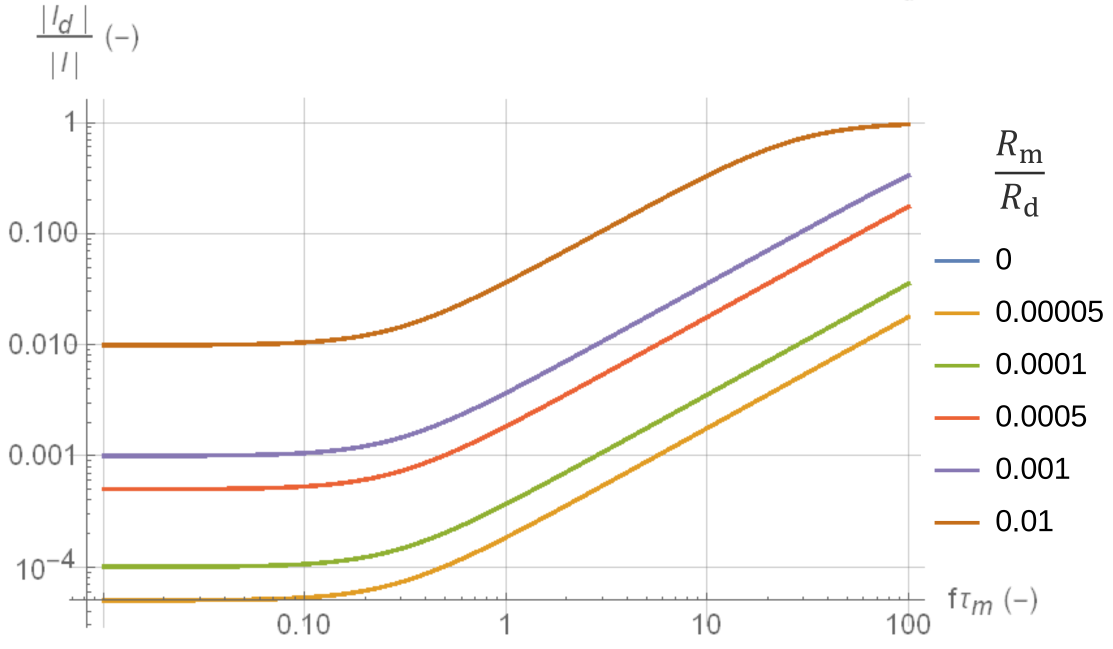

Open-loop control with mathematical models

Lumped-parameters mathematical models

- Single DOF, (if possible) analytical models **$B(t) = f(I, dI/dt, t, I(t' \leq t) \ldots) = F(I(t))$**

- Applications of the forward model:

  1. provide real-time field information to machine operation and other users
  2. predict cycle-to-cycle hysteresis effects to pre-set lattice corrections
  3. complement or replace real-time field measurement systems (“B-trains”): internal diagnostics, replacement during failures or dry runs, of long-term full replacement
  4. provide realistic data to train more sophisticated models (e.g. Machine Learning)

- Applications of the inverse model: **$I(t) = F^{-1}(B(t))$**

  1. Obtain off-line the current cycles required to obtain the desired field

Mathematical models @ CERN

PS Booster

- crude replacement for the B-train
- did not work too well

$$B = B_\mathrm{r} + k_1 I_\mathrm{m} - k_2 \frac{dI_\mathrm{m}}{dt}$$

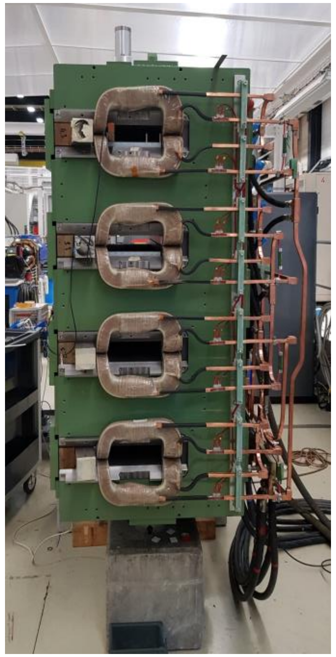

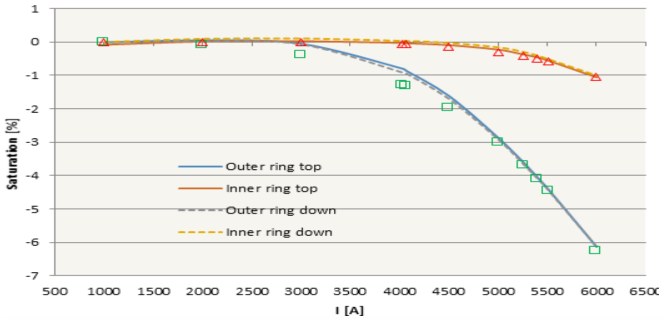

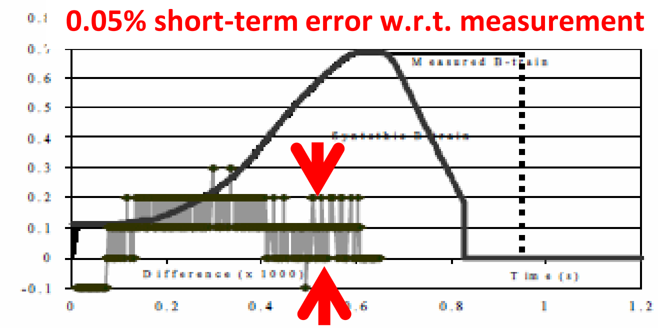
0.05% short-term error w.r.t. measurement

F. Caspers *et al.*, Alternative to Classical Real-time Field Measurements using a Magnet Model, ICALEPCS 97

Antiproton Decelerator

- works very well for unique repeated cycle
- emphasis on smooth B(t) feedback to RF (pbar beam is very fragile)

$$B = B_\mathrm{r} + \beta_1 I_\mathrm{m} + \beta_2 I_\mathrm{m}^2 + \beta_3 I_\mathrm{m}^3 - kL \frac{dI_\mathrm{m}}{dt}$$

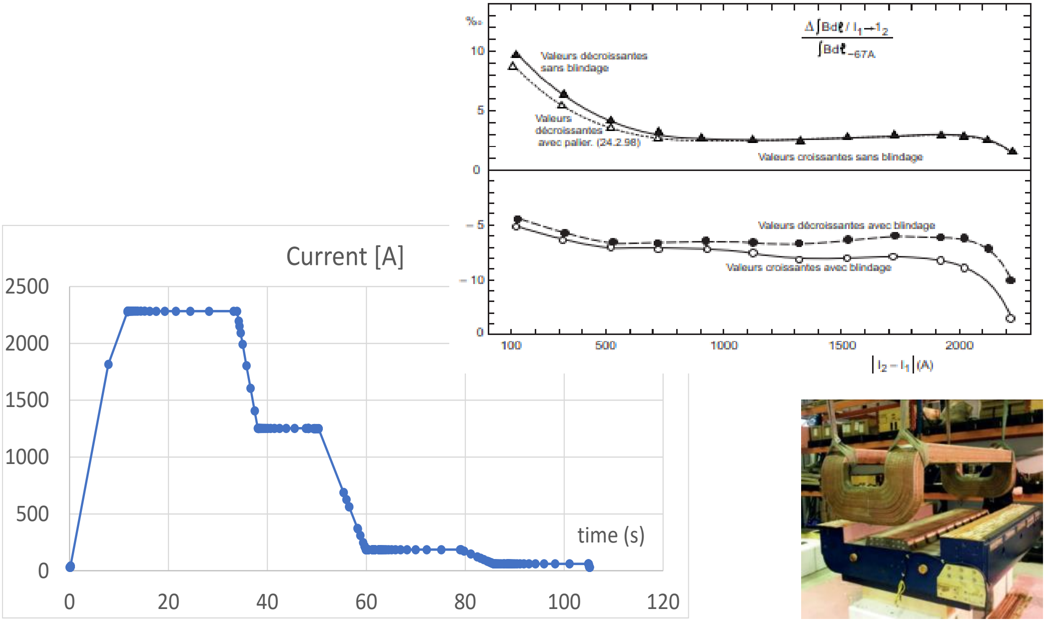

ELENA bending dipole model

- unique case at CERN: ELENA needs both accelerating and decelerating cycles
- First approximation: neglect hysteresis and eddy currents, use polynomial anhysteretic curve
- Stable cycling obtained within the correction capabilities of the RF radial loop

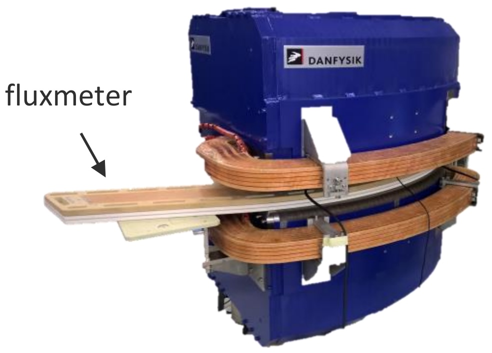

$$\frac{\int B d\ell}{I} = a\left(1-\left(\frac{I}{I_o}\right)^5\right)$$

a = 1.278 mTm, $I_0 \approx 350$ A

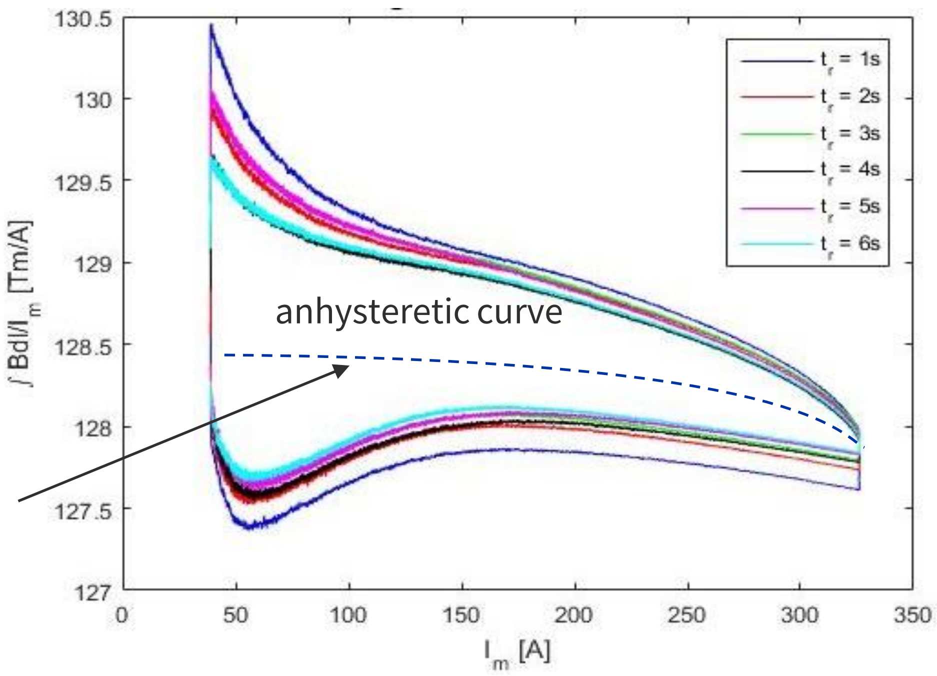

Approximate inversion of the polynomial

Assume: $I \approx \frac{\int B d\ell}{a} + \varepsilon$

$$I \approx \frac{\int B d\ell}{a}\left(1+\frac{1}{a^5\left(\frac{I_o}{\int B d\ell}\right)^5 - 5}\right)$$

Credit: Lajos Bojtar

Machine Learning

- Very promising approach for the interpolation of non-linear dynamical effects
- Studies in progress for open- and closed-loop applications

Modelling the pole field of a small test quadrupole
On the right, a sequence of training cycles
with gradually increasing flat-top.

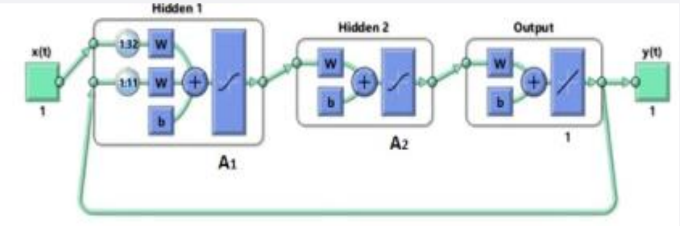

3-layer, 8-node autoregressive NN implemented in Matlab.

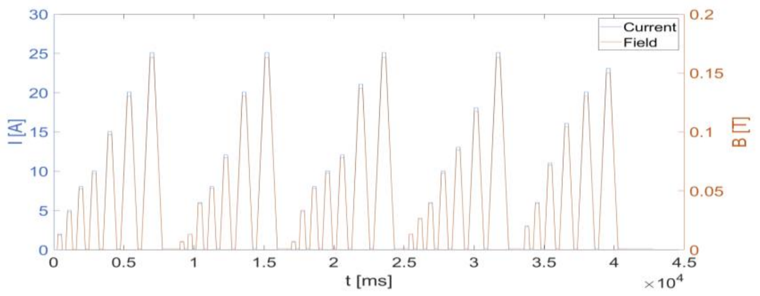

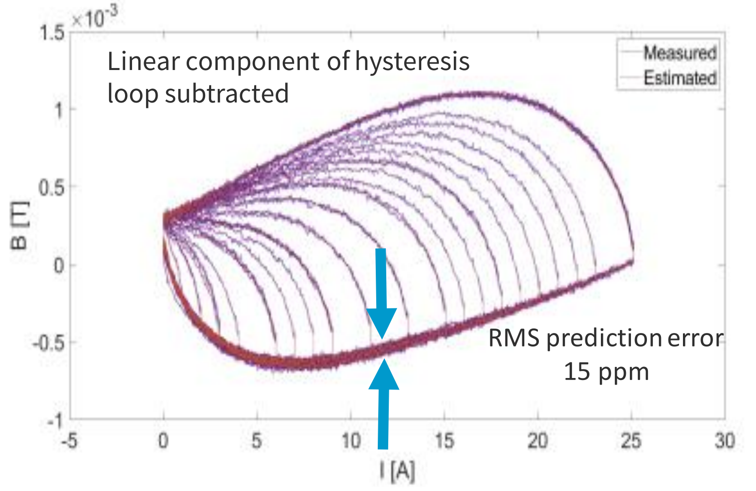

Linear component of hysteresis loop subtracted

RMS prediction error 15 ppm

Comparison prediction/measurement on cycles with increasing, but different flat-top levels respect to training (only the non-linear component is shown in the figure). In this simple case, the interpolating capability of the autoregressive NN is excellent.

(V Di Capua, "Hysteresis modeling in iron-dominated magnets based on a Deep Neural Network approach", *Int. Journal of Neural Systems*)

SPS main dipole field prediction vs measured, for fixed target cycles

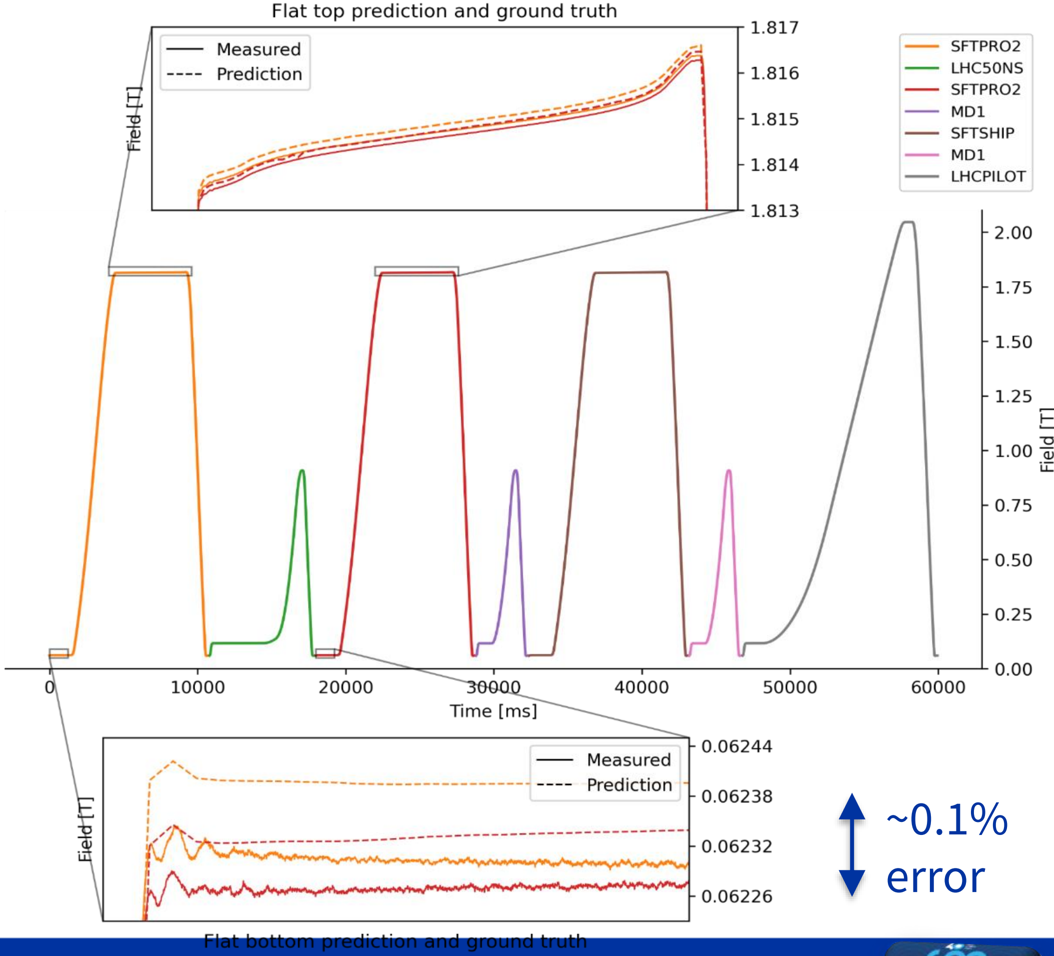

~0.1% error

Credit: Anton Lu

Open-loop control of hysteresis effects

Cycle reproducibility examples

ELENA dipole

Integral transfer function

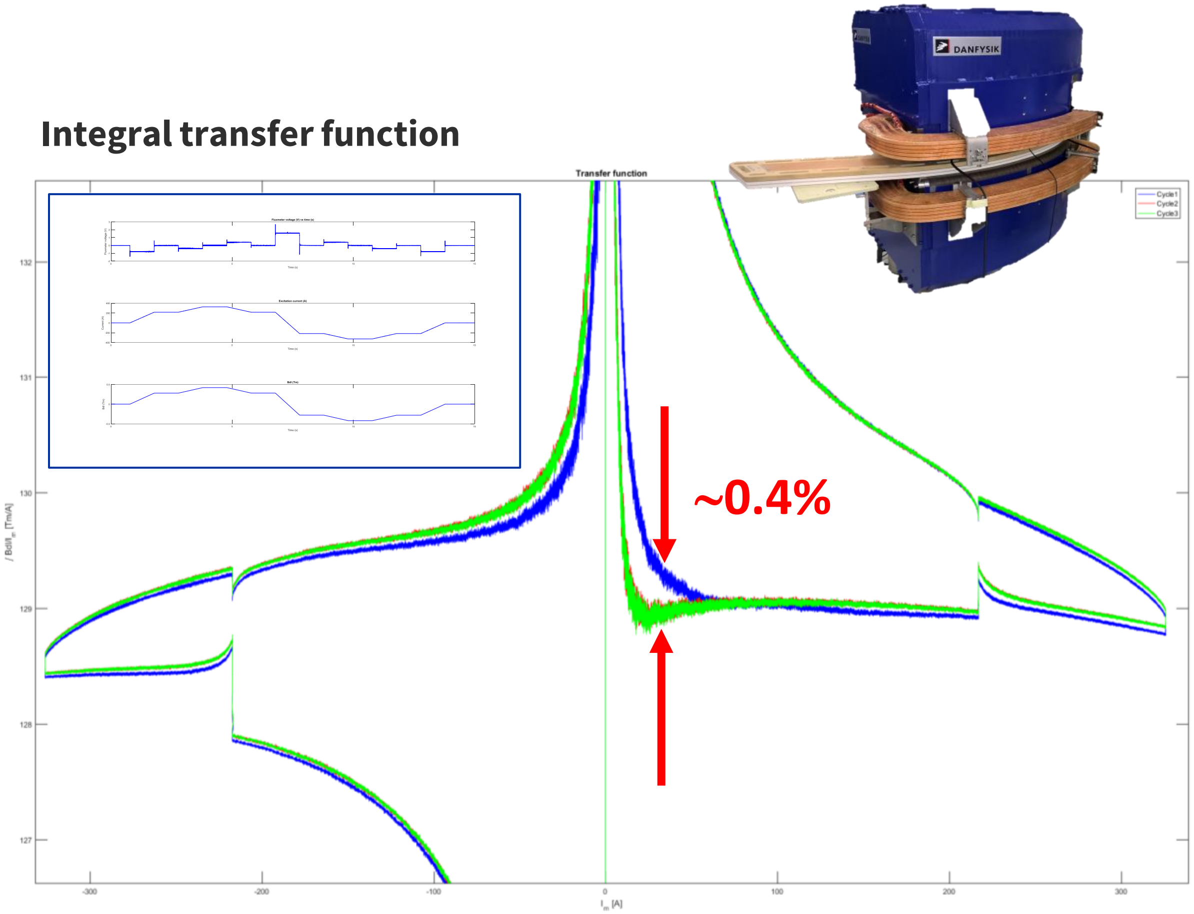

ISOLDE TL dipole

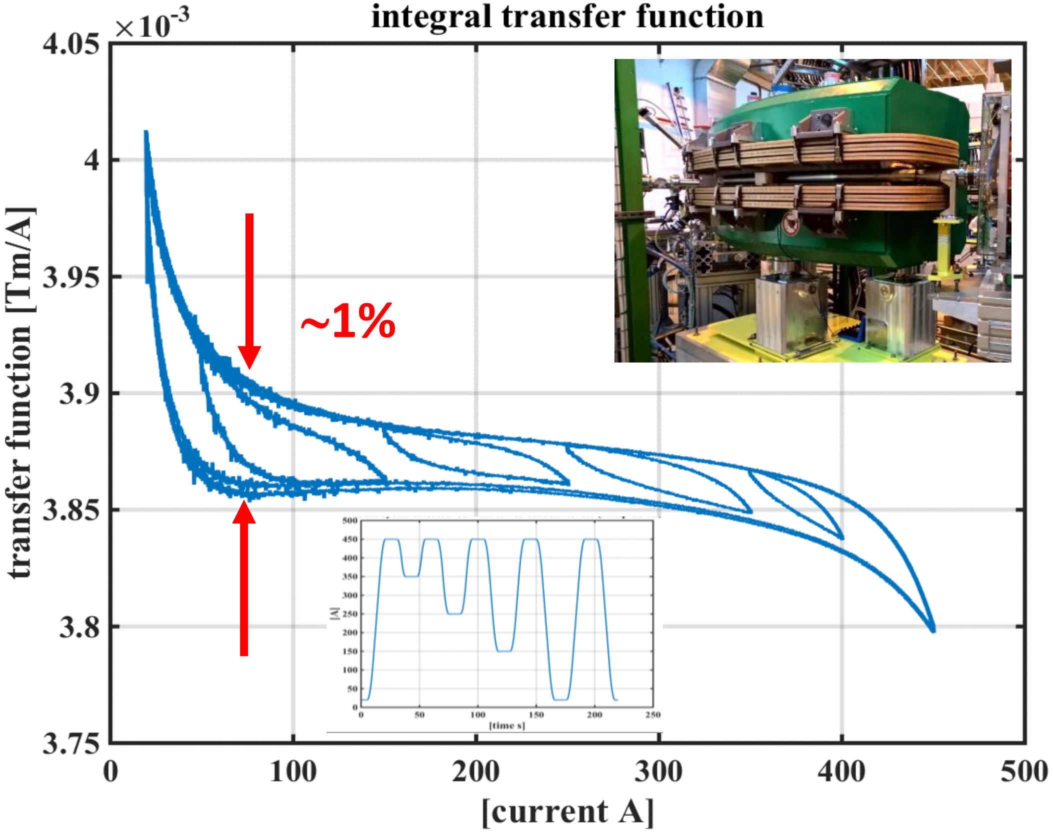

Credit: Christian Grech, Giancarlo Golluccio

Pre-cycling strategies for reproducibility

- Magnetic field reproducibility improves by resetting the magnetic state with current pre-cycles
- The normal **operating mode** of the magnet should be respected
- Dot change the current direction (**monotonic cycling**) or the ramp rate
- Prefer **high currents**: maximum (go into saturation) and minimum (avoid remanent field)

Demagnetization (degaussing)

- Best for <u>bipolar</u> magnets (correctors, steerers …)
- Requires bipolar (better 4-quadrant) power supply … and patience

Normalization

- <u>Unipolar</u> “washing” or “normalization”
- Best when mirroring the typical operational cycles (at least, the extrema)

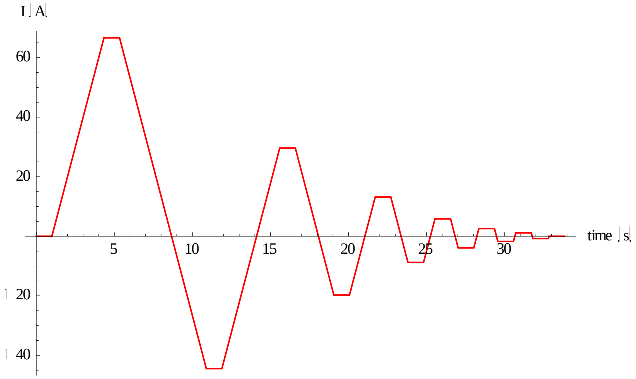

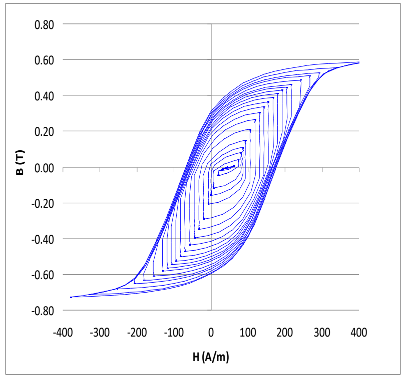

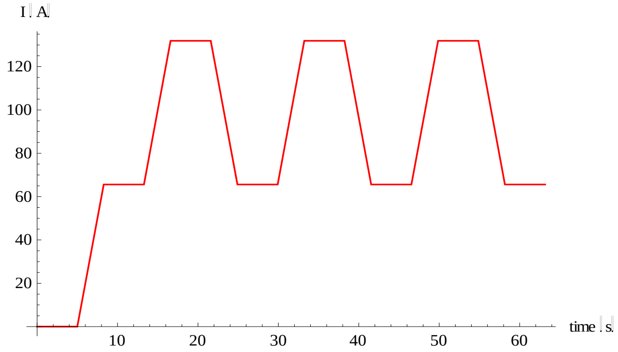

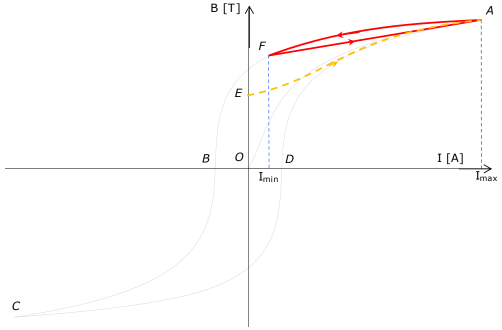

Pre-cycling example – RCS Proto 3

- Start from a stabilized state, then test transitions between ±1.4 and ±2.0 GeV
- The first cycle after a transition may differ up to $2 \cdot 10^{-3}$ from the stabilized value
- After any transition, integrated field stable within **$4 \cdot 10^{-5}$ after 2~3 reps** (limit: power supply stability, measurement noise)

- Results consistent with changes in measured $B_r \leq 1.6$ mT
- Highest |BdL| jumps associated with excitation sign change
- Central field stabilizes more quickly
- Changes of magnetic length **~$3 \cdot 10^{-3}$**

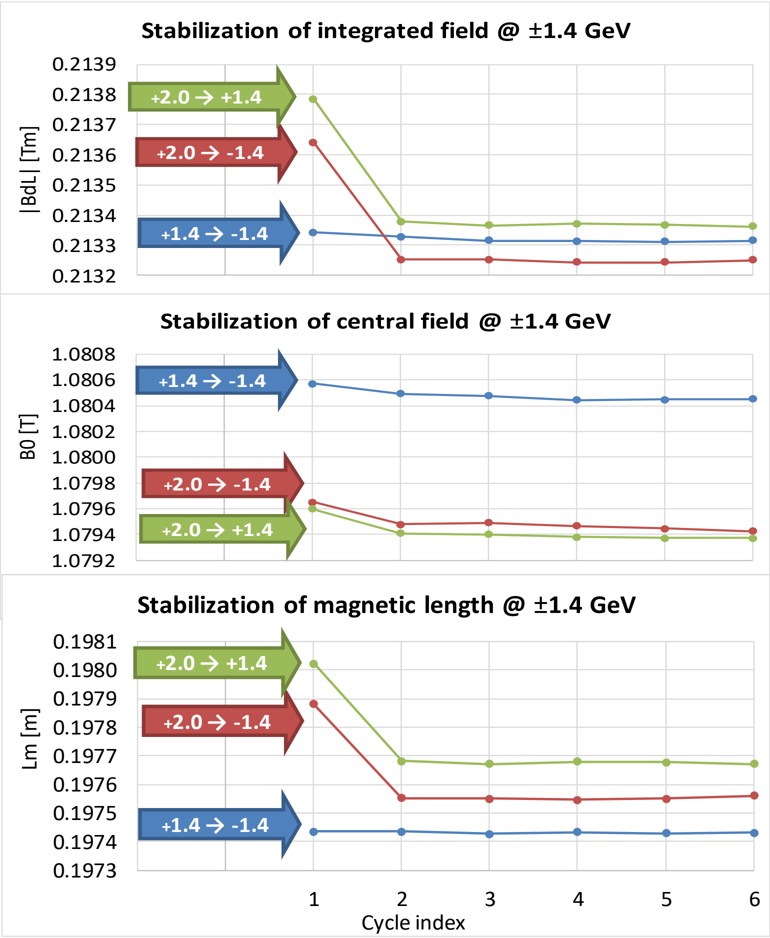

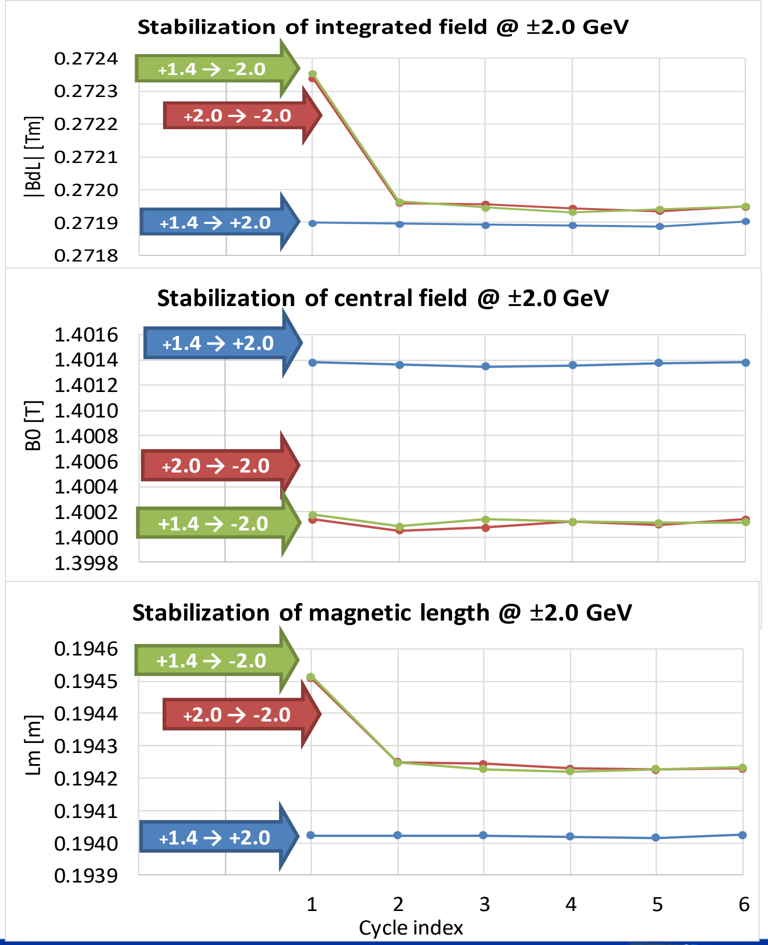

Demagnetization methods

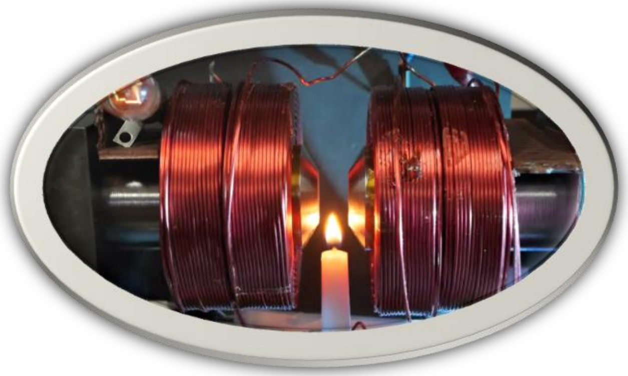

1) Thermal cycling

Guarantees a true thermodynamic reset of a randomly magnetized state

Drawback: requires $T \geq T_{curie} \approx 948$ °C …

2) Less orthodox methods

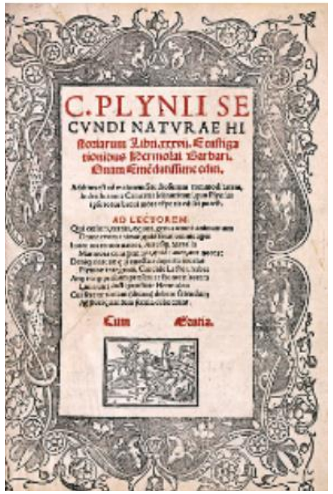

Pliny the Elder,
Natural History, Book XX

Some *alium*

Giambattista Della Porta
(Napoli, 1535-1615)

> La calamita non tira il ferro, se sarà fregata con l'aglio [...] Havendo fatto esperienza di questa cosa, l'ho ritrovata falsa, che non solo i fiati, e i rutti di coloro, che hanno mangiato agli non bastano à far che la calamita non facci l'ufficio suo, ma ongendola tutta di succo di agli, così facea le sue operationi, come se mai fusse stata di aglio bagnata, nè alcuna, ò nulla differenza si conosceva.

De Miracoli & Maravigliosi Effetti dalla Natura prodotti (1665)

AC Demagnetization

- Practical alternative to thermal cycling, when bipolar power supply is available
- Iterate cycling between extrema decreasing in absolute value: typically, $\frac{I_{k+1}}{I_k} = -\frac{2}{3}$

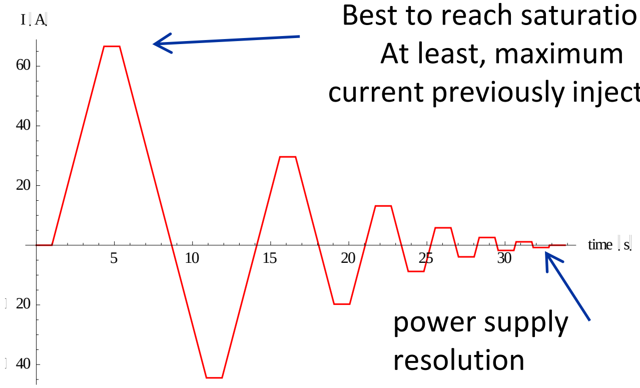

Best to reach saturation:
At least, maximum
current previously injected

power supply
resolution

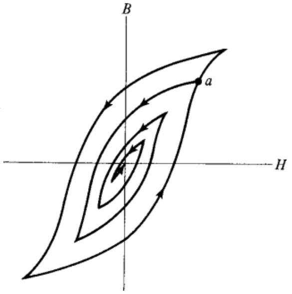

Stop-and-go linear ramps *or*
continuously decreasing
sinusoidal cycles
equally effective

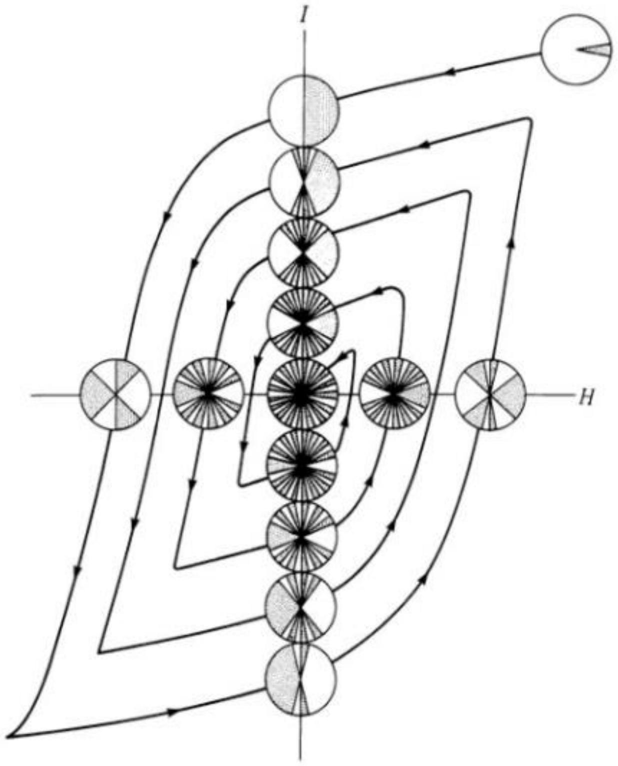

Cullity, *Introduction to Magnetic Materials*, Wiley 2009,

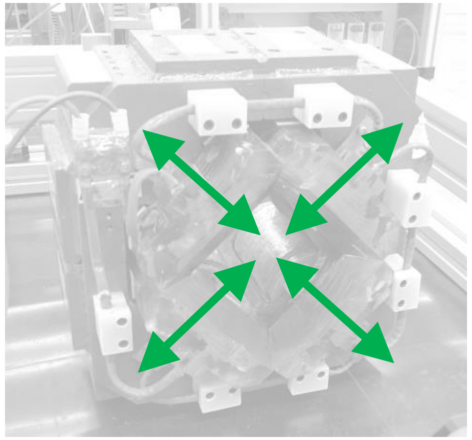

Easy case: ***B*** has mostly a fixed direction at any location (ignoring saturation, leakage) → degaussing needs only decreasing <u>amplitude</u>

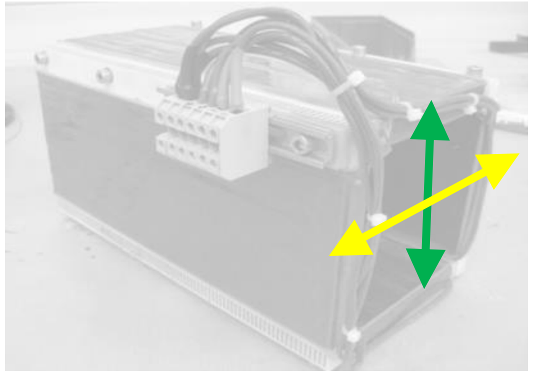

If variable ***B*** direction (XY correctors, trim or coupled excitation circuits) → degaussing must be done with a **rotating field** of decreasing <u>amplitude</u>

AC Demagnetization example – ELENA dipole

- I_{max}= 400 A (0.49 Tm): **0.45 → 0.02 mTm** (~25:1, **$3\cdot10^{-5}$** of full range)
- I_{max}= 326 A (0.43 Tm): **0.86 → 0.03 mTm** (~29:1, **$8\cdot10^{-5}$** of full range)

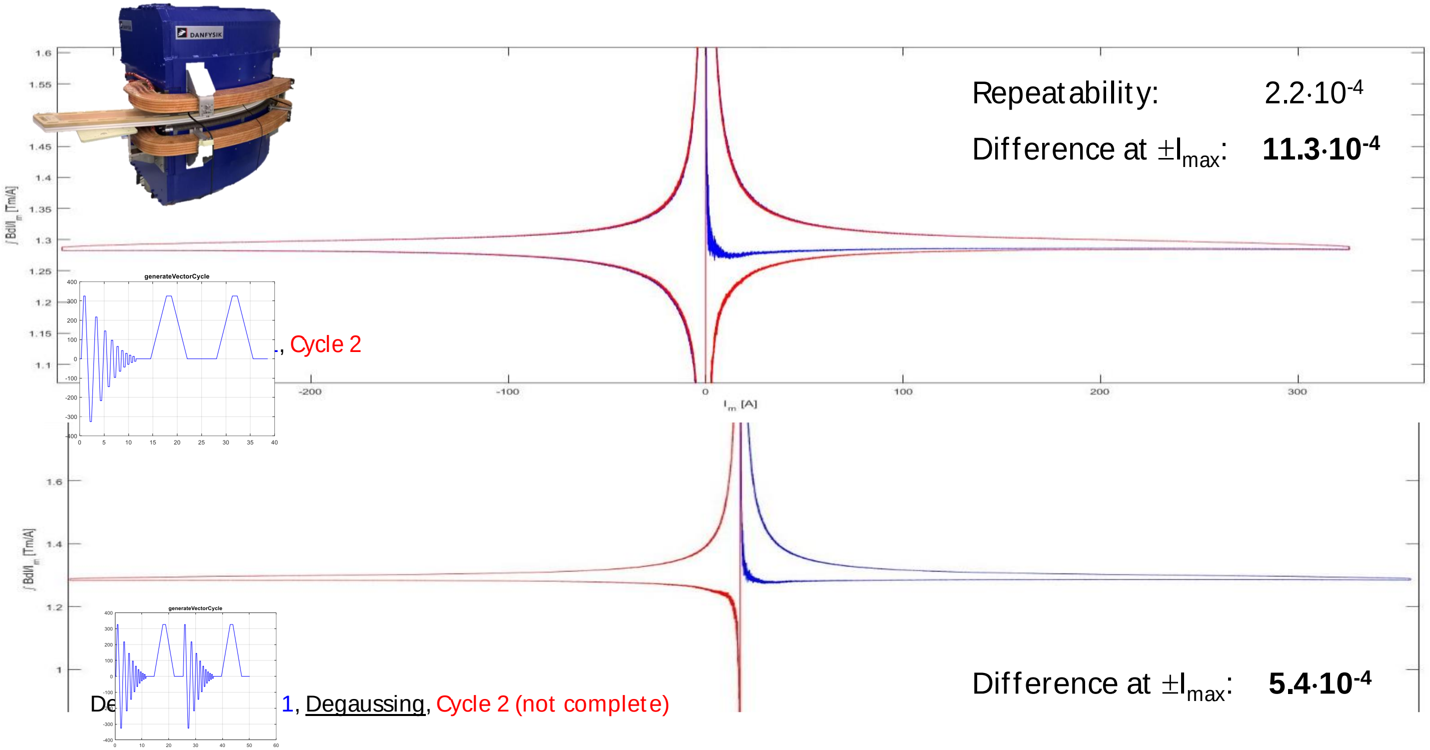

Repeatability: $2.2{\cdot}10^{-4}$

Difference at $\pm I_{max}$: **$11.3{\cdot}10^{-4}$**

, Cycle 2

Difference at $\pm I_{max}$: **$5.4{\cdot}10^{-4}$**

De 1, Degaussing, Cycle 2 (not complete)

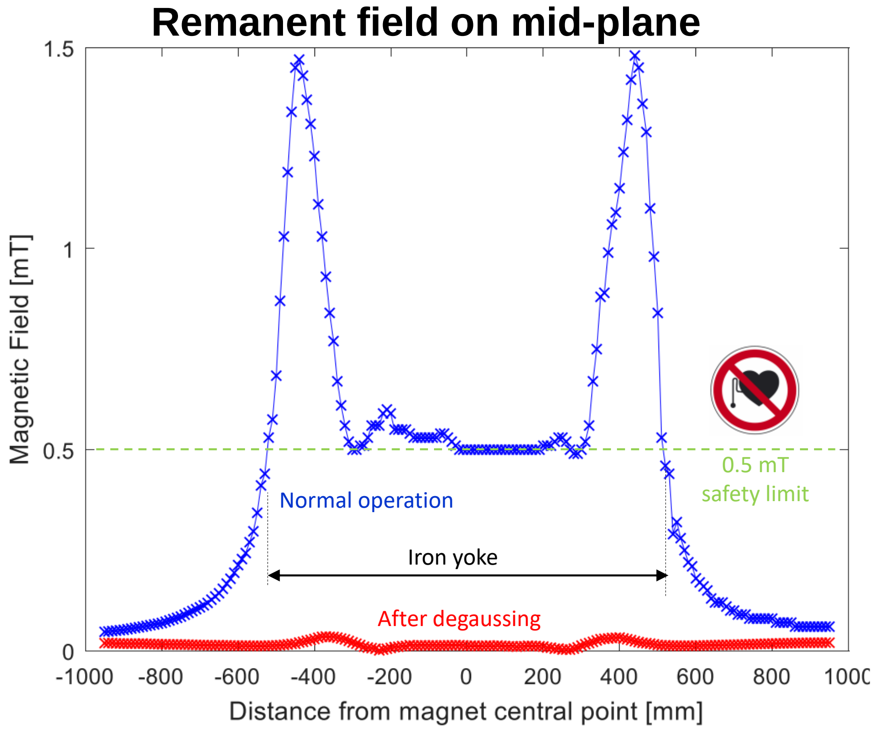

Credit: Christian Grech

One-shot degaussing

- Key idea: find the optimal ($-H^*$, B^*) point that allows to reach (0,0) with only two ramps
- Practical implementation: iterate based on approximation of the intrinsic coercivity

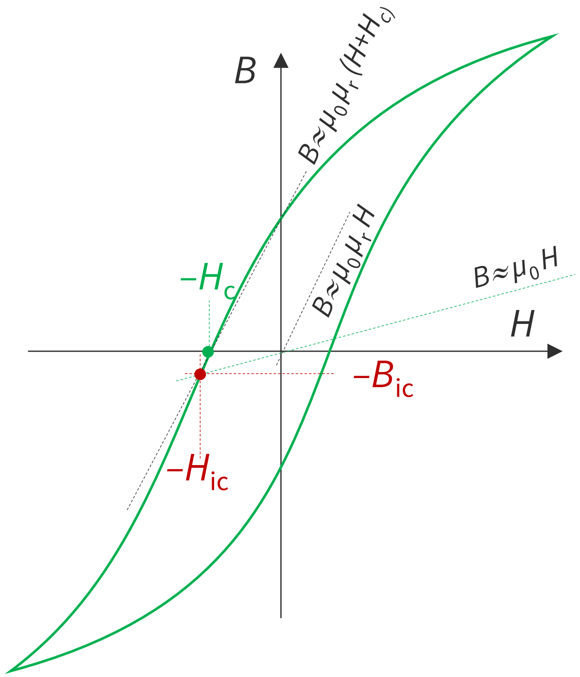

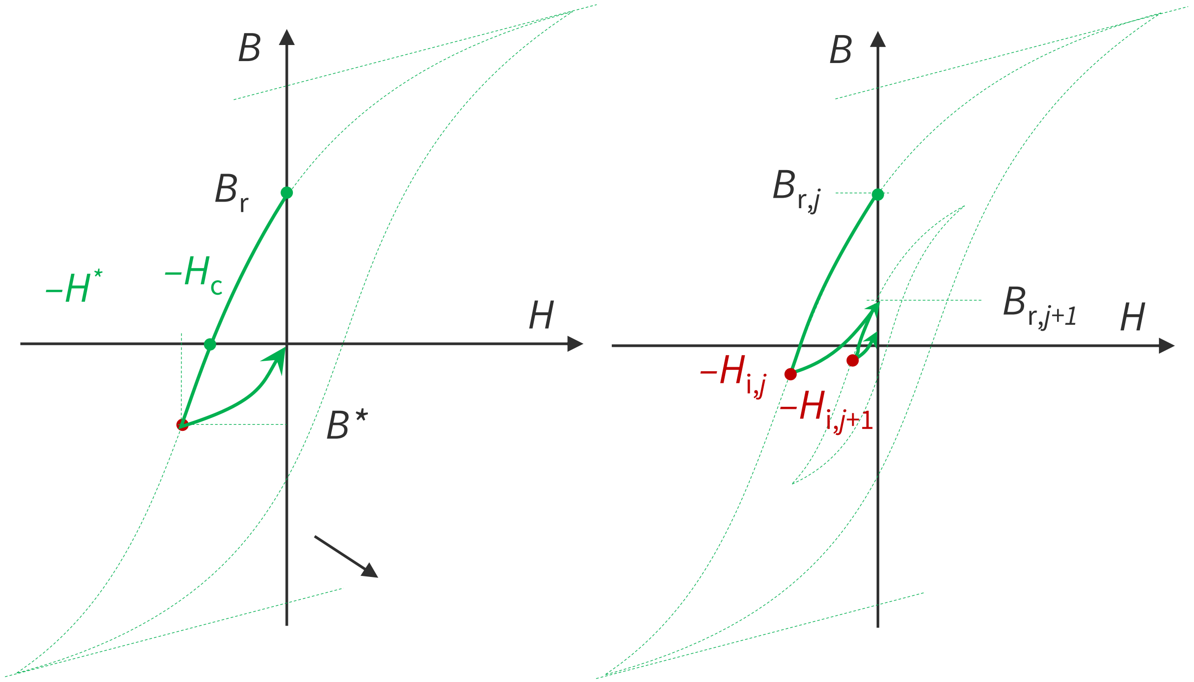

$$\begin{cases} B = \mu_0 \mu_r (H + H_c) \\ B = \mu_0 H \end{cases} \Longrightarrow H_{ic} \approx= -\frac{\mu_r}{\mu_r - 1} H_c$$

μ_r measured from the whole loop, or estimated as –Br/Hc

Virginia de Prieto, Degaussing application for medium and small magnets, *to be published*

Part IV – Closed-loop magnet control

Instrumentation for feedback control systems

Real-time magnetic field feedback

$$f_{\text{prg}} = \frac{c}{2\pi R}\sqrt{1 - \frac{1}{1 + \left(\frac{\bar{B}\rho q}{m_0 c}\right)^2}}$$

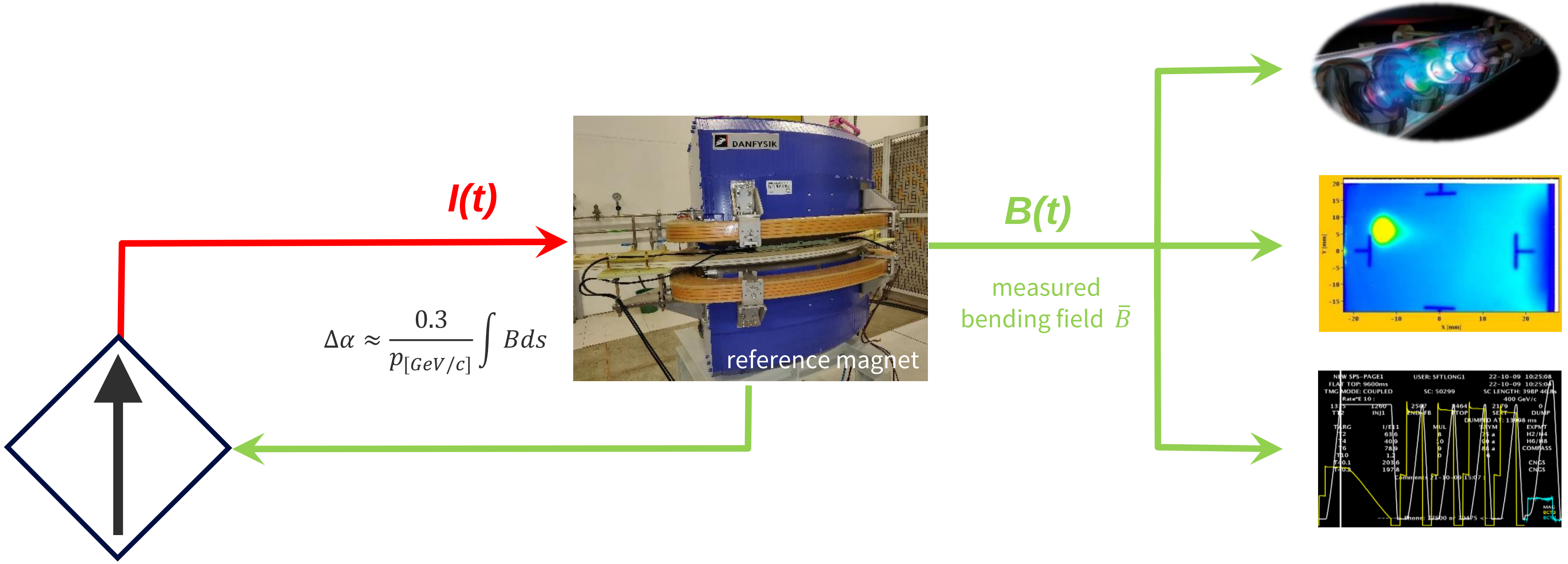

$$\Delta\alpha \approx \frac{0.3}{p_{[GeV/c]}}\int B ds$$

measured
bending field $\bar{B}$

RF control

BW ~ 100 kHz, latency ~ 20 µs

beam instrumentation

monitoring
diagnostics
qualitative feedback to operators

BW 1~ 10 kHz, latency ~ 1 ccyle

BW ~ 1 kHz, latency ~ 1 ms

control of individual magnets

control of synchrotron magnet circuits (“B-trains”)

Real-time measurement options

- Assume room available to install sensors on/close to the beam path
- Crucial factor: accuracy of magnetic length coefficient

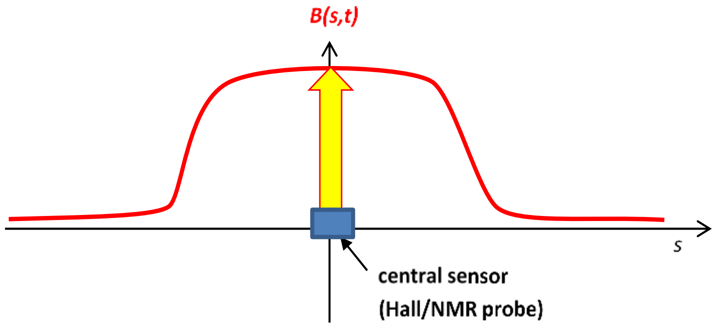	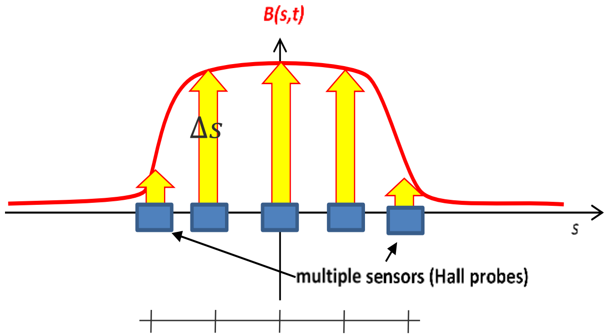	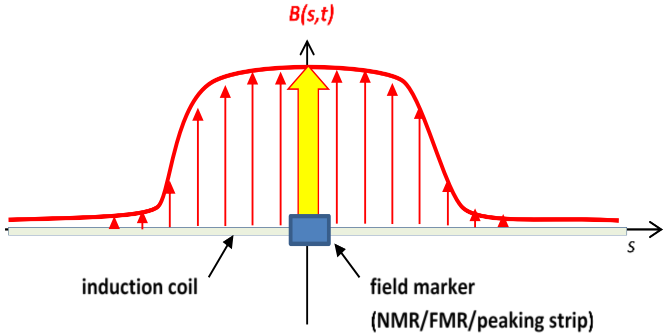
Single-sensor setup	**Multi-sensor setup**	**B-train system**
$\int B(s,t)ds = \ell_{\mathrm{m}}B(0,t)$	$\int B(s,t)ds = \sum_{k=1}^{n} \ell_{\mathrm{m},k}B(s_k,t)$	$\int B(s,t)ds = \ell_m B(0{,}0) + \int_0^t V_c(\tau)d\tau$
• classic solution (e.g. CERN ISOLDE and MEDICIS, Heidelberg B-train) • Bandwidth: few kHz for Hall probes, ~ 1 Hz for NMR (but: higher precision!) • limitations: calibration of ℓ_{m} by trial and error; best on stable hysteresis loops	• based on *n* inexpensive Hall probes • equivalent to classic map with one probe, moved at regular steps • advantages: $\lim_{n\to\infty} \ell_{\mathrm{m},k} = \Delta s = \mathrm{const.}$ • *n* to be optimized case-by-case	• high bandwidth and linearity thanks to integral induction coils • limitations: high deployment and maintenance cost

Local vs integral transfer function

$$l^* = \frac{2\pi R}{N_{\mathrm{BD}}}$$

$$\begin{cases} \ell_{\mathrm{m}} = \dfrac{1}{B_{\mathrm{m}}}\displaystyle\int_{-\infty}^{\infty} B(s)ds \\ \bar{B} = \dfrac{1}{l^*}\displaystyle\int_{-\infty}^{\infty} B(s)ds \end{cases} \Rightarrow \qquad \bar{B} = \frac{\ell_{\mathrm{m}}(s, I(t), I(\tau \le t))}{l^*} B_{\mathrm{m}}$$

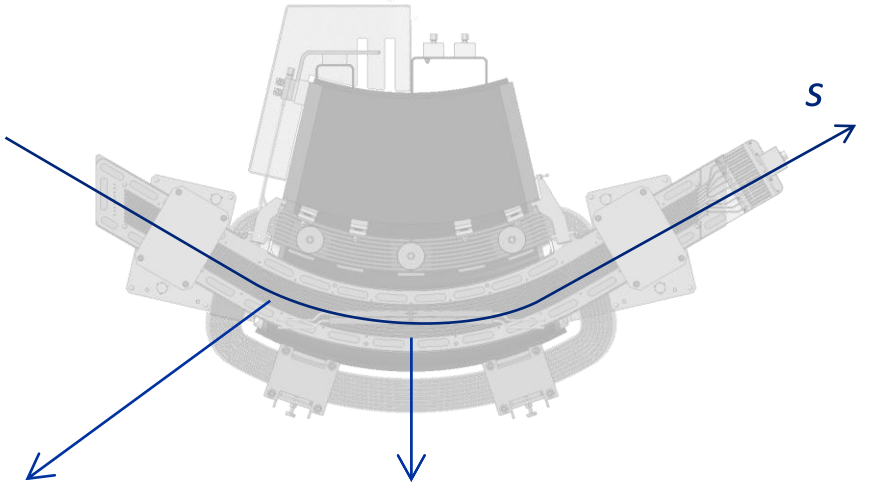

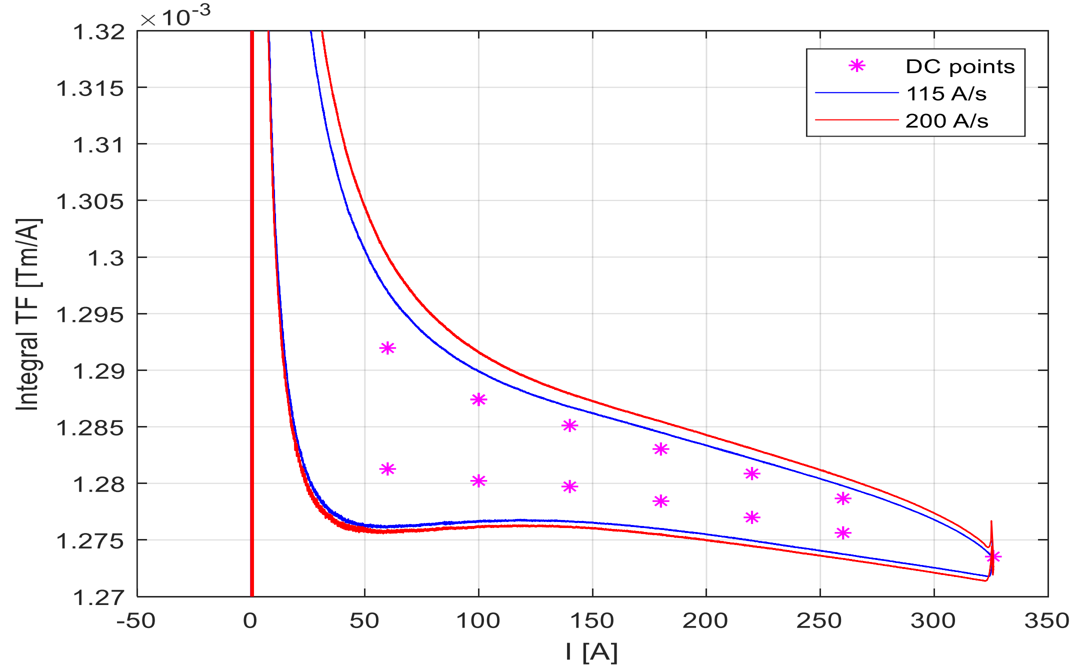

Edge Transfer Function

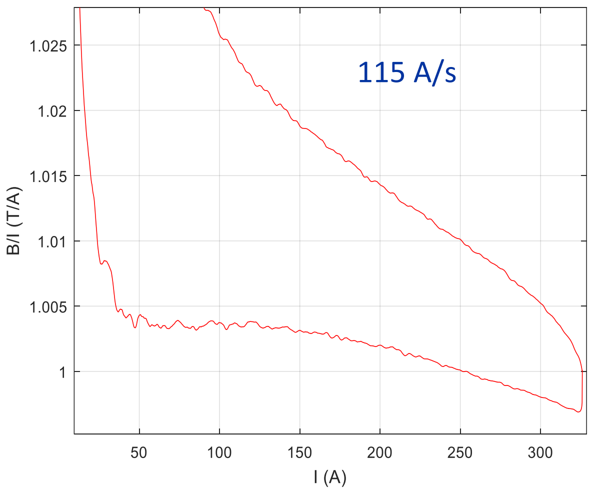

Central Transfer Function

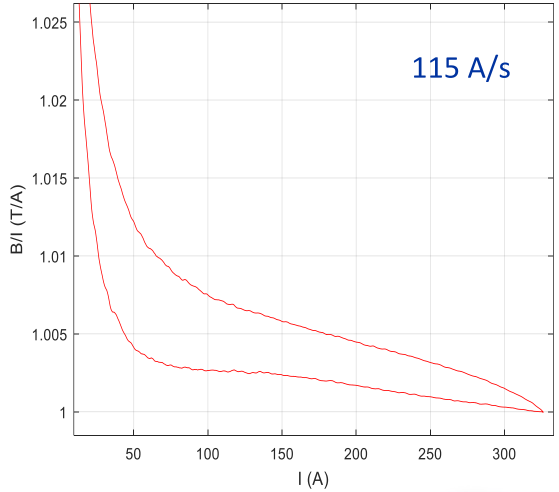

Optimal sensor location 1/3

- Goal: find longitudinal location s^* where the magnetic length does not depend upon excitation current
- Assume: field profile = linear + saturating components; gaussian shape functions

$$B(s,I) = B_0 \frac{I}{I_0}\left(\lambda(s) + \varsigma\left(\frac{I}{I_0}\right)\sigma(s)\right)$$

linearly scaling component associated coils/linear iron Gaussian shape, realistic for short magnets

non-linear components associated with saturating iron centered on pole edges

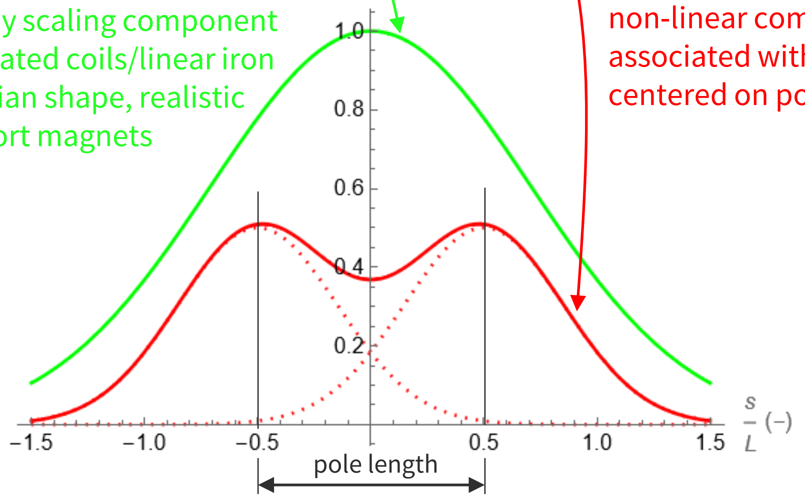

$$\varsigma\left(\frac{I}{I_0}\right) = 1 - \alpha\left(\frac{I}{I_0}\right)^n$$

Saturation characteristic
(as seen e.g. in the inductance model)

$$\ell_{\mathrm{m}}(s,I) = \frac{\int_{-\infty}^{\infty} B(\mathscr{s},I)\,d\mathscr{s}}{B(s,I)} = \frac{\int_{-\infty}^{\infty} \lambda(\mathscr{s})\,d\mathscr{s} + \varsigma\left(\frac{I}{I_0}\right)\int_{-\infty}^{\infty} \sigma(\mathscr{s})\,d\mathscr{s}}{\lambda(s) + \varsigma\left(\frac{I}{I_0}\right)\sigma(s)}$$

$$\ell_0 = \lim_{\substack{I\to 0\\ \eta_S\to 0}} \ell_{\mathrm{m}}(0,I) \qquad \frac{\partial \ell_{\mathrm{m}}}{\partial I} = 0 \implies \ell_{\mathrm{m}}\,(s^*) = \frac{\int_{-\infty}^{\infty} \lambda(\mathscr{s})\,d\mathscr{s}}{\lambda(s^*)} = \frac{\int_{-\infty}^{\infty} \sigma(\mathscr{s})\,d\mathscr{s}}{\sigma(s^*)}$$

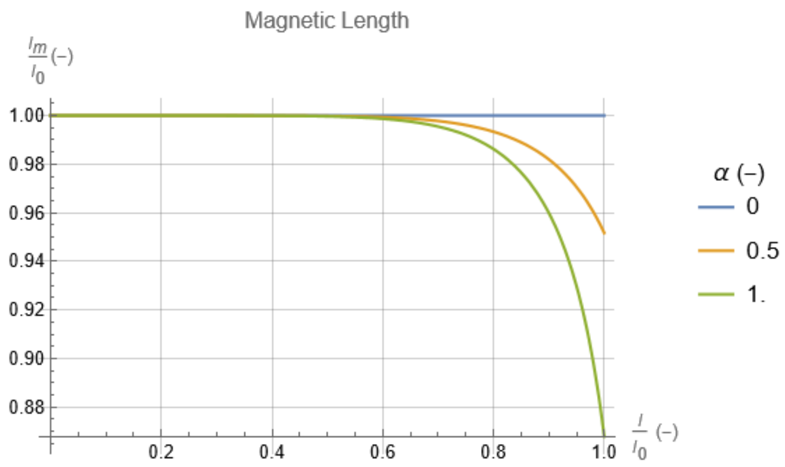

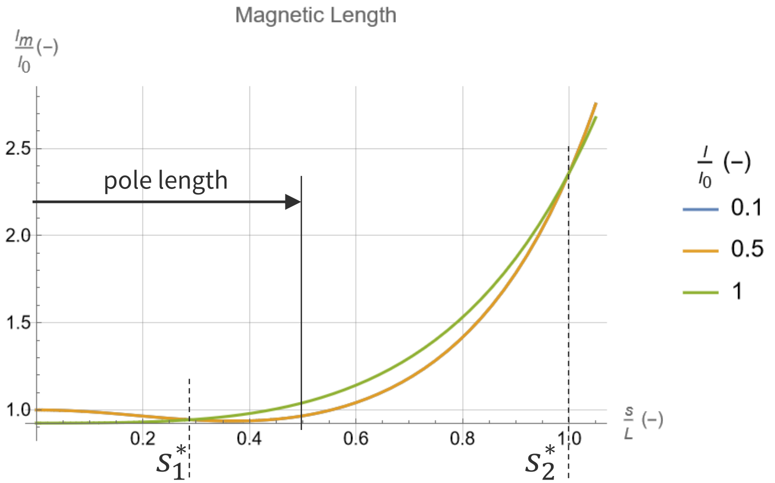

Optimal sensor location 2/3

- Further assume: non-overlapping edge components ($\eta_s \lesssim 0.2$)

$$\begin{cases} \lambda(s) = \mathrm{e}^{-\frac{s^2}{\eta_l{}^2 L^2}} \\ \sigma(s) = \mathrm{e}^{-\frac{\left(s+\frac{L}{2}\right)^2}{\eta_s{}^2 L^2}} + \mathrm{e}^{-\frac{\left(s-\frac{L}{2}\right)^2}{\eta_s{}^2 L^2}} \end{cases}$$

$$\lim_{\substack{\eta_l \to 1 \\ \eta_s \to 0}} \ell_\mathrm{m}^* = \frac{\sqrt{\pi}}{1+\mathrm{e}^{-\frac{1}{4}}} L \approx L$$

$$\ell_\mathrm{m}(s, I) = \sqrt{\pi} L \frac{\eta_\mathrm{L} + 2\eta_S \varsigma\left(\frac{I}{I_0}\right)}{\mathrm{e}^{-\frac{s^2}{\eta_\mathrm{L}{}^2 L^2}} + \varsigma\left(\frac{I}{I_0}\right)\left(\mathrm{e}^{-\frac{\left(s-\frac{L}{2}\right)^2}{\eta_\mathrm{S}{}^2 L^2}} + \mathrm{e}^{-\frac{\left(s+\frac{L}{2}\right)^2}{\eta_\mathrm{S}{}^2 L^2}}\right)}$$

$$\lim_{\eta_s \to 0} s^* = \pm \frac{1}{2} L$$

$$s^* \approx \frac{L}{2} \frac{1 \pm \sqrt{1 - \left(1 - \frac{\eta_S^2}{\eta_L^2}\right)\left(1 + 4\eta_S^2 \ln 2 \frac{\eta_S}{\eta_L}\right)}}{1 - \frac{\eta_S^2}{\eta_L^2}}$$

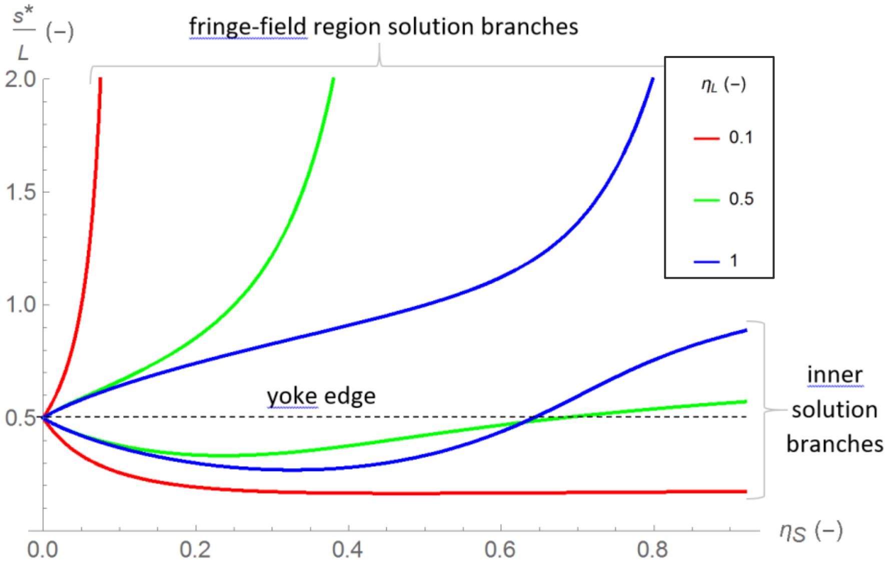

But: with dynamic effects ⇒
the optimal magnetic length cannot be a constant
seek s^* where the change of magnetic length is minimal

Optimal sensor location 3/3 – validation

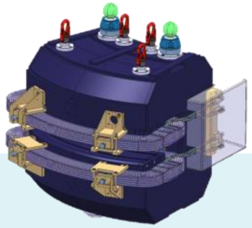

FE simulation of ELENA dipole

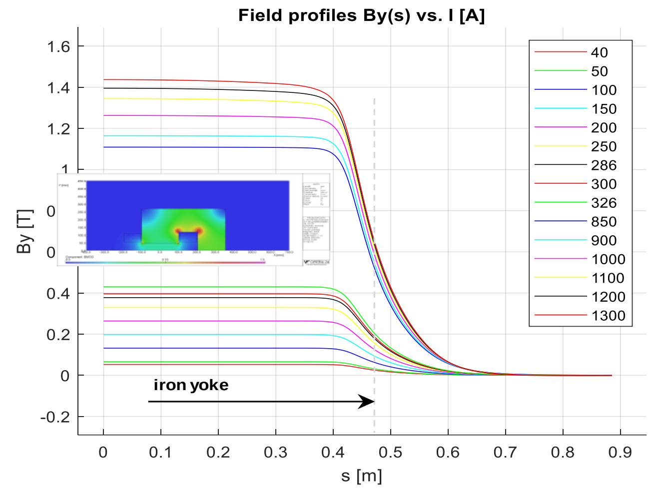

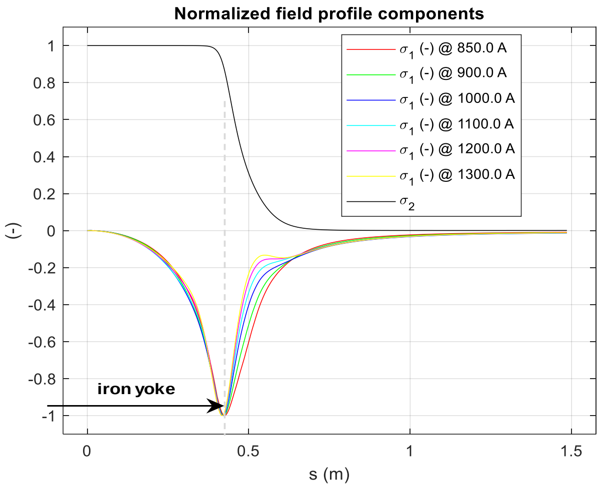

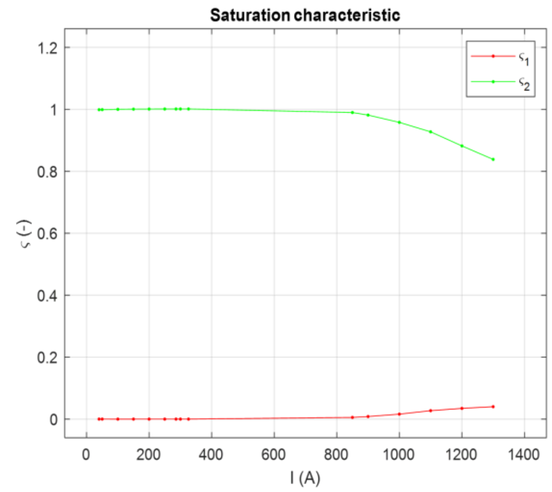

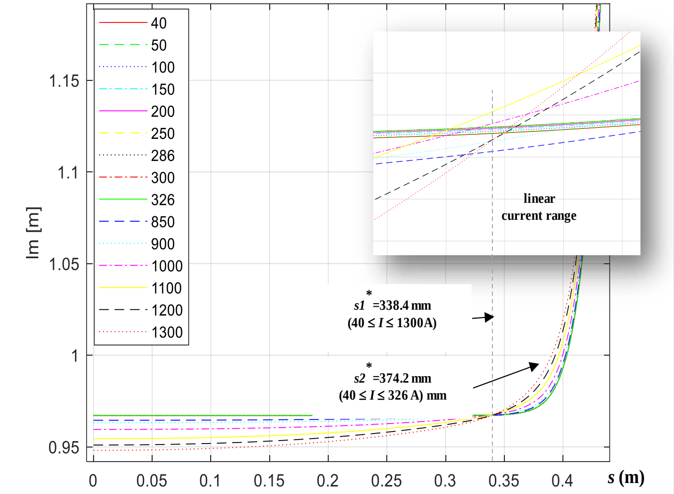

Measurements of ELENA dipole

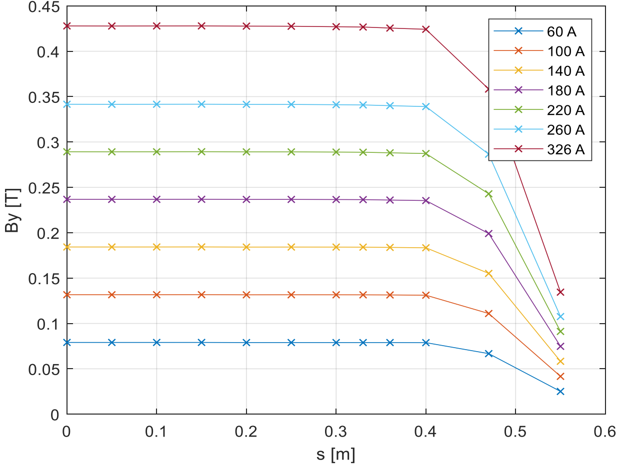

Model with two non-linear contributions:

$$B(s,I)=B_0\frac{I}{I_0}\left(\varsigma_1\left(\frac{I}{I_0}\right)\sigma_1(s)+\varsigma_2\left(\frac{I}{I_0}\right)\sigma_2(s)\right)$$

DC: measured *s** = 352 mm (FE: 369 mm)
200 A/s: measured *s** = 334 mm

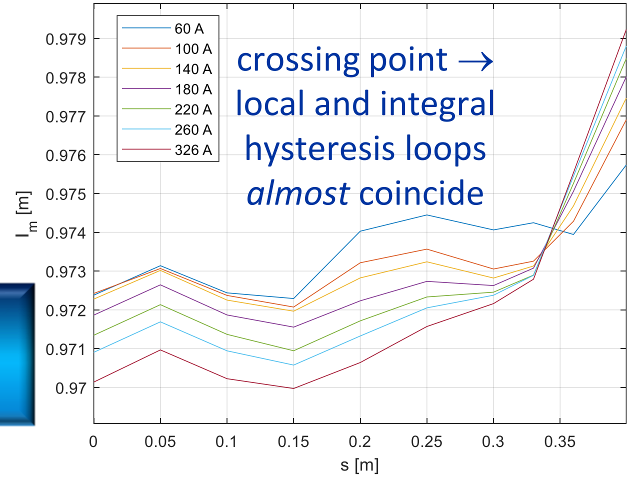

crossing point →
local and integral
hysteresis loops
almost coincide

Credit: Daniel Schoerling, Christian Grech

CERN B-train systems

- Real-time feedback from reference magnets in series with ring (at CERN: LEIR, PSB, PS, SPS, AD, ELENA)
- Principle: periodic integration reset with a local field marker (integrator drift correction)
- Typical requirements: resolution 50 µT, uncertainty 100 µT, bandwidth 100 kHz, latency 30 µs

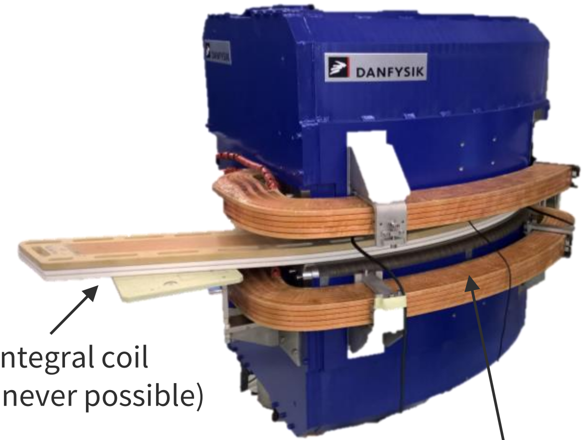

Integral coil
(whenever possible)

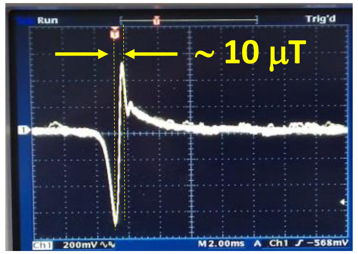

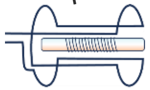

NMR probe in
Marker mode
(fixed RF frequency)

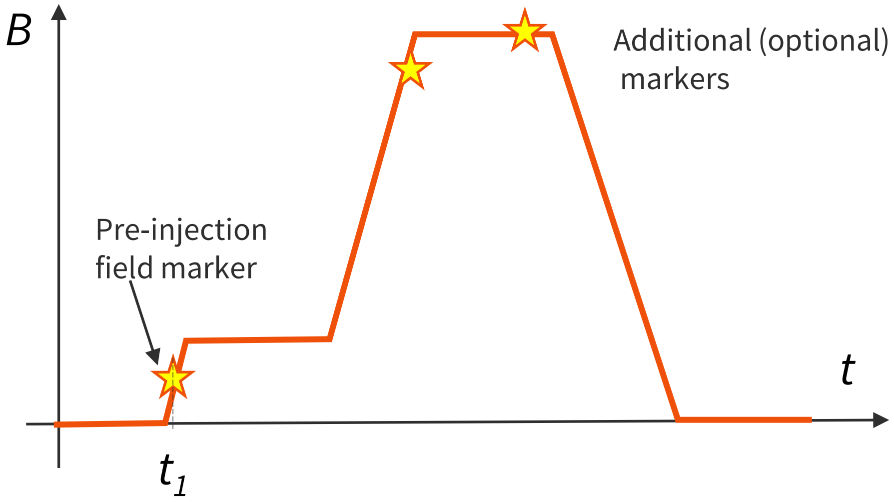

$$B(t) = B_{\text{marker}}(t_1) + \frac{1}{A_c}\int_{t_1}^{t} V_{coil}(\tau)d\tau$$

preset **effective coil area** **marker trigger pulse**

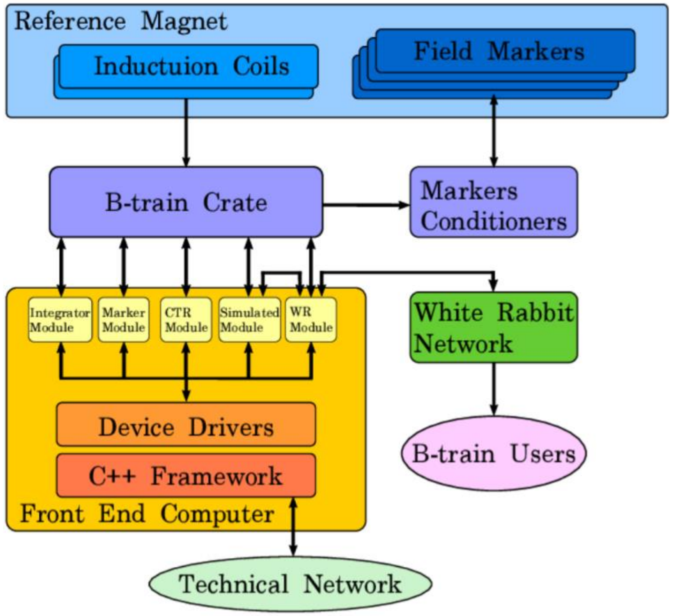

Reference Magnet

Induction Coils

Field Markers

B-train Crate

Markers Conditioners

Integrator Module

Marker Module

CTR Module

Simulated Module

WR Module

White Rabbit Network

Device Drivers

C++ Framework

Front End Computer

B-train Users

Technical Network

B-train electronics

- Tight HW/SW/FW/MW coupling to accelerator control infrastructure for remote configuration, diagnostics
- 2× redundant acquisition chains

White Rabbit patch panel

Timing distribution

WRS/3-18 White Rabbit switch

Auxiliary crate (crosspower switch, Btrain/Bdot selection, power supply)

OASIS DAQ crate

INCAA signal patch panel

Acquisition Chain #1 (OPERATIONAL)

Frequency Generators (excitation of resonance-based field markers)

Metrolab PT2025 NMR teslameters (Hi/Low field markers)

Standard oscilloscope for maintenance

Fluxmeter coil patch panel

B-train crate
(diagnostic display,
analog/digital B-train interface,
marker signal distribution,
power supplies)

Front End Computer (FEC) industrial PC

Acquisition Chain #2 (SPARE)

custom FMC (ANSI/VITA 57 FPGA Mezzanine Cards) on commercial SPEC PCIe carriers to **implement analog/digital I/O**

- Dual-channel voltage integrator
- Dual-channel field marker peak detector
- White Rabbit interface /simulated B-train/predicted B-train

White Rabbit B(t) distribution
Deterministic Ethernet on fiber
Sub-ns synch/GPS disciplined
OA with commercial support

Find it in CERN Open Hardware Repository (https://ohwr.org)

Example: LEIR B-train system

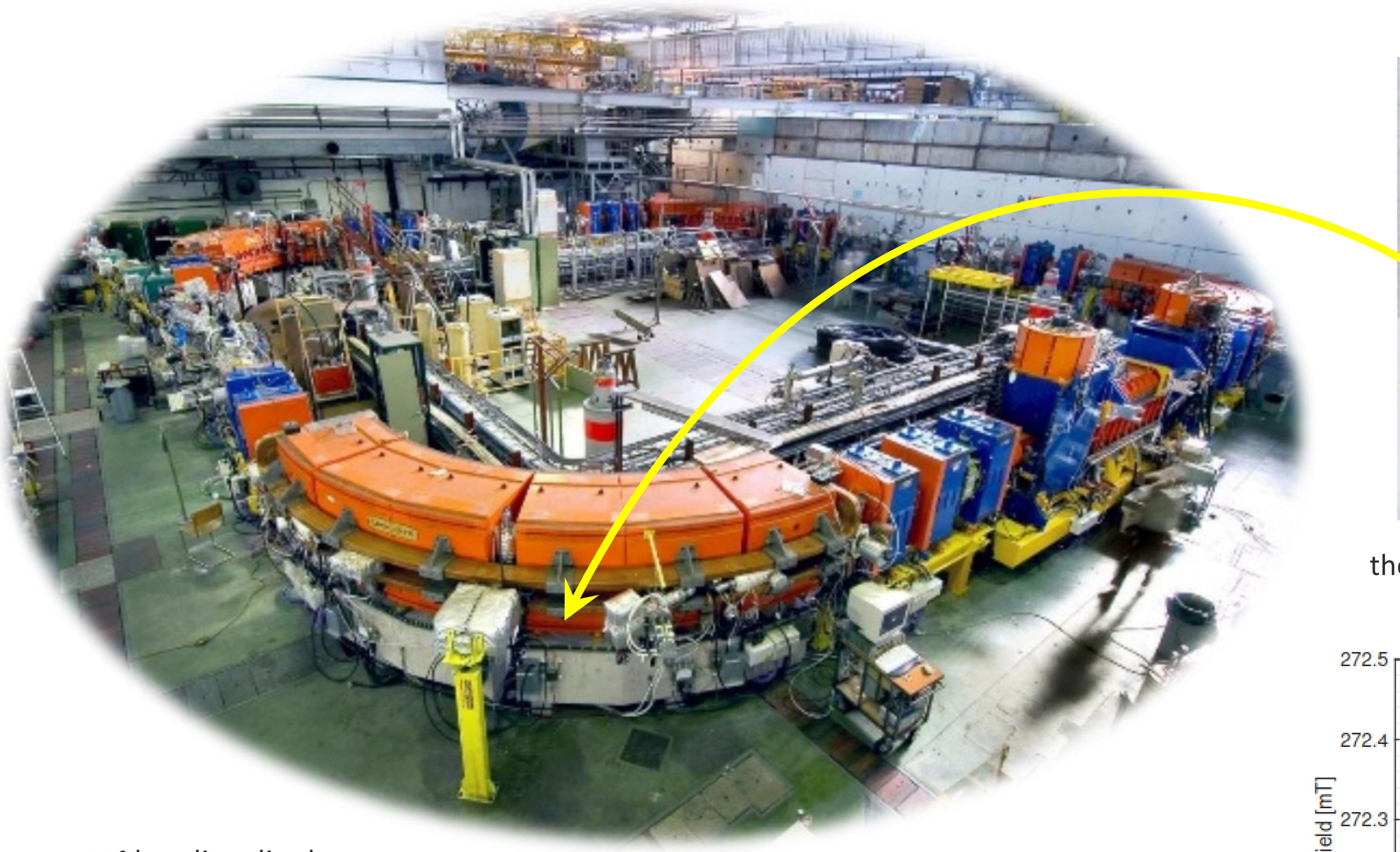

4× 90° bending dipoles

No spare/reference magnet
B-train sensor positioned in fringe field

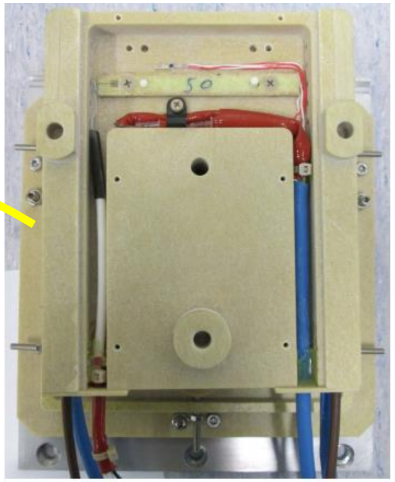

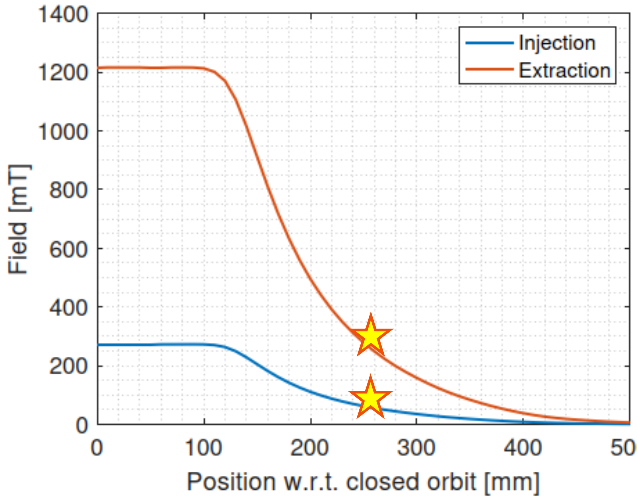

thermostated assembly with induction coil +
106 mT FMR waveguide resonator

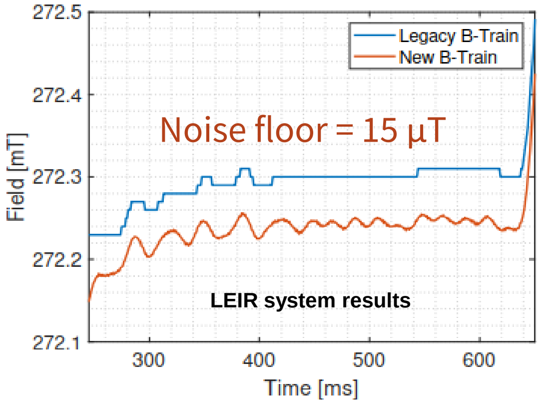

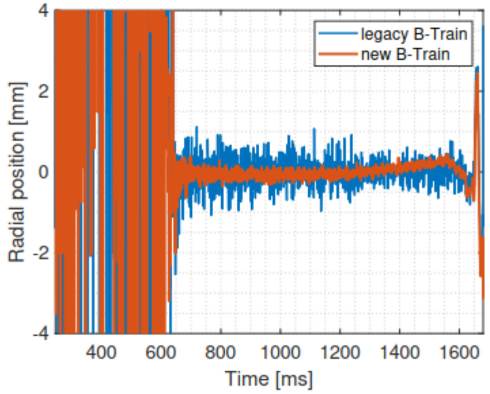

A. Beaumont *et al.*, Error Characterization and Calibration of Real-Time Magnetic Field Measurement Systems, *Nuclear Instr. and Methods*

Conclusions

- Simplified analytical and numerical **hysteresis and eddy currents models** may be useful to gain insight and feed-forward information in simple applications
- Accurate magnetic field control can be achieved by means of **cycle normalization** strategies, or **real-time measurement feedback**. Time and cost are an issue.
- Challenges on the horizon:
  — **simplify and optimize** instrumentation to scale beyond mere bending dipoles ("Baby B-train" systems for multipoles, transfer lines)
  —more demanding requirements (**fast-cycled magnets**, accuracy, reliability) for physics and medical accelerators
  — leverage safely the promising capabilities of **Machine Learning** approaches